

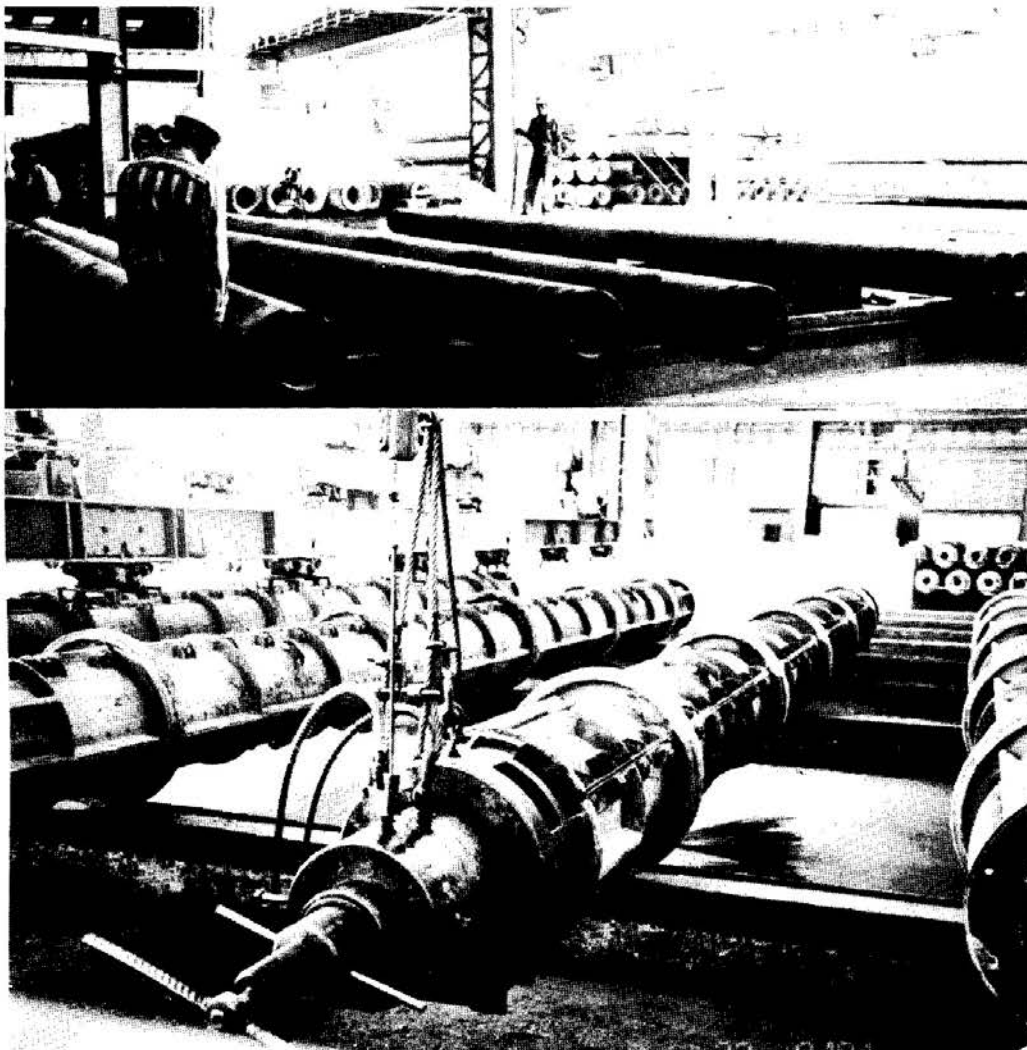
Volume 25 Number 2 December 1994

ISSN 0046-5828

GEOTECHNICAL ENGINEERING

Journal of
SOUTHEAST ASIAN GEOTECHNICAL SOCIETY

Sponsored by
ASIAN INSTITUTE OF TECHNOLOGY



GEOTECHNICAL ENGINEERING

CONTENTS

Photographic Feature:

Seismic Response of Steep Natural Slopes by S.A. ASHFORD.....	1
--	---

Main Papers:

Behaviour of Pile Groups in Calcareous Sand by R.H. AL-DOURI and H.G. POULOS.....	3
Land Subsidence and Negative Skin Friction in Piles by P. KARASUDHI and P. POONSAWAT.....	21
Behaviour of Model Batter Piles in Soft Clays Under Lateral Loads by S. NARASIMHA RAO, C. VEERESH and G.V.S. SHANKARANARAYANA.....	37
Load Transfer Through A Gravel Bed on Stone Column Reinforced Soil by M.R. MADHAV and W.F. VAN IMPE.....	47
A Comparison of the Cyclic Pullout Behaviour of Model Plate and Pile Anchors in Soft Clay by M. DATTA, S.K. GULHATI and N.U. KHAN.....	63
Geotechnical Properties of the Cohesive Sungshan Deposits, Taipei by C.T. CHIN, J.H.A. CROOKS and Z.C. MOH.....	77

Abstracted and/or Indexed in *Geotechnical Abstracts*

PHOTOGRAPHIC FEATURE

SEISMIC RESPONSE OF STEEP NATURAL SLOPES

S.A. Ashford¹

There is a long history of seismically induced failures in steep slopes composed of weakly cemented soils such as loess, volcanic ash, and marine terrace deposits. This photograph shows a failure in a 150-meter high slope in Daly City, California, as a result of the 1989 Loma Prieta earthquake. Failures in these materials are typified by their brittle nature.

One aspect of these seismically induced failures is the effect of topographic amplification on the seismic response. Research recently conducted at the University of California at Berkeley and ongoing at A.I.T. show that strong motion near the crest of these steep slopes can be amplified by over 50 percent due to the effect of topography alone. Recommendations are forthcoming on how to account for these effects in seismic slope stability analyses.



¹ School of Civil Engineering, Asian Institute of Technology, GPO Box 2754, Bangkok, 10501, Thailand

BEHAVIOUR OF PILE GROUPS IN CALCAREOUS SAND

R.H. Al-Douri¹ and H.G. Poulos²

SYNOPSIS

Static loading tests have been performed on model pile groups jacked into reconstituted calcareous sand beds consolidated under different overburden pressures. The results of the tests have shown the influence of overburden pressure and density on both pile group capacity and stiffness. Specifically, the results have shown that as the number of piles increases, the pile group efficiency increases and the group stiffness decreases.

A modified form of boundary element analysis has been used to predict the static behaviour of a pile group using input parameters derived from experimental results. Comparisons between the measured and predicted results show reasonable agreement.

INTRODUCTION

The ultimate axial load capacity and settlement response under design loadings are important considerations in the design of pile groups subjected to the static loading. A number of researchers have studied the behaviour of pile groups in silica sand (e.g. Hanna, 1963; Kishida, 1967; Vesic, 1967; Tejchman, 1973; Ranganatham & Kaniraj, 1978; O'Neill, 1983). In contrast, very few studies of the behaviour of pile groups and the interaction between piles in calcareous sand have been reported (eg. Baus & Ray, 1988; Al-Douri & Poulos, 1994).

In this paper, the results of axial static loading tests on 2- and 4-pile groups in calcareous sand are described. The piles have been jacked into medium-dense and dense sand consolidated under various pressures applied at both the top and ends of the sand bed, using a specially designed test chamber. The results of these tests show the effects of number of piles, soil density and overburden pressure on the pile group efficiency and group stiffness. In addition, measurements have been made of the load distribution along one pile in each group during installation and tensile loading.

A boundary element analysis has been used to predict the static behaviour of a pile group using input parameters derived from experimental results for a single pile. Comparisons between the measured and predicted behaviour have then been made.

¹ Researcher, Centre for Geotechnical Research, School of Civil and Mining Engineering, The University of Sydney, NSW 2006, Australia.

² Professor, School of Civil and Mining Engineering, Sydney University, NSW 2006, Australia, Senior Principal of Coffey Partners Int. Ltd, NSW, Australia.

CHARACTERISTICS OF CALCAREOUS SANDS

The sediment employed in this investigation is designated as “N.R.A” calcareous sand, and was obtained from the seabed at the site of the North Rankin A platform on the North-West Shelf of Australia. The grading curve for this sand is given by Al-Douri (1992). The soil has minimum and maximum particle sizes of about 0.06mm and 2mm respectively, with a value of D_{50} of 0.15mm. The minimum and maximum dry densities are 9.4 and 13.0kN/m³ respectively.

This soil can be classified as a carbonate sand of mainly bioclastic and pelletal origin, with an average carbonate content of 97%. Microscopic examinations (Al-Douri, 1992) have shown the angular nature of the particles, with a high incidence of intra-particle voids. This angularity leads to a high friction angle and a high void ratio, and consequently, a high compressibility. Drained triaxial compression tests performed on N.R.A. sand have indicated that the drained friction angle ϕ' and the initial tangent drained Young's modulus E_{max}' can be estimated from the following relationships (Hull et al 1988):

$$\phi = 46.8 - 0.02\sigma_c' \quad (1)$$

$$E_{max}' = 7.8 + 0.32\sigma_c' \quad (2)$$

where σ_c' = effective confining stress in MPa (within the range 0.10 to 0.40 MPa). The drained Poisson's ratio (ν_{min}') at low strain level was found to be about 0.15.

APPARATUS AND PROCEDURE

The apparatus used for testing the model pile groups is shown diagrammatically in Figure 1. The test chamber had a 590 mm internal diameter and a total height of 680 mm. The vessel was composed of three parts. The top and bottom parts contained water and were used to supply pressure to consolidate the soil. The central vessel body had a height of 480 mm and contained the soil which was separated from the top and bottom parts by rubber membranes. The soil was rained in to the central vessel body, and then consolidated initially by an equal applied pressure at the top and bottom boundaries. The piles were made of 25 mm external diameter aluminium tube, with a 3 mm wall thickness. Each group contained one instrumented pile, with the remainder of the piles being uninstrumented. Details of the dimensions and design of the test chamber, the piles, the pile collars and the pile caps, have been given by Al-Douri (1992).

The sand bed was prepared by raining the sand through a special raining device placed on the body of the vessel, thus producing a relatively uniform sand bed (Al-Douri, 1992). The range of dry density produced by this raining procedure was 9.6 kN/m³ to 10.5 kN/m³, depending on the height of the sand fall. This range of density represented “loose” and “medium-dense” sand. “Dense” samples were produced by vibrating the rained sand in the vessel using two vibrators installed opposite each other on the top flange of the test vessel,

BEHAVIOUR OF PILE GROUPS

as shown in Figure 1. After placement of the sand, the desired overburden pressure was applied for a period of at least 24 hours prior to installation and testing of piles.

The tests were carried out on 4-pile and 2-pile groups. The test procedure involved jacking the piles into the sand until they reached their final penetration of about 290 mm, after which then the load was released. After about 3 hours, the loading machine connecting the pile cap and the model pile group applied an increasing tensile load until failure occurred.

The overburden pressure remained constant during the jacking and loading of the piles. The procedure for jacking the piles was one of two methods:

- 1) Jacking piles individually: In this method, the loading machine and each pile in the group was aligned in turn. The instrumented pile was jacked first, followed by the other piles. The head load for each pile was recorded by a calibrated proving ring, while the load distribution along the instrumented pile was monitored by strain gauges during jacking of the piles. Further details are given by Al-Douri (1992) and Al-Douri & Poulos (1994).
- 2) Jacking all the piles simultaneously: This method is similar to that used for pile tests in silica sand by Vesic (1967). In this method, the piles in the group were connected by a pile cap and then jacked together into the consolidated sand. The jacking load was recorded by the proving ring attached the pile cap, while the load developed along the instrumented pile was recorded at various stages by the strain gauges along the pile.

For both methods, the four pile group was jacked in a symmetrical square pattern with a centre-to-centre spacing of $4d$, while the 2-pile configuration had centre-to-centre spacings of $3d$, $4d$ and $5d$ (where d = pile diameter) as shown in Figure 1.

BEHAVIOUR DURING JACKING

Piles Jacked Individually, Two series of tests were performed. The first was performed on pairs of piles of study the interaction between two piles during jacking, static and cyclic loading. The results have been discussed by Al-Douri & Poulos (1994). The results for the jacking response of pairs of piles are summarized in Table 1. This table shows for each test, the dry density, overburden pressure, pack and ultimate jacking loads, end bearing capacity, and ultimate skin friction measured during jacking of the piles. The following observations have been made by Al-Douri & Poulos (1994):

- a) The jacking force generally increases as the sand density increases or as the overburden pressure increases.
- b) The earlier jacked piles carry less load than those which have been jacked later. This behaviour is similar to that observed by Kishida (1967), who studied the effect of the order of installation in a group of piles driven into silica sand.
- c) There is interaction between the piles being jacked, as evidenced by the change in

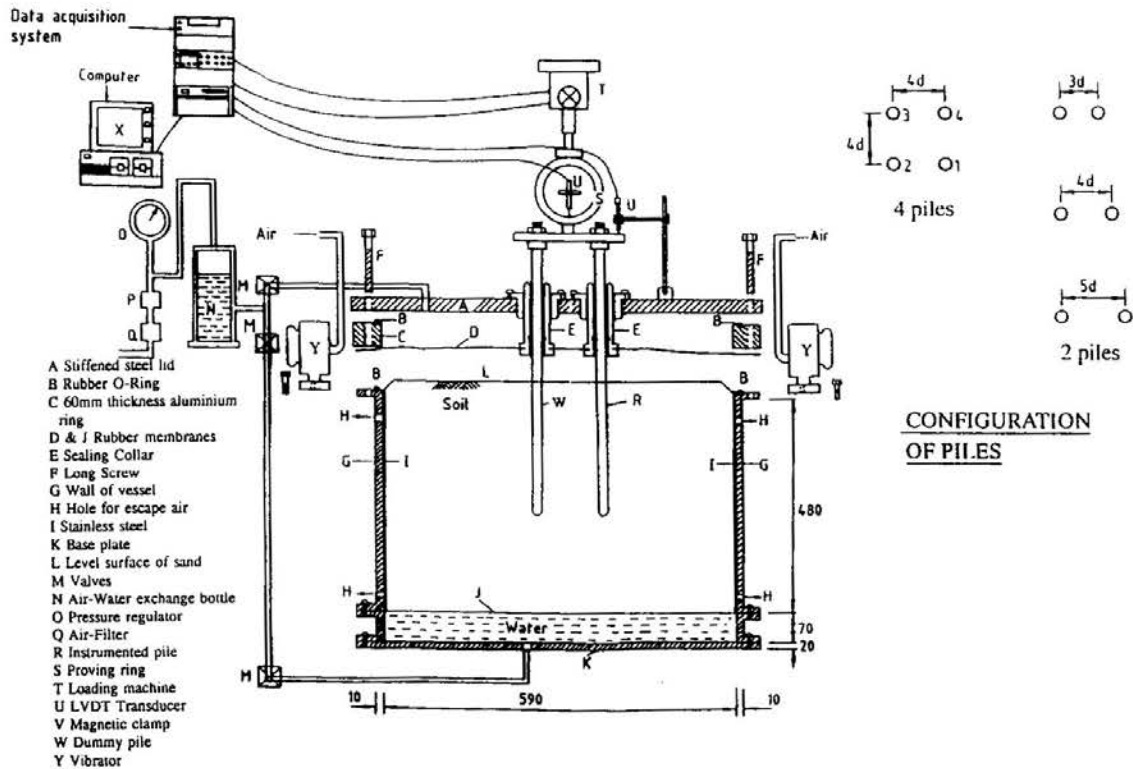


Fig. 1 Schematic Diagram of Test Setup.

head movement of the first pile as the second pile is installed.

The second series comprised tests on 4-pile groups and the results of these tests are summarized in Table 2.

Figure 2 shows relationships between head load and penetration for each of the four piles when jacked into medium dense sand. The jacking load for each pile generally increases with increasing penetration. The required jacking load increases as the number of piles previously installed increases.

The results in Figure 2, and the results from the other tests in Table 2, display a general trend whereby rapid increases in jacking load occur as the penetration depth increases until the peak is reached, after which there is a small decrease to an ultimate value which appears to be dependent on the sand density of the sample.

Pile Jacked Together in a Group, The total jacking load (P_g) on the group was measured by a proving ring, while the strain gauges along the instrumented pile measured the force distribution for various amounts of penetration. For each test, the mean jacking load is defined as the total load P_g divided by the number of piles in the group. The results of jacking 2- and 4-piles simultaneously are summarized in Tables 3.

The peak end bearing capacity developed during jacking under different overburden pressures is shown in Figure 3. The general trend is for end bearing capacity to increase with increasing overburden pressure. The regression line for 4-pile groups plots slightly above

BEHAVIOUR OF PILE GROUPS

Table 1 Results from Installation of Pile Groups (By Jacking the Two Piles Individually).

Test No.	Dry Density (kN/m ³)	Vertical Pressure (kPa)	Jacked Pile No.	Spacing Between Two Piles d=Pile Dia (mm)	Residual Load at Base Prior to Test Sg1 (N)	Peak Base Load Sg1 (N)	Peak End Bearing Capacity (kPa)	Peak Head Load Sg5 (N)	Ultimate Base Load Sg1 (N)	Ult. End Bearing Capacity (kPa)	Ultimate Head Load Sg5 (N)	Ultimate Skin Friction (kPa)
Int-1	10.20	100	1st 2nd	3d 3d	92.0	1198.0	2440.5	1295.0 1460.0	1186.5	2417.1	1371.0	8.2
Int-2	10.40	100	1st 2nd	3d 3d	101.5	1336.0	2721.7	1443.5 1539.0	1115.0	2271.5	1319.0	9.1
Int-3	10.10	200	1st 2nd	3d 3d	114.0	2121.0	4320.9	2238.0 2540.0	1812.0	3691.4	2123.0	13.9
Int-4	11.50	100	1st 2nd	3d 3d	103.0	1675.0	3412.3	2008.0 1755.0	1005.0	2047.4	1352.0	15.5
Int-5	11.40	200	1st 2nd	3d 3d	132.0	2597.0	5290.6	2980.0 3100.0	2230.5	4543.9	2769.0	24.1
Int-6	10.00	200	1st 2nd	3d 3d	85.0	2248.0	4579.6	2471.0 2602.0	2006.0	4086.6	2306.0	13.4
Int-7	11.30	100	1st 2nd	4d 4d	106.0	1745.0	3554.9	1830.0 1815.0	1307.5	2662.6	1598.6	13.0
Int-8	10.50	200	1st 2nd	5d 5d	94.0	2261.0	4606.1	2456.0 1815.0	1853.0	3774.9	2272.0	18.7

Table 2 Results from Installation and Static Tensile Tests of Pile Groups (By Jacking the Four Piles Individually).

Test No.	Dry Density (kN/m ³)	Vertical Pressure (kPa)	Jacked Pile No.	Results of Jacking Tests						Results of Static Tests				
				Residual Load at Base Prior to Test Sg1 (N)	Peak Base Load Sg1 (N)	Peak Head Load Sg5 (N)	Ultimate Base Load SG1 (N)	Ult. End Bearing Capacity (kPa)	Ultimate Head Load Sg5 (N)	Ultimate Skin Friction (kPa)	Mean Static Load *(P.R)/4 (N)	Head Load Sg5 (N)	Static Skin Friction fs (kPa)	
4PDC-1	10.40	100	1st	85.5	1254.0	1360.0	1280.0	2607.6	1445.0	7.4	353.8	295.0	16.1	
			2nd			1520.0								
			3rd			1571.0								
			4th			1658.0								
4PDC-2	10.90	100	1st	90.0	2148.0	2242.0	1817.0	3701.6	2116.0	13.4	475.0	383.0	21.6	
			2nd			2446.0								
			3rd			2520.0								
			4th			2456.0								
4PDC-3	10.60	200	1st	91.7	2644.0	2810.5	2218.0	4518.5	2654.8	19.5	693.8	640.0	31.5	
			2nd			2714.0								
			3rd			3119.0								
			4th			3066.0								
4PDC-4	10.30	200	1st	113.0	2257.0	2413.0	1964.0	4001.0	2272.0	13.8	548.0	486.0	24.9	
			2nd			2779.0								
			3rd			3011.0								
			4th			3128.0								

* P.R = Proving ring reading for total load on group during static tensile load, P.R/4 = Reading of total static load on group/No. of Piles.

BEHAVIOUR OF PILE GROUPS

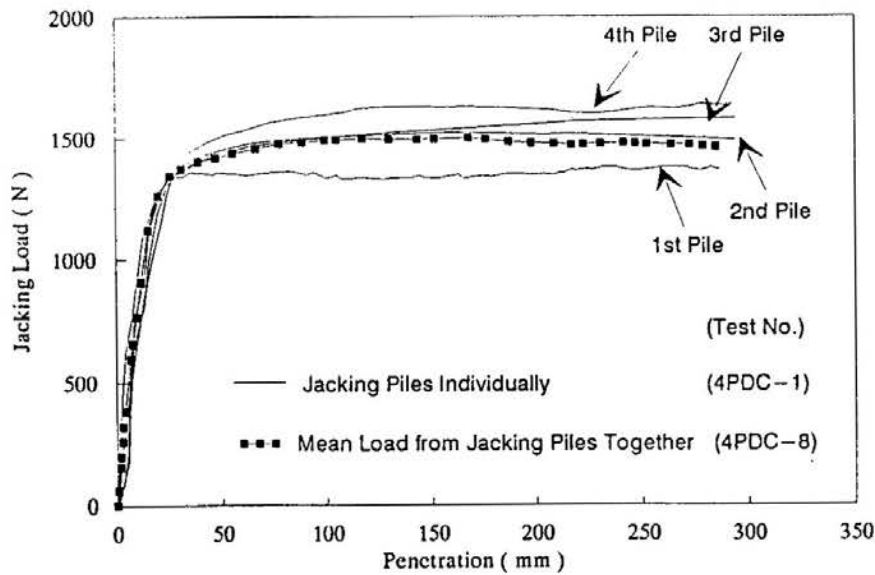


Fig. 2 Jacking Load vs Penetration for Jacking 4 Piles in Different Method (Jacking Individually and Jacking Piles all Together)

that for 2-pile groups which in turn is slightly higher than that for single piles.

Figure 4 shows typical residual load distributions in the instrumented pile, for single piles and pile groups in medium-dense sand. For the same overburden pressure and density, the residual load observed in the 4-pile group is slightly higher than that in the 2-pile group which in turn is higher than that for single pile.

The influence of overburden pressure on the maximum residual load mobilized along a pile in the group is shown in Figure 5. The residual load in all groups increases with increasing overburden pressure, and with the number of piles in the group.

A comparison can be made between the results obtained from jacking piles individually and those for jacking piles together. Figure 2 shows that the mean load from jacking four piles together lies between the load for the first and second jacked piles when jacked individually. However, the general shape of the load-penetration curves are the same for both jacking techniques.

BEHAVIOUR UNDER STATIC TENSILE LOADING

In this study, the effects of the residual load mobilized from jacking of the group are taken into account by distinguishing between the “actual load” which is the measured load change minus the residual load, and the “apparent load”, which is in the measured load change (taking no account of the existence of the residual load). The results of static tests carried out on both 4-pile groups and 2-pile groups are categorized according to the jacking method.

Piles Jacked Individually. Four tensile static tests have been performed on group

Table 3 Results from Jacking and Static Tests of 2- & 4-Pile Groups (Jacking all Piles in the Group Together).

Test No.	Dry Density (kN/m ³)	Vertical Pressure (kPa)	Residual Load at Base Prior To test Sg1 (N)	Mean Jacking Load *(P.R)/N (N)	Peak Head Load Sg5 (N)	Ultimate Head Load Sg5 (N)	Ultimate Base Load Sg1 (N)	Peak End Bearing Capacity (kPa)	Ultimate Skin Friction (kPa)	Total Static Load Pg = P.R (N)	Static Skin Friction fs (kPa)	Secant Pile Stiffness (N/mm)	Group Efficiency (Pg/NPs)
*2PDC-1	10.10	75	41.0	1342.3	1300.0	1128.0	1010.0	2508.4	5.2	324.3	7.1	4587.9	1.12
2PDC-1	10.20	100	74.0	1542.5	1568.4	1260.0	1148.0	3009.3	5.0	430.1	9.6	5282.1	1.10
2PDC-3	9.90	100	98.0	1791.6	1772.1	1655.0	1513.0	3296.4	6.3	423.4	9.4	4301.2	1.09
2PDC-4	10.50	100	106.0	1700.2	1669.8	1320.0	1140.0	3236.7	8.0	498.6	11.2	6338.6	1.28
2PDC-5	10.20	200	128.0	2411.6	2457.4	1813.0	1587.0	4708.7	10.4	816.0	18.6	7153.5	1.04
2PDC-6	10.30	200	112.0	2733.7	2699.5	1535.0	1382.0	5153.3	6.8	906.4	20.2	8994.7	1.16
2PDC-7	10.00	100		1576.9	1586.8	1478.0	1247.0	3060.7	10.2	390.0	8.9	3742.8	1.00
*4PDC-4	10.20	50	38.0	1011.5	1053.6	980.0	865.0	2006.6	5.1	470.0	5.2	3833.3	1.31
4PDC-5	10.00	75	53.0	1239.5	1252.9	1180.0	1059.0	2414.1	5.4	600.0	6.7	3320.2	1.07
4PDC-6	10.80	100	142.0	2197.0	2233.5	1825.0	1578.0	4354.7	11.2	1370.0	15.1	3893.7	1.22
4PDC-7	10.00	100		1458.4	1481.9	1348.0	1104.0	2831.7	10.9	952.0	10.5	3471.1	1.12
4PDC-8	9.90	100	113.0	1596.6	1608.6	1668.0	1482.0	3088.8	8.3	875.0	9.7	4678.5	1.05
4PDC-9	10.20	100	107.0	1580.5	1597.4	1685.0	1456.0	3065.6	10.3	781.0	8.6	5689.6	1.15
4PDC-10	9.95	200	136.0	2511.7	2545.9	1343.0	1125.0	4930.2	9.9	1811.0	20.0	6640.4	1.37
4PDC-11	10.30	200	158.0	2896.3	2995.5	1607.0	1340.0	5640.1	12.1				

* 2PDC = 2 Pile group test, 4PDC = 4 Pile group test.

** P.R = Proving ring reading for total load on group during jacking or static load, P.R/N = Reading of total jacking or static load on group/No. of Piles.

BEHAVIOUR OF PILE GROUPS

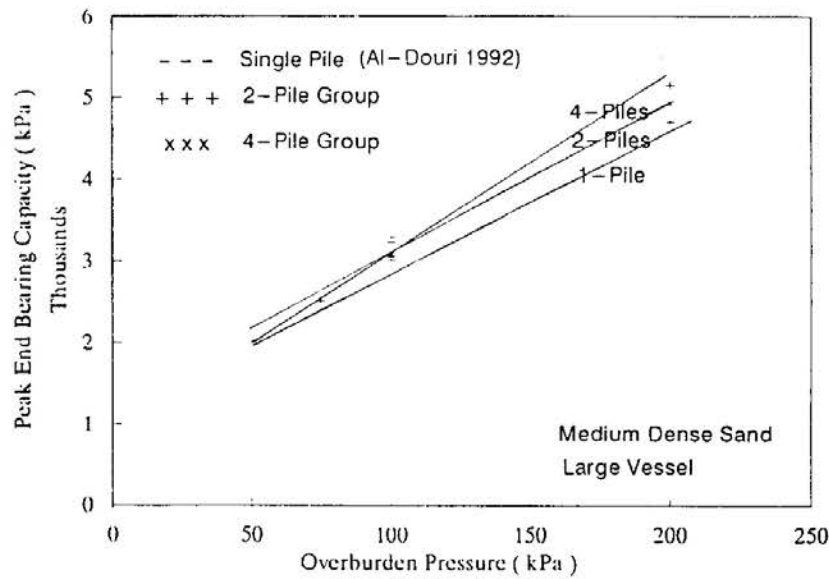


Fig. 3 The Influence of Overburden Pressure on Peak End Bearing Capacity of Pile Groups During Jacking.

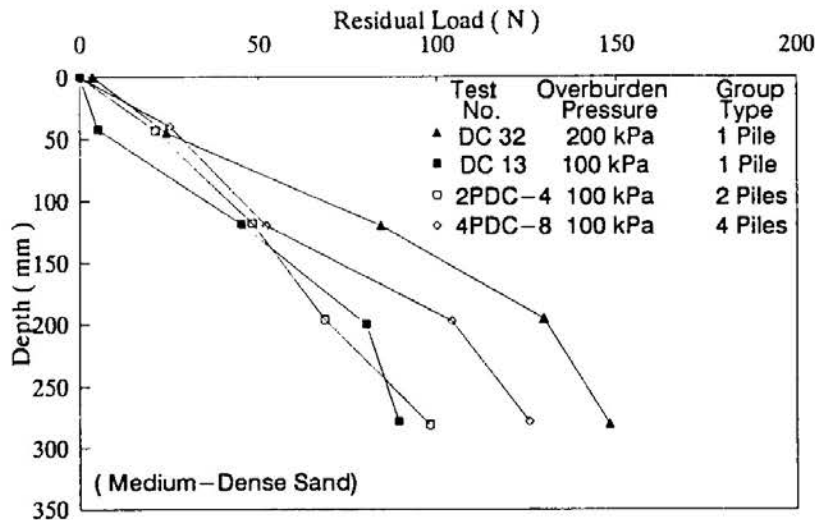


Fig. 4 Residual Load Distribution Along the Length of One Pile in Group.

installed by this method and the results are summarized in Table 2. This table shows the values of mean static load, head load and deduced average skin friction for various sand densities and overburden pressures.

For different positions along the instrumented piles, typical “actual” load-settlement curves from static tensile loading of a 4-pile group in medium-dense sand (4PDC-1) are shown in Figure 6. As the applied tensile load increases, the loads measured from all strain gauges in the instrumented pile (except the top strain gauge Sg5), are initially compressive, but become tensile. However, the total load on the group as measured by the proving ring starts from zero. As was observed for the case of a single pile (Poulos & Al-Douri, 1992), the high compressive load observed at the bottom strain gauge Sg1 decreases with axial

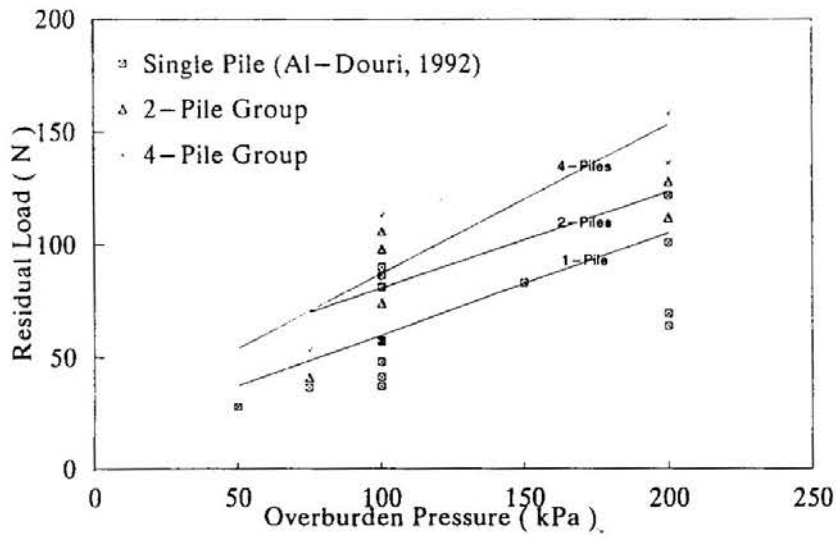


Fig. 5 Effect of Piles on the Residual Load (Prior to Testing).

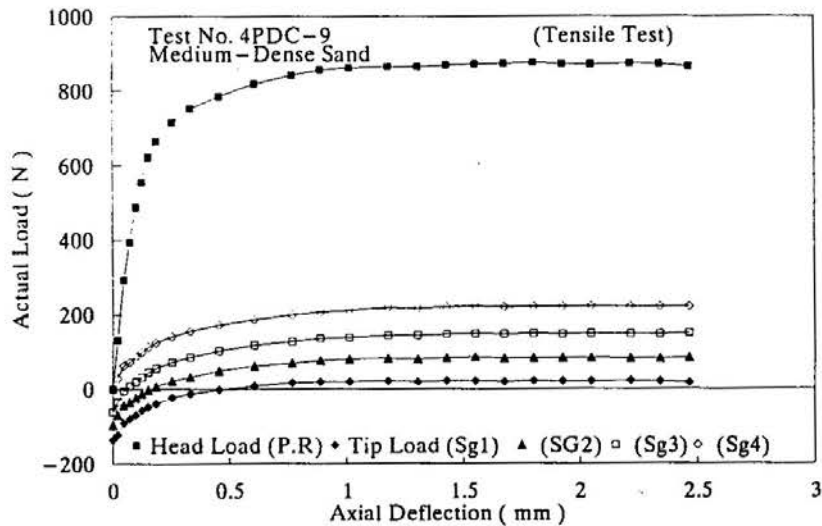


Fig. 6 Load-Deflection Curve for 4-Pile Group (100 kPa Overburden Pressure).

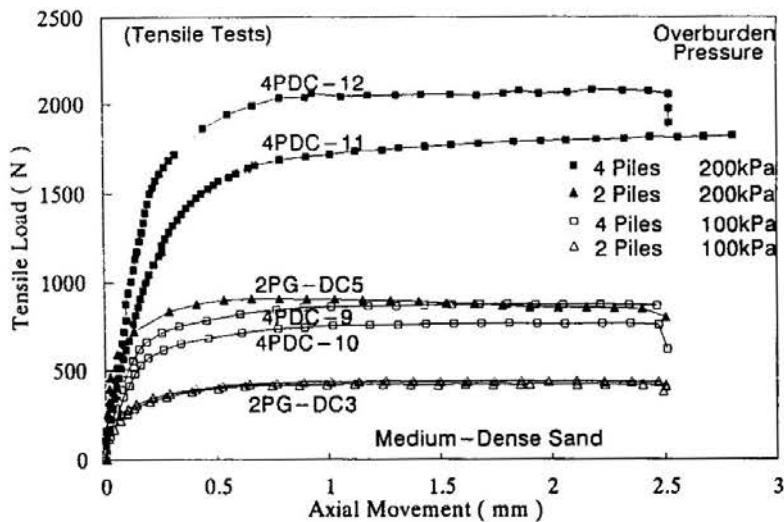


Fig. 7 Load-Deflection Curve During Static Loading for 2- and 4-Pile Groups Under Different Overburden Pressure.

BEHAVIOUR OF PILE GROUPS

deflection until it reaches a more or less zero tensile load value, indicating essentially zero tip resistance in uplift, as would be expected. Similar behaviour is found for all pile groups tested.

Piles Jacked Together in a Group. Two series of tensile static tests on 2- and 4-pile groups have been performed using this jacking technique, and the results of these tests are summarized in Table 3.

Two groups of load-deflection curves obtained from tensile loading of 2-pile groups and of 4-pile groups are shown in Figure 7. For a particular overburden pressure and group type, the difference in load capacity is not more than 15%, indicating a reasonable degree of repeatability. As expected the load capacity increases as the overburden pressure increases, and the capacity of 4-pile groups is higher than that of 2-pile groups for the same overburden pressure and soil density.

Comparisons between the settlement obtained from the results of pile group tests shown in Figure 8 and those from single pile tests performed by Al-Douri (1992) can be made. The results indicate that the settlement increases as the number of the piles in group increases, with identical loads. Similar behaviour is observed from model pile groups in silica sand by Tejchman (1973).

Comparisons between the results obtained from jacking piles individually and those for jacking piles together can be made from the results shown in Figures 6 and 7 and the results presented in Tables 2 and 3. The mean head loads and loads along one pile for individual jacking are higher than those for the group jacking, and in general, the differences in the behaviour of piles under static loading are similar to the differences in behaviour during jacking using both jacking techniques.

The influence of number of piles in a groups on the group efficiency (η) under an overburden pressure of 100kPa is shown in Figure 8. η is defined as the ultimated load of the group divided by the number of piles times the ultimate load of a single isolated pile. The

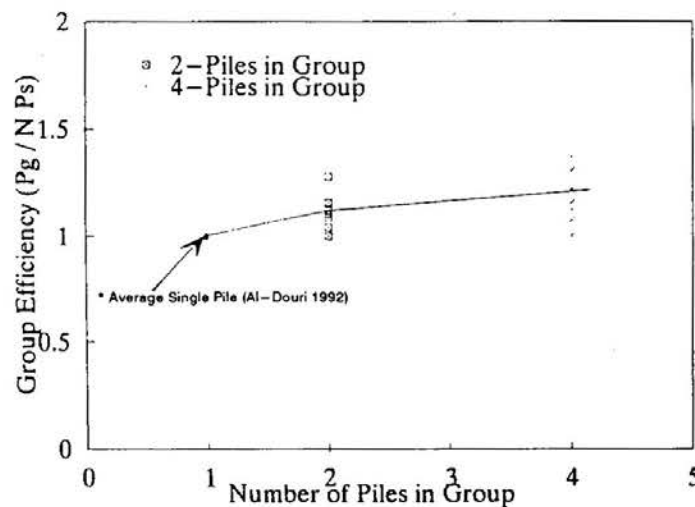


Fig. 8 Group Efficiency Versus Number of Piles in Group.

group efficiency appears to increase slightly as the number of piles in the group increases.

Figure 9 shows the relationship between the group efficiency η of 2-pile and 4-pile groups and sand density. η appears to increase with increasing sand density, and similar observations on jacked pile groups in silica sand have been made by Vesic (1967), Das et al. (1976) and Ranganatham & Kaniraj (1978), again indicating that the soil density plays an important role in determining the pile capacity. Vesic (1967) reported that the soil density may affect pile group efficiency more than the number of piles in a group, and this conclusion appears to be confirmed by the present test results.

The secant stiffness of the different pile groups tests is shown in Figure 10, for a load level $P/P_s = 25\%$. The general trend is for the secant stiffness to decrease with increasing number of piles and also for increasing load level. Figure 10 shows also the predicted relationship between group stiffness and number of piles, which will be discussed later.

Load Distribution

Figure 11a presents the relationship between the tensile load in the pile and depth during tensile loading for the instrumented pile in a 2-pile group (2PDC-4) jacked in medium dense sands subjected to 100kPa applied pressure. The following observations may be made from this Figure:

- 1) the load at each point along the instrumented pile starts from a compressive residual value, except that measured by the top strain gauge,
- 2) the base load decreases with increasing pile movement until it becomes close to zero at failure, and
- 3) the slope of the load distribution curve is nearly constant, implying that the skin friction is almost constant with depth.

The development of skin friction along a pile in a 2-pile group can be further studied by converting the relationships in Figure 11a to shear stress versus depth relationships. As

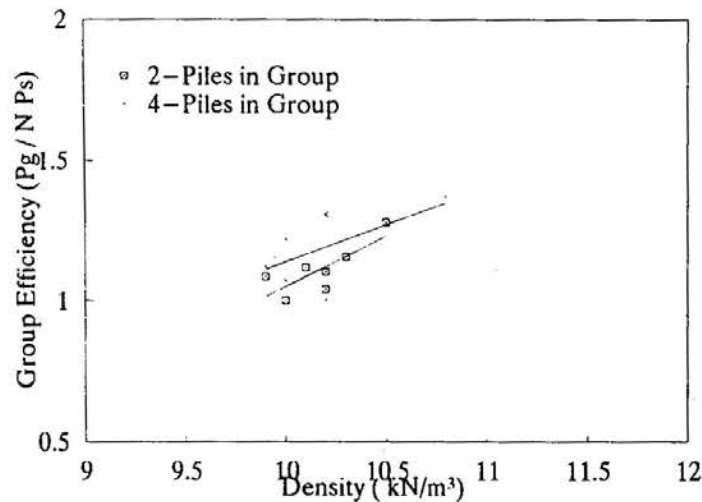


Fig. 9 Effect of Dry Density on Group Efficiency.

BEHAVIOUR OF PILE GROUPS

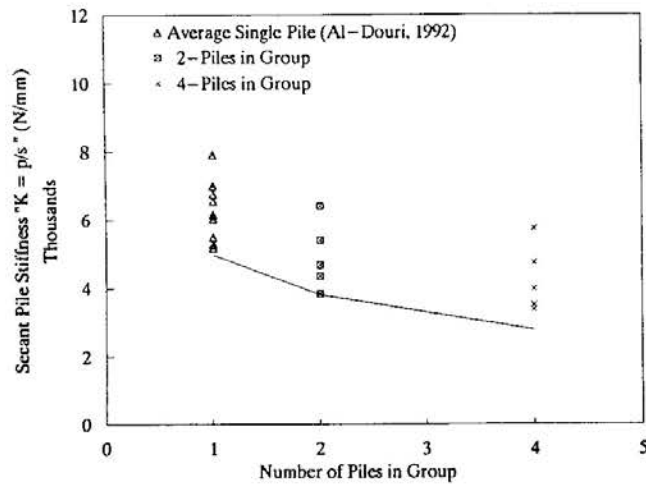


Fig. 10 Secant Pile Stiffness vs Number of Piles in the Group (25% Load Level).

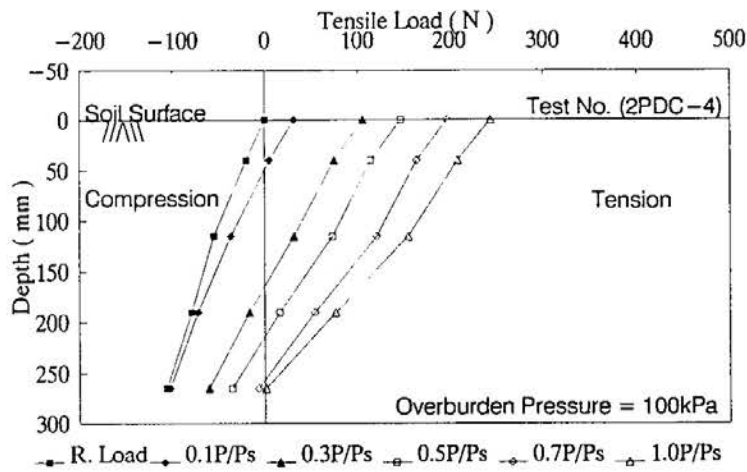


Fig. 11a Effect of Pile Load Level on Tensile Loads Along Instrumented Pile in the 2-Pile Group.

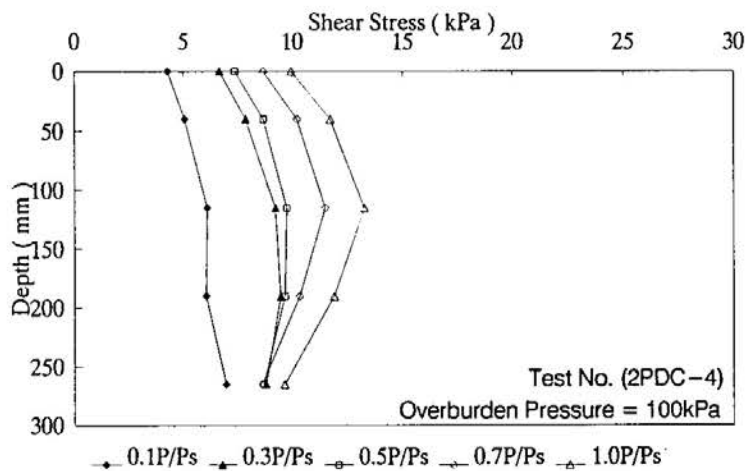


Fig. 11b Effect of Pile Load Level on Shear Stress Along Instrumented Pile in the 2-Pile Group.

shown in Figure 11b, it can be seen that the skin friction increases with increasing tensile displacement, and is reasonably constant with depth.

COMPARISON BETWEEN MEASURED AND PREDICTED RESULTS

A simplified form of boundary analysis for both axial static and cyclic response was described by Poulos (1989a) and has been used to predict the residual load after installation, the load-settlement behaviour, and the load distribution in a single pile and a pile within a group. This analysis represents the pile shaft as a series of elastic cylindrical elements surrounded by a soil mass which is modelled as an elastic continuum. The analysis allows for local pile-soil slip along the shaft and bearing failure at the pile tip. The analysis is implemented via the program "SCARP" (Poulos, 1989b). The loading can be specified as either displacement-controlled or load-controlled.

Although SCARP can incorporate non-homogeneous soil profiles, it has been assumed for the model tests that both the soil Young's modulus (E_s) and the Poisson's ratio (ν_s) are constant with depth. ν_s has been assumed to be 0.3 while E_s has been backfigured from the measured single pile head stiffness at 25% of load level using elastic theory by Randolph and Worth (1978). The average value of secant Young's modulus at 25% load level for medium dense sand under 100kPa overburden pressure was found to be about 20MPa.

Pile Installation

In order to model pile jacking, the pile has been loaded to failure in the analysis and then unloaded, and it has been assumed that; i) the limiting shear stress is uniformly distributed along the pile; ii) the values of limiting shear stress and Young's modulus used in the analysis are the values derived from the single pile tests; iii) the installation has involved the generation of full slip and end bearing before removal of the load.

Figure 12 shows the predicted and observed relationships between residual load and

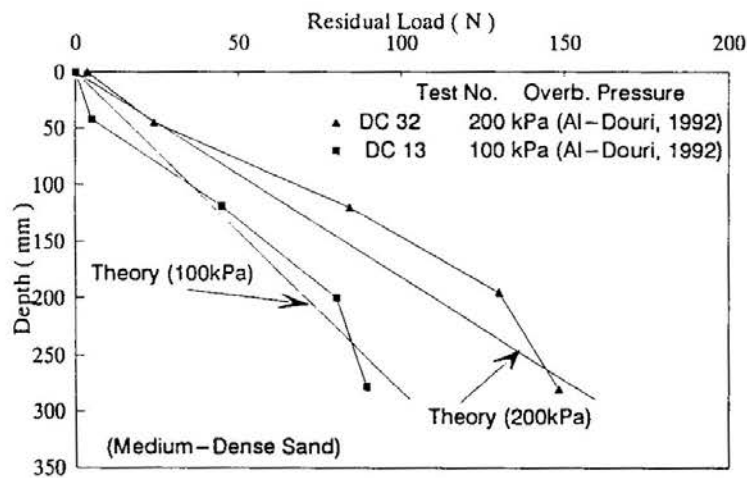


Fig. 12 Measured and Predicted Residual Load vs Depth for Single Pile .

BEHAVIOUR OF PILE GROUPS

depth of a single pile jacked into medium-dense sand under 100kPa and 200kPa overburden pressures. The theoretical residual load increases linearly from the base to the top of the pile, and the maximum value is about 100 N for the soil subjected to 100kPa (Figure 12) and about 150 N for the sand subjected to 200 kPa. The general trend and the maximum predicted value of residual load are similar to those obtained from the tests.

The predicted results for residual load in a single pile, and a pile within a group, are the same, if the same soil parameters are used. It is interesting to note that the experimental results also show little difference between a single pile and a pile in a group, under the same conditions of sand density and overburden pressure.

Static Behaviour

Comparison between predicted and measured results of the secant pile stiffness obtained from different pile groups tests are summarized in Figure 10. The general trends in both the measured and theoretical behaviour for the secant stiffness to decrease as the number of piles in the group increases. However the predicted values of stiffness are generally somewhat lower than the average of measured results.

Figure 13 shows the measured and predicted load distributions at failure along the pile jacked into medium dense sand and subjected to two different overburden pressures. For both overburden pressures, the general trend of load distribution for both measured and predicted results is for an almost linear decrease from the pile head to the pile tip. The predicted and measured distributions of load are about the same, indicating that the distribution of ultimate skin friction is nearly uniform with depth.

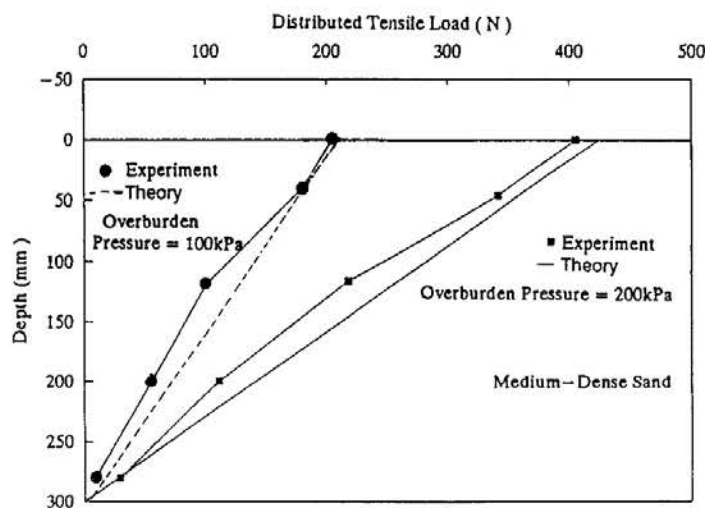


Fig. 13 Measured and Computed Load Distributions at Failure During Static Loading.

CONCLUSIONS

Several tests on model 2-pile groups and 4-pile groups jacked into New North Rankin calcareous sand have been carried out to investigate the factors that influence the load-

settlement behaviour and the skin friction behaviour along piles and small pile groups. The main conclusions are summarized below.

Behaviour During Jacking

- 1) The end bearing resistance and the skin friction developed during jacking generally increase as the initial sand density increases or overburden pressure increases.
- 2) Jacking the piles together in a group results in a more uniform distribution of load among and along these piles than if the piles are jacked individually.
- 3) The residual load mobilized along a pile in dense sand is higher than that in medium dense sand.
- 4) The maximum residual load developed within a pile in a group in dense sand is higher than that in medium-dense sand.
- 5) The predicted and experimental values of residual load within a pile in a group, are similar, and are also similar to those for a single pile.

Static Response

- 1) For both techniques of jacking piles (individually and simultaneously), the tensile group load increases to a peak load and then drops to an ultimate value for both dense and medium-dense sands. The values of mean static load from jacking piles simultaneously is slightly less than those for jacking piles individually.
- 2) As the tensile load increases, the initial compressive residual loads reduce, and at failure, the tip load is eventually zero.
- 3) The group efficiency (η) increases as the number of piles in group increases, and also increases with increasing sand density.
- 4) For single piles and pile groups, the secant stiffness decreases with increasing load level.
- 5) The stiffness of single piles is higher than that of the 2-pile group which is in turn stiffer than the 4-pile group.

Comparisons between the predicted and experimental load-deflection behaviour during tensile static loading of single piles and pile groups show that the load capacity and stiffness obtained from theoretical analyses correspond reasonably well with the measured values.

In summary, the work described in this paper shows that group action influences both pile capacity and pile stiffness, but that the effects on stiffness are more significant than on load capacity. Theoretical analysis based on a simplified form of boundary element analysis appears to provide a reasonable means of assessing pile group stiffness.

BEHAVIOUR OF PILE GROUPS

ACKNOWLEDGEMENTS

The work presented in this paper forms part of a research project of the Mechanics of Calcareous Sediments carried out at the University of Sydney and supported by a grant from the Australian Research Council. The tests were carried out using the facilities of Centre for Geotechnical Research. The authors are indebted to Dr. T. Hull and Mr R Barker for assistance with the experimental work.

REFERENCE

- AL-DOURI R.H. (1992). "Behaviour of Jacked Single Piles and Pile Groups in Calcareous Sediments". PhD Thesis, The University of Sydney.
- AL-DOURI R.H. and POULOS H.G. (1994). "Interaction Between Jacked Piles In Calcareous Sand" XIII Int. Conf. Soil Mech. (ICSMFE), New Delhi, India.
- BAUS, R.L. and RAY, R.P. (1988). "Axial Pile Capacity Study for Piles in Calcareous Marl". Proc. Int. Conf. on Calc. Sediments, Perth, Australia Vol. 1, pp. 185-191.
- DAS, B.M., SEELEY, G.R. and SMITH, J.E. (1976). "Uplift Capacity of Group Piles in Sand". Jnl. of Geot. Engrg. Div., ASCE, Vol. 102, No. GT3, pp. 282-286.
- HANNA, T.H. (1963). "Model Studies of Foundation Group in Sand". Geotechnique, Vol. 13, No. 4, pp. 341-351.
- HULL, T.S. POULOS, H.G. and ALEHOSSEIN, H. (1988). "The Static Behaviour of Various Calcareous Sediments". Proc. Int. Conf. on Calc. Sediments, Perth, Vol, 1, pp. 87-96.
- KISHIDA, H. (1967). "Ultimate Bearing Capacity of Piles Driven into Loose Sand", Soil and Found., Vol. 7, No. 3, pp. 20-29.
- O'NEILL, M.W. (1983). "Group Action in Offshore Piles". Proc. ASCE Special Conf. on Geotechnical Practice in Offshore Engineering Austin, pp 25-64.
- POULOS, H.G. (1989a). "Cyclic Axial Loading Analysis of Piles in Sand." Jnl. of Geot. Engrng. Div., ASCE, Vol. 115, No. 6, pp. 836-852.
- POULOS, H.G. (1989b). "Program SCARP. Static and Cyclic Axial Response of Piles." Centre for Geotechnical Research University of Sydney Australia.
- POULOS, H.G. and AL-DOURI, R.H. (1992). "Influence of Soil Density on Pile Skin Friction in Calcareous Sediments", Proc. 6th ANZ Conf. on Geomechs., Christchurch, New Zealand, pp. 375-380.
- RANGANATHAM B.V. and KANIRAJ S.R. (1978) "Settlement of Model Pile Foundation in Sand". Indian Geot. Jnl. Vol. 3, No. 1, pp. 1-26.
- TEJCHMAN, A.F. (1973). "Model Investigations of Pile Groups in Sand". Jnl. of Geot. Engrng. Div., ASCE, Vol. 99, No. SM2, pp. 199-217.
- VESIC, A.S. (1967). "A Study of Bearing Capacity of Deep Foundations". Final Report, project B-189, School of Civil Engineering Georgia, Institute of Technology, U.S.A.

LAND SUBSIDENCE AND NEGATIVE SKIN FRICTION IN PILES

P. Karasudhi¹; and P. Poonsawat²

SYNOPSIS

Land subsidence and negative skin friction in piles, due to water withdrawal from artesian wells, are analyzed by discretizing the near field into finite elements, and the rest into infinite elements. The shape functions of the infinite elements are derived analytically from simple problems. The Biot's theory for quasi-statics of saturated porous isotropic elastic solids is assumed to govern the soil media. The Laplace transform of governing conditions are solved numerically first, then the inverse Laplace transform of any solution function is obtained by a curve-fitting method. Subsidence results agree closely with those obtained by others.

INTRODUCTION

The problems of negative skin friction in piles, due to fill surcharge and water withdrawal from deep artesian wells, have been subjected to numerous investigations, e.g. Ng, Karasudhi & Lee (1976), and Lee, Chin & Chow (1990). Exact analytical solutions for such problems are possible only for simple cases. For multilayered saturated elastic half spaces the analytical approach is very complicated and mathematically intractable. The most suitable and efficient way to solve such problems is to employ numerical techniques without restrictions on geometry, inhomogeneity, anisotropy and boundary conditions. Since Sandhu & Wilson (1969), the conventional finite element technique is used to solve any type of complex problems of saturated elastic half space, by truncating the semi-infinite domain into a large but finite field which is then discretized into standard finite element. By this way, it needs a higher computational effort and cost because of large number of degrees of freedom.

To avoid this difficulty, Rajapakse & Karasudhi (1985) proposed three types of infinite elements for solving elastostatic multilayered half space by investigating the elastostatic far-field behavior of a homogeneous half space and a layered half space. However, a successful application of this scheme for the present study depends upon the use of far-field functions which can represent the actual far-field behaviors. The objective of this paper is to present an efficient scheme, to calculate land subsidence and negative skin friction due to water withdrawal from deep artesian wells, employing infinite elements to discretize the far field and analytically derived far field functions as shape functions for such infinite

¹ Professor, ²Former Graduate Student, School of Civil Engineering, Asian Institute of Technology, P.O. Box 2754, Bangkok 10501, Thailand.

elements. The proposed scheme also involves an efficient inverse Laplace transform technique to obtain the quasi-static time functions.

FINITE ELEMENT FORMULATION

Formulation of Proper Functional

The proper functional to represent the total potential energy of a quasi-static saturated elastic soil media can be formulated, in the indicial notation of Cartesian tensors, as follows.

$$\Pi \equiv \int_V [\sigma_{ij} * \epsilon_{ij} + p_f * \epsilon_{ii} - H(t) * \frac{\partial w_i}{\partial t} * p_{f,i}] dV + \int_S [H(t) * \bar{Q} * p_f - \bar{X}_i * u_i] dS \quad (1)$$

where σ_{ij} is the effective stress tensor, ϵ_{ij} the strain tensor, u_i is a displacement component of a solid matrix, ϵ_{ii} the dilatation, p_f the excess pore pressure (positive in tension), w_i is the displacement of fluid relative to the solid matrix of soil, $H(t)$ the Heaviside step function, t the time, S the surface, V the volume completely enclosed by S , \bar{Q} the outflow rate, \bar{X}_i the surface force, and $*$ denotes the standard convolution integral, i.e.

$$v_1 * v_2 \equiv \int_0^t v_1(t-s) v_2(s) ds, \quad v_1 * v_2 = v_2 * v_1 \quad (2a, b)$$

in which 0^- is infinitesimally less than zero. Thus

$$\tilde{\Pi} = \int_V (\tilde{\sigma}_{ij} \tilde{u}_{ij} + \tilde{p}_f \tilde{u}_{ii} - \tilde{w}_i \tilde{p}_{f,i}) dV + \int_S (p^{-1} \tilde{Q} \tilde{p}_f - \tilde{X}_i \tilde{u}_i) dS \quad (3)$$

$$\delta \tilde{\Pi}(\tilde{u}_i, \tilde{p}_f) = \int_V (\tilde{\sigma}_{ij} \delta \tilde{u}_{ij} + \tilde{u}_{ii} \delta \tilde{p}_f + \tilde{p}_f \delta \tilde{u}_{ii} - \tilde{w}_i \delta \tilde{p}_{f,i}) dV + \int_S (p^{-1} \tilde{Q} \delta \tilde{p}_f - \tilde{X}_i \delta \tilde{u}_i) dS \quad (4)$$

where \tilde{u}_i and \tilde{p}_f are selected as the primary field variables in the variation above, p is the Laplace transform parameter versus the time t , δ is that variational symbol signifying a virtual quantity, $\tilde{v}(p)$ the Laplace transform of $v(t)$, i.e.

$$\tilde{v}(p) \equiv \int_0^\infty \exp(-pt) v(t) dt \quad (5)$$

Incorporating Darcy's law in Eq. 4, all equilibrium, perfect saturation conditions and well-posed boundary conditions, as proposed by Biot (1941) and reviewed by Karasudhi (1992) for quasi-statics, can be obtained simultaneously by the condition $\delta \tilde{\Pi} = 0$. For finite element formulation, Eq. 4 should be put in the form of matrices as follows.

$$\delta \tilde{\Pi} = \int_V (\delta \tilde{E}^T \tilde{S} + \delta \tilde{p}_f \tilde{\epsilon}_{kk} + \delta \tilde{\epsilon}_{kk} \tilde{p}_f - k p^{-1} \delta \tilde{P}_g^T \tilde{P}_g) dV + \int_S (p^{-1} \delta \tilde{p}_f \tilde{Q} - \delta \tilde{U}^T \tilde{X}) dS \quad (6)$$

where S , E , P_g , \tilde{X} and U are respectively representing the following column vectors;

LAND SUBSIDENCE AND NEGATIVE SKIN FRICTION

effective stress, strain, pore pressure gradient (hydraulic gradient), prescribed surface force and displacement, and k the coefficient of permeability. In the present study these vectors are used either in cylindrical coordinates (r, θ, z) or spherical coordinates (R, ϕ, θ) depicted in Fig. 1.

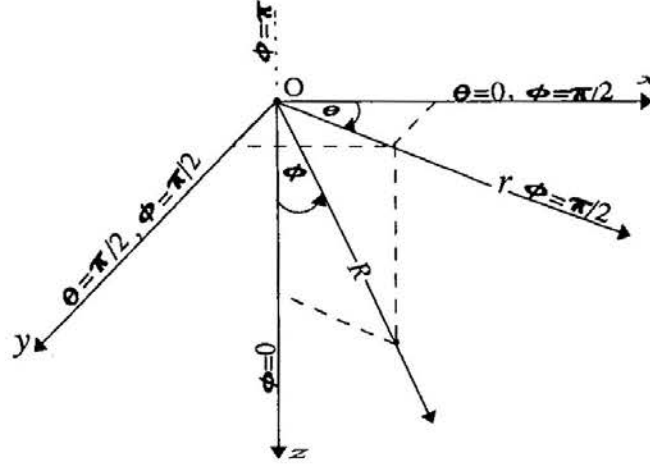


Fig. 1 Cartesian (x, y, z) , Cylindrical (r, θ, z) , and Spherical (R, ϕ, θ) Coordinates.

Finite Element Discretization

Expressing all functions involved in $\delta\tilde{\Pi}$ (Eq. 6) in terms of $\tilde{u}_r, \tilde{u}_\theta, \tilde{u}_z$, and \tilde{p}_f at nodes of each element; then setting $\delta\tilde{\Pi} = 0$; we get the characteristic matrix, which is equivalent to the stiffness matrix in pure solid problems, of that element. Hence, the displacement field vector u of an element for the axisymmetric case can be expressed in terms of their nodal values as follows

$$\tilde{u}(r, z, p) = \begin{Bmatrix} \tilde{u}_r(r, z, p) \\ \tilde{u}_z(r, z, p) \end{Bmatrix} = N^u(r, z) \tilde{U}^e(p) \quad (7a)$$

where

$$N^u(r, z) = \begin{bmatrix} N^{u_r} & 0 \\ 0 & N^{u_z} \end{bmatrix}, \quad \tilde{U}^e(p) = \begin{bmatrix} \tilde{U}^r(p) \\ \tilde{U}^z(p) \end{bmatrix} \quad (7b,c)$$

in which N^{u_r} is the row vector of nodal displacement shape functions in the r direction, 0 is the null row vector of the same size as the previous one, N^{u_z} is the row vector of nodal displacement shape functions in z direction, $\tilde{U}^r(p)$ is the column vector of nodal displacements in r direction, and $\tilde{U}^z(p)$ is the column vector of nodal displacement in the z direction. Similarly, the fluid pore pressure p_f is discretized as given below,

$$\tilde{p}_j(r, z, p) = N^{pj}(r, z)\tilde{P}^e(p) \quad (8)$$

where $N^{pj}(r, z)$ is the row vector of pore pressure shape functions and $\tilde{P}^e(p)$ is the column vector of nodal pore pressures.

By substituting Eq. 7a into the strain-displacement relationship, the strain vector $E(r, z, p)$ and the stress-strain relationship can be expressed, respectively, as the following

$$\tilde{E}(r, z, p) = B\tilde{U}^e, \quad \tilde{S}(r, z, p) = D\tilde{E} \quad (9a,b)$$

where the explicit forms of B and D are given in Appendix.

By substituting Eqs. 7 to 9 into Eq. 6, $\delta\Pi^e$ of an element can be written as

$$\delta\Pi^e = \delta\tilde{U}^{eT}K^e\tilde{U}^e + \delta\tilde{P}^{eT}C^e\tilde{U}^e + \delta\tilde{U}^{eT}C^e\tilde{P}^e - p^{-1}\delta P^eL^e\tilde{P}^e - \delta\tilde{U}^{eT}\tilde{R}_1^e + p^{-1}\delta\tilde{P}^{eT}\tilde{R}_2^e \quad (10a)$$

where

$$K^e = \int_{V^e} B^TDBdV \quad C^e = \int_{V^e} AN^{pj}dV \quad (10b,c)$$

$$L^e = \int_{V^e} kA^pA^pdV \quad \tilde{R}_1^e = \int_{S^e} N^uT\tilde{X}dS \quad \tilde{R}_2^e = \int_{S^e} N^{pjT}\tilde{Q}dS \quad (10d-f)$$

in which matrices A , A^p are given in Appendix.

For whole system, we can write

$$\tilde{\Pi}(\tilde{u}, \tilde{p}_p) = \sum_e \tilde{\Pi}^e(\tilde{u}, \tilde{p}_p) \quad (11)$$

By setting $\delta\tilde{\Pi} = 0$, the characteristic matrix, which is equivalent to the stiffness matrix in pure solid problems, is obtained in the form :

$$\begin{bmatrix} K & C \\ C^T & -L \\ & P \end{bmatrix} \begin{Bmatrix} \tilde{U} \\ \tilde{P} \end{Bmatrix} = \begin{Bmatrix} \tilde{R}_1 \\ 1 \\ -\tilde{R}_2 \\ P \end{Bmatrix} \quad (12a)$$

in which

$$K = \sum_e K^e \quad C = \sum_e C^e \quad L = \sum_e L^e \quad \tilde{U} = \sum_e \tilde{U}^e \quad (12b-e)$$

$$\tilde{R}_1 = \sum_e \tilde{R}_1^e \quad \tilde{R}_2 = \sum_e \tilde{R}_2^e \quad \tilde{P} = \sum_e \tilde{P}^e \quad (12f-h)$$

The first of Eq. 12a is the discretized equilibrium equation in which K is the usual elastic stiffness of the medium, C the coupling matrix, \tilde{R}_1 the load vector due to boundary traction.

LAND SUBSIDENCE AND NEGATIVE SKIN FRICTION

The second equation of Eq. 12b represents the discretized flow equation which relates volumetric strain to the inflow due to the nodal pore pressure and the outflow rate R_2 . Equation 12a gives a set of equations to be solved to find the numerical solutions of the problem at the nodes.

INFINITE ELEMENTS

Discretization of Material Domains

Since, the conventional finite element method is computationally expensive for problems of multilayered semi-infinite soil media, a discretization of the material domains into finite elements in the near field and infinite elements in the rest is proposed as in Fig. 2. There are two types of infinite elements; horizontal elements (HE) in the horizontal layers in the upper part of such a multilayered half space, and radiating elements (RE) inside the underlying half space. Each infinite element has nodes only where it is connected to a conventional finite element (see Fig. 3).

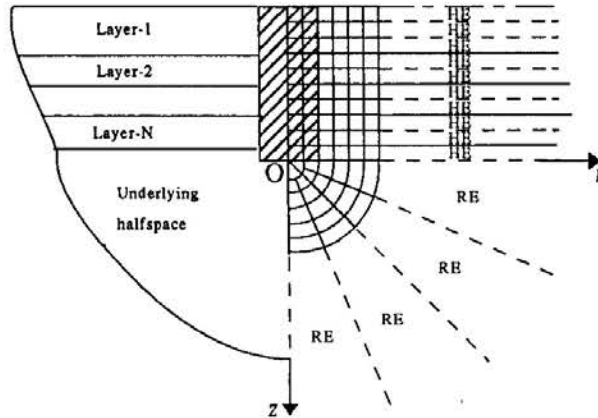


Fig. 2 Discretization of Multilayered Half Space.

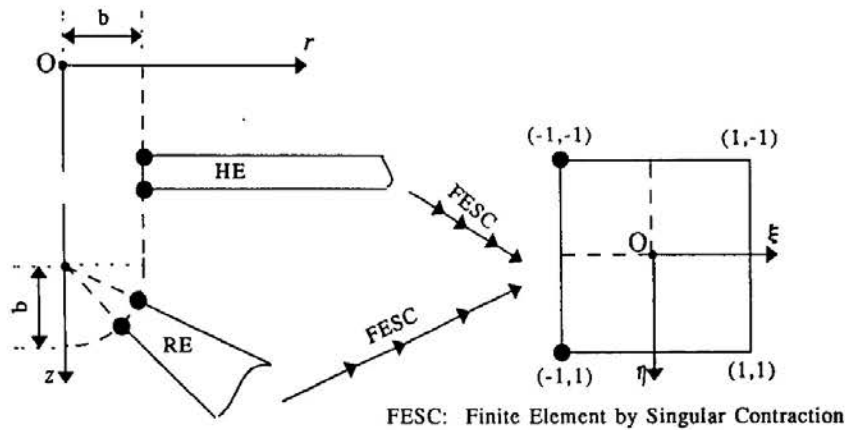


Fig. 3 Contraction of Infinite Elements into Finite Element

Mapping of Infinite Elements into Finite Elements

Rajapakse and Karasudhi (1985) presented a contraction to map an infinite element in the rz -plane into a finite element in the $\xi\eta$ -plane by employing a simple singular function along $\xi = -1$ as shown in Fig. 3. The coordinate transformation for HE is

$$r = \sum_j 2(1-\xi)^{-1} L_j(\eta) r_j, \quad z = \sum_j L_j(\eta) z_j \tag{13a,b}$$

and for RE is

$$r = \sum_j 2(1-\xi)^{-1} L_j(\eta) r_j, \quad z = \sum_j 2(1-\xi)^{-1} L_j(\eta) z_j \tag{13c,d}$$

where $L_j(\eta)$ is the Lagrangian polynomial. Accordingly, the nodes of the infinite elements are mapped on the $\xi = +1$ side of the finite element.

Interpolation Functions for Infinite Elements

Interpolation functions for the primary field variables of infinite elements are obtained in view of; analytical far field shape functions proposed by Karasudhi (1993), and coordinate transformation functions proposed by Rajapakse & Karasudhi (1985). Coordinate transformation functions are presented in Eqs. 13. Karasudhi (1993) presented appropriate analytical far field functions by analyzing the far field behavior of three fundamental problems; a homogeneous half space, a homogeneous full space, and two different half spaces perfectly bonded together. These fundamental problems were analyzed separately for three types of loadings; a point sink, a point force in z -direction, a point force in x -direction. These loads are applied at $r = z = 0$ (see Fig. 1). It has been already shown that the far field behavior for all three fundamental problems are identical, but different for various types of loadings considered. These far field functions are compiled in Table 1.

Table 1 Far-field Functions.

Type of loading	$u_r(r,z,p)$	$u_z(r,z,p)$	$p_f(r,z,p)$
Point Sink	rR^{-3}	zR^{-3}	zR^{-3}
Force in z -direction	rzR^{-3}	R^{-1}	zR^{-3}

As mentioned earlier using the far field functions in Table 1 and the coordinate transformation functions in Eqs. 13, following interpolation functions are derived and presented below.

For a point sink, for node j of a HE,

LAND SUBSIDENCE AND NEGATIVE SKIN FRICTION

$$N_j^{u_r}(\xi, \eta) = \frac{(1-\xi)^2}{4} L_j(\eta), \quad N_j^{u_z}(\xi, \eta) = N_j^{p_f}(\xi, \eta) = \frac{(1-\xi)^3}{8} L_j(\eta) \quad (14a-d)$$

and for node j between two adjacent RE's, as

$$N_j^{u_r}(\xi, \eta) = N_j^{u_z}(\xi, \eta) = N_j^{p_f}(\xi, \eta) = \frac{(1-\xi)^2}{4} L_j(\eta) \quad (14e-g)$$

For node j at the interface between a HE and a RE, the shape functions as Eqs. 14a-d hold.

For loading in the z -direction, for node j of a HE,

$$N_j^{u_r}(\xi, \eta) = \frac{(1-\xi)^2}{4} L_j(\eta), \quad N_j^{u_z}(\xi, \eta) = \frac{1-\xi}{2} L_j(\eta) \quad (15a,b)$$

$$N_j^{p_f}(\xi, \eta) = \frac{(1-\xi)^2}{8} L_j(\eta) \quad (15c)$$

and for node j between two adjacent RE's, as

$$N_j^{u_r}(\xi, \eta) = N_j^{u_z}(\xi, \eta) = \frac{1-\xi}{2} L_j(\eta), \quad N_j^{p_f}(\xi, \eta) = \frac{(1-\xi)^2}{4} L_j(\eta) \quad (15d-f)$$

For node j at the interface between a HE and a RE, the shape functions as Eqs. 15a-c hold.

These elements also satisfy the compatibility and completeness requirements. Another major advantage of this algorithm is that due to the proper coordinate transformation functions and primary field variable interpolation functions presented above, the proposed infinite elements can be treated as standard finite elements. In the formulation of infinite element characteristic matrices, we shall involve integrals with respect to ξ , which are proper and closed formed as the following,

However, in real practice, it is very laborious to factor out the integral above (with respect to ξ) from the simultaneous integration with respect to both natural coordinates ξ and η . It is more practical to perform such simultaneous integration directly by means of a standard method.

LAND SUBSIDENCE AND NEGATIVE SKIN FRICTION

Water withdrawal from deep artesian wells, symbolized by the point sink in Fig. 4a, can

cause land subsidence, different consolidation at different depths in the soil mass, and negative skin friction in piles embedded in such soil media.

Problem Composition

The problem of negative skin friction in piles can be treated as being composed of three systems, namely;

- (1) free-field subsidence due to water withdrawal from artesian wells such as depicted in Fig. 4a,
- (2) the half space subjected to the 'bond' forces q_i as shown in Fig. 4b, and
- (3) the fictitious bar subjected to $-q_i$ as in Fig. 4b.

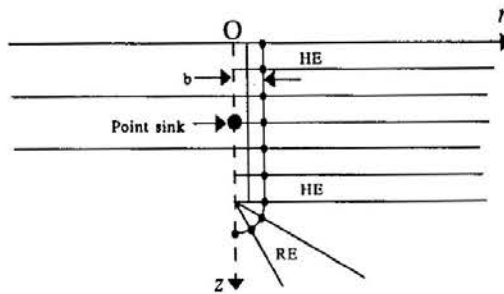


Fig. 4a System (1) with Point Sink.

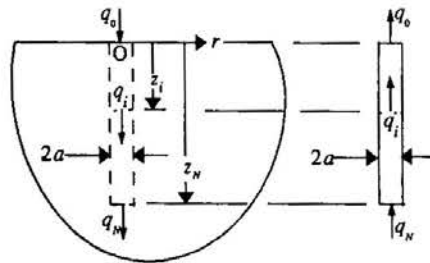


Fig. 4b Interacting Systems (2) and (3).

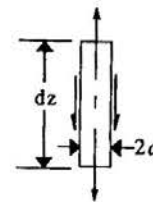


Fig. 4c Small Segment of Actual Pile.

The fictitious bar has the same dimensions as the actual pile, but its stiffness is equal to the difference between those of the latter and the half space, i.e.

$$E^{(3)}(z) = E^{(p)} - E^{(2)}(z) \tag{17}$$

where E denote a Young's modulus, a supernumerical within parentheses a system number, and the superscript p within parentheses the actual pile. The deformation at a certain point in system (3) is equal to the sum of those at the corresponding points in systems (1) and (2). The total forces or stresses are the appropriate sums of those in all three systems. Consider the fictitious pile as a uniaxial member and divide it into N elements with nodal points at z_i ; $i=0$ to N ; $z_0=0$, z_N =pile length (Figs. 4). Accordingly, the equilibrium of axial forces acting

LAND SUBSIDENCE AND NEGATIVE SKIN FRICTION

on the fictitious bar, and its axial displacements at various values of z_i can be written as

$$\sum_{i=0}^N \tilde{q}_i = 0, \quad \tilde{w}_0^{(3)} = \tilde{w}_0^{(1)} + \sum_{i=0}^N b_{0i} \tilde{q}_i \quad (18a,b)$$

$$w_j^{(3)} = w_{j-1}^{(3)} + \frac{z_j - z_{j-1}}{E_j^{(3)}} \sum_{k=0}^{j-1} \tilde{q}_k = \tilde{w}_j^{(1)} + \sum_{i=0}^N b_{ji} \tilde{q}_i, \quad (j = 1, 2, \dots, N) \quad (18c)$$

where $b_{ji} = \tilde{w}_j^{(2)}$ due to unit \tilde{q}_i . Equation 18 gives a set of equations to be solved to find the bond forces \tilde{q}_i and one displacement, say $\tilde{w}_0^{(3)}$. The stress of the real pile $\tilde{\sigma}_{zz}^{(p)}$ will be obtained as follows,

$$\tilde{\sigma}_{zz}^{(p)} = \tilde{\sigma}_{zz}^{(1)} + \tilde{\sigma}_{zz}^{(2)} + \tilde{\sigma}_{zz}^{(3)} \quad (19)$$

It should be noted that the inverse Laplace transform is carried out after the above stage.

Actual Negative Skin Friction

The equilibrium of the axial forces and the negative skin friction acting upon the actual pile element where $z_{i-1} < z < z_i$ is

$$P_i - P_{i-1} + 2\pi a h_i \tau_i = 0 \quad (20)$$

where τ_i and P_i are the negative skin friction assumed constant along element i , and the axial force, respectively, at $z = z_i$, a the radius of the pile and $h_i = z_i - z_{i-1}$. We can obtain τ_i as follows,

$$\tau_i = -\frac{P_i - P_{i-1}}{2\pi a h_i} \quad (21)$$

APPROXIMATE INVERSE LAPLACE TRANSFORMS

It is proposed in this study that the Laplace transform of all governing conditions are satisfied first at each numerical value of the parameter p , then the inverse Laplace transform of any solution function is obtained as a function of time t by the following method:

Constant Outflow Rate and Force Problems

For problems of the outflow rate $\bar{Q} = H(t)$ and the applied force $\bar{P} = H(t)$, the solution is likely to be in the form

$$v(t) = g_0 [1 - \exp(-\alpha t)] \quad (22)$$

satisfying the initial condition $v(0^+) = 0$. The Laplace transform of Eq. 22 gives

$$p\tilde{v}(p) = g_0 \left\{ 1 - \frac{p}{p + \alpha} \right\} \quad (23)$$

Respectively, the final and initial values of $v(t)$ are

$$v(\infty) = [p\tilde{v}(p)]_{p \rightarrow 0^+} = g_0, \quad v(0^+) = [p\tilde{v}(p)]_{p \rightarrow \infty} \quad (24a,b)$$

The quantity g_0 is to be determined by Eq. 24a, and α by curve-fitting Eq. 23.

Asymptotic Outflow Rate Problem

For problems of the outflow rate $Q = 1 - \exp(-\alpha^*t)$ and the applied forces $P = 1 - \exp(-\alpha^*t)$, the solution is likely to be in the form

$$v(t) = g_0[1 - \exp(-\alpha t)] \quad (25)$$

and α and g_0 can be determined in the same way as in the preceding case.

RESULTS AND DISCUSSIONS

Groundwater withdrawal in Bangkok area is analyzed by the proposed method. The rates of withdrawal from different aquifers are compiled in Table 2. Thickness and depth of aquifers are presented in Table 3, and aquifer properties are tabulated in Table 4.

Table 2 Rates of Pumping in (m³/day).

Bangkok	Phra Padaeng	Nakhon Luang	Nonthabuti
120,000	227,500	310,000	142,500

Table 3 Aquifer Thickness and Depth.

Aquifers	Approximate depth to mid layers(m)	Approximate thickness(m)
Bangkok	35	10
Phra Padaeng	67.5	35
Nakhon Luang	132.5	35
Nonthaburi	182.5	35

Water is assumed to be withdrawn from the mid-depth of each aquifer. With the relationship among the rates of withdrawal from different aquifers being the same as in Table 2, the amount of the withdrawal from each aquifer is adjusted in such a way that the settlement at the surface at the horizontal distance of 350m from every well at 10 years agrees closely with that predicted by Premchitt (1978), by means of a geological model. The numerical results of the Laplace transforms of the land surface subsidence and their approximations are illustrated in Fig.5. The real time functions of such subsidence are compared in Fig.6. The vertical displacement profile along the depth (z-direction) is as shown in Fig. 7, and this shows that the largest settlement occurs at surface and decreases with the soil depth. The displacement at the pile tip is a little bit less than the free surface subsidence.

LAND SUBSIDENCE AND NEGATIVE SKIN FRICTION

Table 4 Aquitard and Aquifer Properties.

Layer No.	Soil Types	Thickness (m)	Permeability k, (mm/day)	Young's modulus E, (MN/m ²)	Poisson's ratio ν
1	Clay	30	0.864	15	0.4
2	Sand	10	864.0	40	0.25
3	Clay	10	0.432	20	0.35
4	Sand	35	691.2	50	0.25
5	Clay	30	0.173	20	0.35
6	Sand	35	432.0	60	0.25
7	Clay	15	0.173	30	0.30
8	Sand	35	432.0	60	0.25
9	Clay	∞	0.043	35	0.35

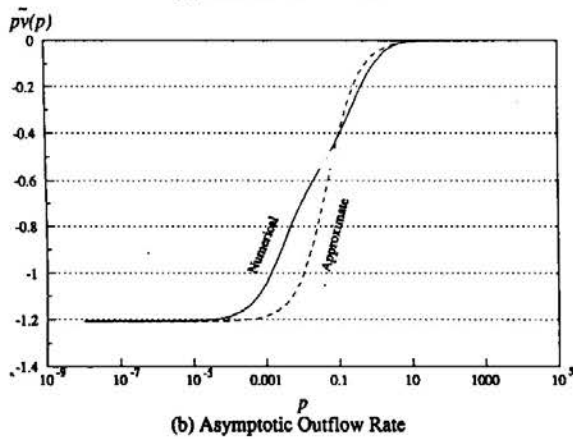
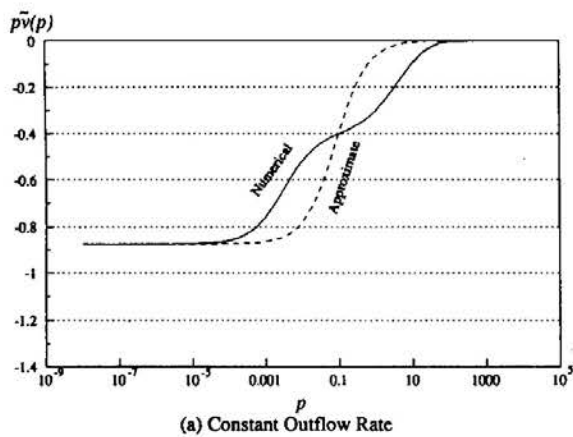


Fig. 5 Land Surface Subsidence.

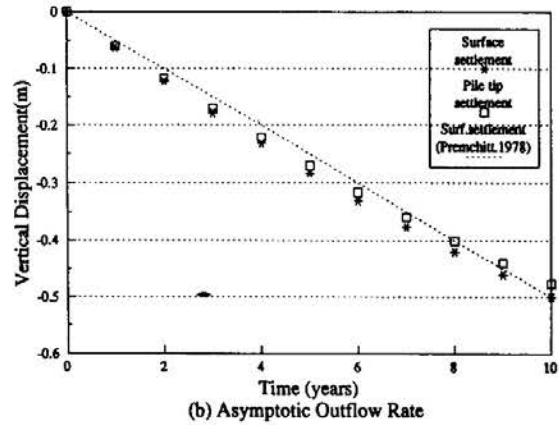
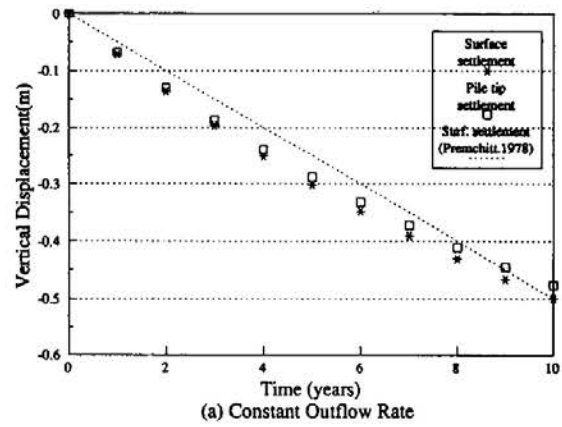


Fig. 6 Surface Settlement in Central Bangkok Due to Water Withdrawal.

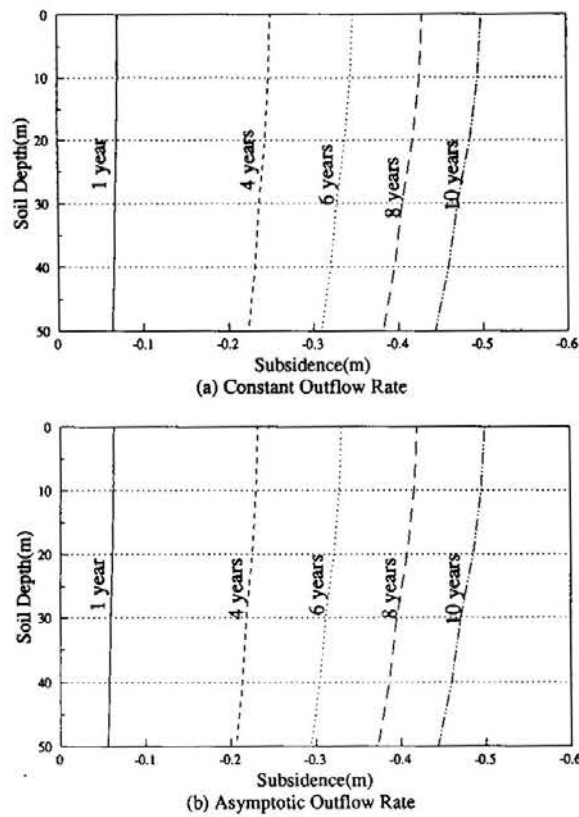


Fig. 7 Vertical Displacement in Central Bangkok due to Water Pumping.

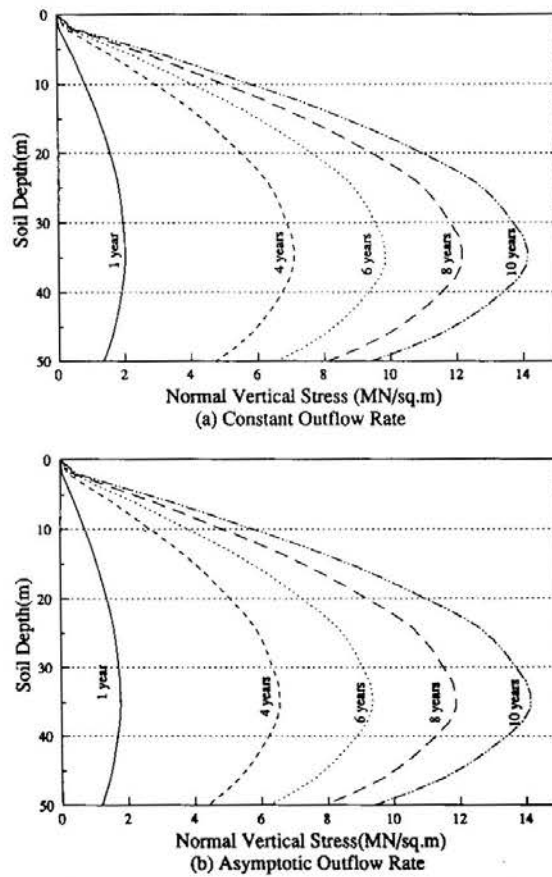


Fig. 8 Total Vertical Stress in Pile.

LAND SUBSIDENCE AND NEGATIVE SKIN FRICTION

The circular cylindrical pile adopted in this study is 50m long, 0.5m in radius, and has Young's modulus $E^{(p)} = 30 \times 10^3 \text{ MN/m}^2$. The total vertical stress profile along the pile depth is illustrated in Fig. 8 for various time durations. This shows that the total vertical stress is very high at the center part and quite low at both ends of the pile, and the stress increases with time at a specific depth.

The graph of skin friction versus soil depth is as shown in Fig. 9 for various time durations. The maximum skin friction occurs at about 4m depth and the neutral point is located in the first sand layer (about 35m deep).

The computer programme used for the above computations was derived from Smith & Griffiths (1988). However, this programme was modified slightly and some new subroutines were added for incorporating the proposed infinite elements. The finite element and infinite element scheme of this problem was carried out by using the element mesh shown in Fig. 2.

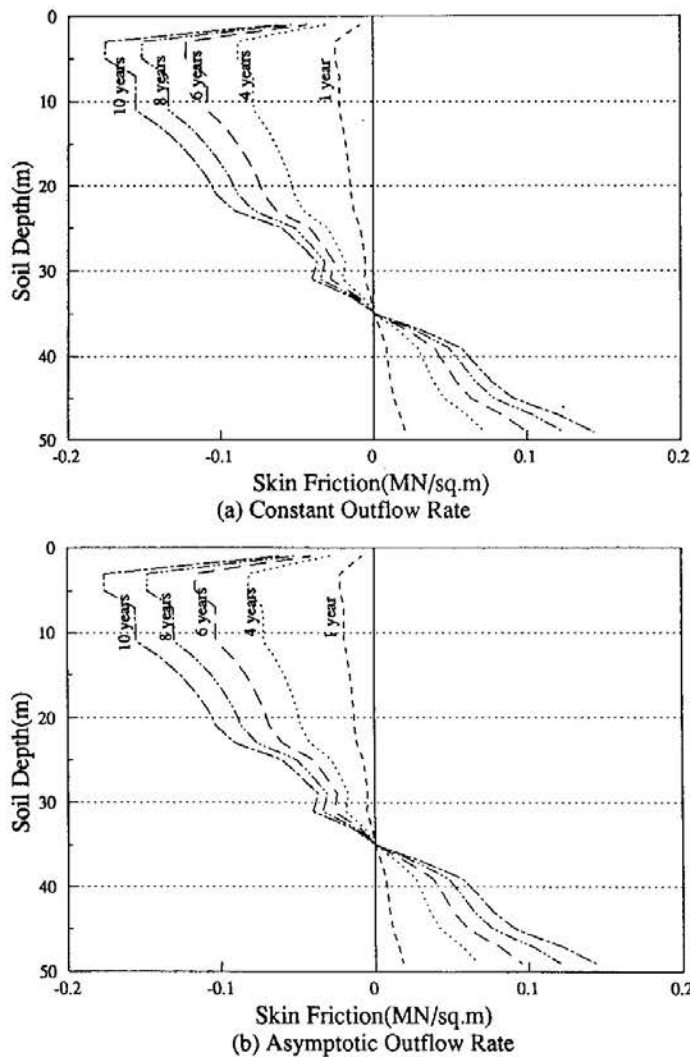


Fig. 9 Negative Skin Friction on Pile due to Water Withdrawal.

CONCLUSIONS

The shape functions of infinite elements are derived analytically from simple problems. All completeness and compatibility requirements are satisfied by such elements. Standard finite element method programs are readily applicable, since all elements involved eventually are finite. The Laplace transform results of all governing conditions are satisfied first, almost in the same manner as in statical analyses (without Laplace transform) of pure elastic solids, at each numerical value of the Laplace transform parameter p . The proposed approximate inverse Laplace transform scheme gives very accurate initial and final results, and fairly accurate real time functions at other time t . Subsidence by the proposed method with a constant outflow rate and an asymptotic rate of outflow for the first ten years varies almost linearly, agreeing very closely with that by Premchitt (1978).

REFERENCES

- BIOT, M.A. (1941). General theory of three dimensional consolidation. *J. Appl. Phys.* Vol.12, pp. 155-164.
- KARASUDHI, P. (1992). A rational infinite element scheme for quasi-statics of saturated elastic half space. *2nd Tri-Lateral (Kyoto University - Korea Advanced Institute of Science and Technology - National Taiwan University) Joint Seminar on Civil Engineering, Taipei*, November 16-18, pp. 109-112.
- KARASUDHI, P. (1993). An efficient scheme for land subsidence and negative skin friction. *Impact of Computational Mechanics on Engineering Problems*, edited by V.A. Pulmano and V. Murti, Balkema, Rotterdam, pp. 55-62.
- LEE, S.L., CHIN, J.T. and CHOW, Y.K. (1990). Negative skin friction on pile groups. *International Journal of Numerical and Analytical Methods for Geomechanics*, Vol.14, pp. 75-91.
- NG, H.K., KARASUDHI, P. and LEE, S.L. (1976). Prediction of negative skin friction and settlement in piles due to fill surcharge. *Geotechnical Engineering*, Vol. 7, pp. 25-45.
- PREMCHITT, J. (1978). Analysis and simulation of land subsidence with special reference to Bangkok. *D.Eng. Dissertation*, Asian Institute of Technology, Thailand.
- RAJAPAKSE, R.K.N.D. and KARASUDHI, P. (1985). Elastostatic infinite elements for layered half spaces. *J. Eng. Mech., ASCE*. Vol. 111, No. 9, pp. 1144-1158.
- SANDHU, R.S. and WILSON, E.L. (1969). Finite element analysis of seepage in elastic media. *Journal of Engineering Mechanics, ASCE*, Vol. 95, pp. 641-652.
- SMITH, I.M. and GRIFFITHS, D.V. (1988). Programming the finite element method. *John Wiley and Sons Ltd., 2nd Edition*, Vol. 1.

APPENDIX

Matrices in formulating element stiffness

Constitutive matrix D is

$$D = \begin{pmatrix} \lambda+2\mu & \lambda & \lambda & 0 \\ \lambda & \lambda+2\mu & \lambda & 0 \\ \lambda & \lambda & \lambda+2\mu & 0 \\ 0 & 0 & 0 & \mu \end{pmatrix} \quad (31)$$

where λ and μ are Lamé's constant.

Matrix of strain-displacement relationship B is

$$B = \begin{pmatrix} \frac{\partial N^{u_r}}{\partial r} & 0 \\ N^{u_r} & 0 \\ r & 0 \\ 0 & \frac{\partial N^{u_z}}{\partial z} \\ \frac{\partial N^{u_r}}{\partial z} & \frac{\partial N^{u_z}}{\partial r} \end{pmatrix} \quad (32)$$

Vector of displacement gradient A and pore pressure gradient A^p are

$$A = \begin{Bmatrix} \frac{N^{u_r}}{r} + \frac{\partial N^u}{\partial r} \\ \frac{\partial N^{u_z}}{\partial z} \end{Bmatrix} \quad A^p = \begin{Bmatrix} \frac{\partial N^{p_f}}{\partial r} \\ \frac{\partial N^{p_f}}{\partial z} \end{Bmatrix} \quad (33a,b)$$

It should be noted here that the matrices presented above are applicable only for axisymmetric problems and the coordinate system referred is the cylindrical coordinate system.

BEHAVIOUR OF MODEL BATTER PILES IN SOFT CLAYS UNDER LATERAL LOADS

S. Narasimha Rao¹, C. Veeresh² and
G.V.S. Shankaranarayana³

SYNOPSIS

When a soil with a low strength extends to a considerable depth, piles are generally used to transmit vertical and lateral loads. For the situations with large lateral loads, vertical piles cannot generally be relied on to withstand the horizontal forces and in such cases, batter piles are adopted in order that the resultant of the external forces is acting axially to the pile. In this paper, the results of experimental investigations carried out on instrumented model piles installed in clayey soils are reported. Tests were conducted with embedment ratios L/D (L is the depth of embedment and D is diameter of the pile) of 15, 20 and 32, and at each of these embedment ratios, piles were tested with batter angles ranging from -30° to $+30^\circ$ with vertical. The results indicate that the piles with negative batter offer more resistance to horizontal load. This aspect is also confirmed by the moments measured along the axis of piles. Failure patterns observed during testing further support the variations in capacity.

INTRODUCTION

When a soil with a low strength extends to a considerable depth, pile foundation becomes an obvious choice to transmit vertical and lateral loads to the surrounding soil. Large lateral loads can act on pile foundations supporting structures such as offshore platforms, quay and harbour structures, transmission line towers, tall structures, bridge abutments, and anchorages for water front structures. The safety of these structures depends on the ability of supporting piles to resist large lateral forces. In situations where large lateral loads are acting, vertical piles cannot be relied upon to withstand the horizontal forces and in these circumstances, inclined or battered piles are generally used. A batter pile has an improved resistance to horizontal loading since a large portion of horizontal component is carried axially by the pile. Batter pile can be called negative batter pile, if the lateral load acts in the direction of batter (Fig.1a), and can be called positive batter pile if the lateral load acts opposite to the direction of batter (Fig.1b).

¹ Professor and Head, Ocean Engineering Centre, Indian Institute of Technology, Madras 600036, India.

² Research Scholar, Ocean Engineering Centre, Indian Institute of Technology, Madras 600036, India.

³ Graduate Student, Ocean Engineering Centre, Indian Institute of Technology, Madras 600036, India.

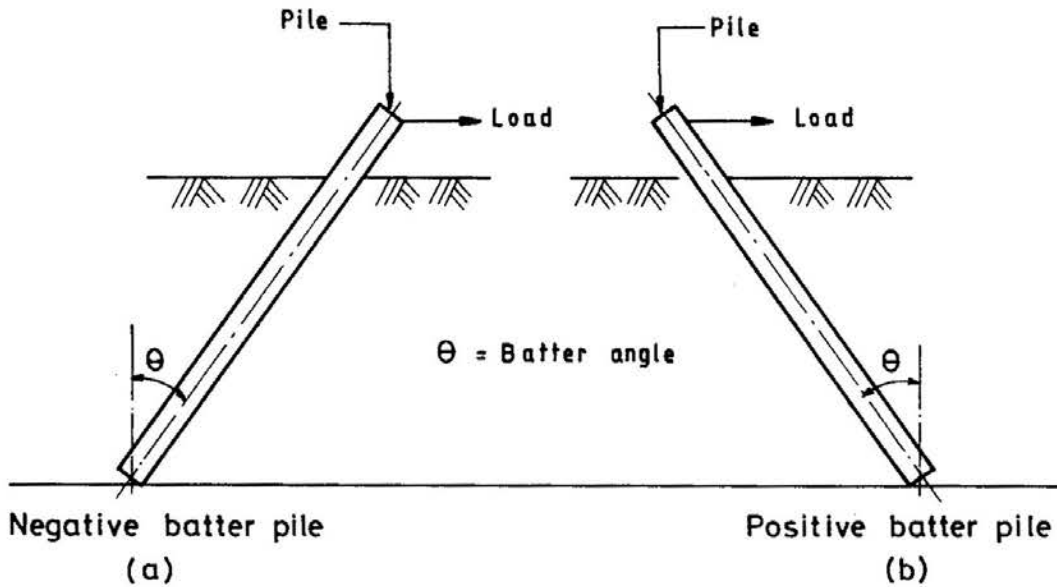


Fig. 1 Types of Batter Piles.

Several investigators have studied the behaviour of batter piles in some detail (Tschebotarioff, 1953; Feagin, 1953; Murthy, 1964; Prakash & Subramanyam, 1965; Awad & Petrasovits, 1969; Ramasamy, 1974 and Gopal Ranjan et al, 1980). Feagin (1953) conducted tests on groups of batter and vertical timber piles with heads fixed in concrete monoliths. The results of these tests indicated that; (i) groups of batter piles combined with vertical piles were more resistant to lateral loads for both positive and negative batter piles than the vertical pile and (ii) for a relative batter pile the resistance to lateral loads exceeds that of a positive batter pile either with or without a vertical load. Tschebotarioff (1953) suggested that the slip surfaces in the case of positive batter piles are deflected upwards and in the case of negative batter piles deflected downwards. He further suggested that, a pile with negative batter offered more resistance than a pile with positive batter. The test results of Murthy (1964) in sands indicated that the resistance to lateral loads increased as the batter angle varied from $+45^\circ$ to -45° . Prakash & Subramanyam (1965), conducted model studies on batter piles embedded in sand under lateral loads and concluded that piles with a negative batter were superior. Results obtained from tests on batter piles in sand by Awad & Petrasovits (1969) also confirmed that negative batter offered more resistance. Ramasamy (1974) carried out two dimensional analysis by assuming the soil behaviour to be elasto-plastic and these results indicated that groups consisting of batter piles offered greater resistance to horizontal loads than those groups consisting of only vertical piles both in cohesive and cohesionless soils. The test results of Gopal Ranjan et al (1980) obtained from batter piles in clayey soils indicated a similar improvement in pile capacity for piles with negative batter.

From the aforementioned literature it is clear that many investigators (Murthy, 1964; Awad & Petrasovits, 1969 and Gopal Ranjan et al, 1980) have confirmed that piles with negative batter offer more resistance to lateral loads than vertical piles and investigators like Tschebotarioff (1953) made an attempt to explain the changes in terms of slip surfaces.

BEHAVIOUR OF MODEL BATTER PILES

Previously only a limited amount of work has been carried out on batter piles in clays. The present study investigates the behaviour of model batter piles in clay under lateral loads. The details of the piles tested, soils used and the experimental set ups are given in the following section.

EXPERIMENTAL INVESTIGATIONS

Tests were conducted on hollow model aluminium piles of 26 mm diameter 1.2 mm thickness and of 1000 mm length. These piles were instrumented with electrical resistance type strain gauges to trace the variations in bending moments with depth. The gauges were fixed (in pairs, diametrically opposite to each other) with a center to center distance of 100 mm along the pile axis in the way shown in Fig.2. This method of connecting each pair of gauges results in automatic temperature compensation (Perry & Lissner,1955). Furthermore, the bending strain readings were magnified because the sum of tension

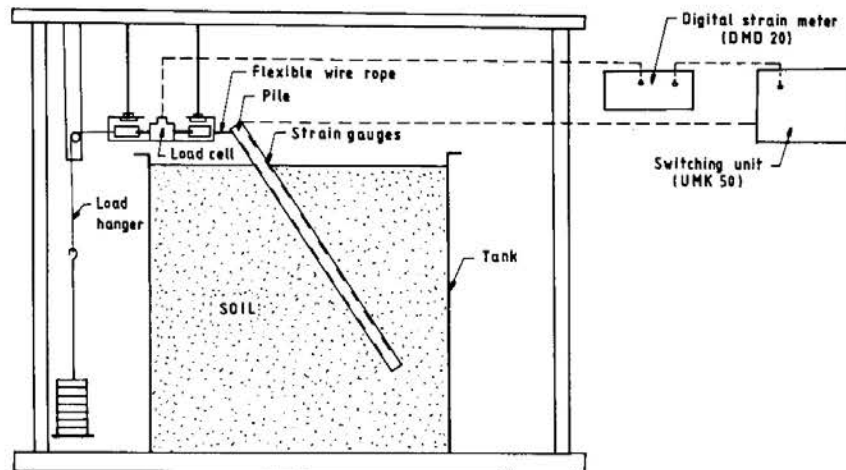


Fig. 2 Experimental Set Up.

Table 1 Details of Piles Tested .

S.No.	Pile dia D (mm)	Embedment depth L (mm)	L/D	Batter Angle
1.	26	390	15	- 30°, - 20°, - 10°, 0°, + 10°, + 20° and + 30°.
2.	26	520	20	- 30°, - 20°, - 10°, 0°, + 10°, + 20° and + 30°.
3.	26	890	32	- 30°, - 20°, - 10°, 0°, + 10°, + 20° and + 30°.

and compression readings had the effect of improving the sensitivity of the strain measurements. The pile was calibrated before testing to provide accurate determinations of bending moments and stresses. Tests were conducted in a test tank of size, 1300mm X 800mm X 1100mm. The size of the tank had to be decided considering the size of the pile to be tested, the zone of influence along and perpendicular to loading, and the batter angle. It was found by Prakash 1964, that the interference zone was limited to a distance equal to 8 to 12 times the pile diameter in the direction of loading and 3 to 4 times the pile diameter normal to the loading. Considering all these factors the tank design was sufficiently large to avoid interference effects. The arrangement of the tank with its loading frame is shown in Fig.2. The loading was applied in increments using cast iron weights placed over a loading pan connected to a flexible wire rope attached to the pile and taken over pulleys. The load applied was measured accurately with a load cell of 2kN capacity. Lateral movement of the pile at the ground surface was measured using a dial gauge having a least count of 0.01 mm. The soil used in this investigation was a soft marine clay obtained from coastal deposits from the East Coast of India. The soil consisted of 90% of clay and silt fraction and 10% fine sand. The index properties of the soil are, liquid limit 82% and plastic limit 32%.

Testing Procedure

The pile was positioned at the required batter angle in the test tank and fully saturated soil was placed in 50mm thick layers. Each layer was hand packed and then compressed with a template to remove entrapped air. All the tests were conducted at a consistency, I_c [(LL-water content)/(LL-PL)] of 0.6. This consistency is low enough for the soil to behave as a soft clay. With this soft consistency there was no difficulty in placing the soil and achieving a homogeneous fill. The homogeneity of the soil bed prepared was checked frequently by taking the measurements of density, water content and undrained shear strength at different depth locations. The tests on the pile were conducted at three embedment ratios L/D (depth of embedment of pile/diameter of pile) of 15, 20 and 32. At each of these embedment ratios, the pile was tested at different batter angles (for both positive and negative batter piles). The loads applied in all these tests were at a height of 90mm above ground level. The details of the tests carried out are given in Table.1.

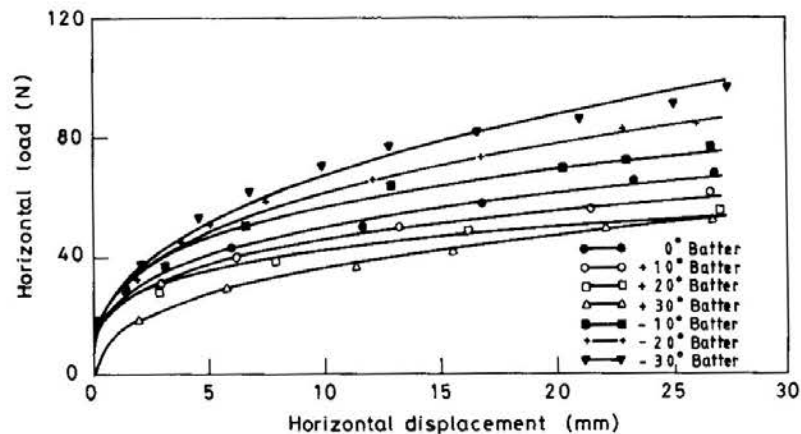


Fig. 3 Lateral Load Versus Displacement Curves.

RESULTS AND DISCUSSIONS

A typical set of load versus displacement curves for embedment ratio of L/D of 15 and at different batter angles tested is presented in Fig.3. With addition of load there is an increase in the displacements and the trend is similar for different batter angles. For a vertical pile (pile with zero batter angle), it can be seen that up to a lateral load of 30N to 40N the deflections are in the order of 3mm to 4mm only. In comparison with vertical piles, the piles with positive batter angle shows larger displacements for the same range of load increments. However, in the case of piles with negative batter the recorded deflections are less. For negative batter piles as the batter angle increases, the displacements are reduced considerably. For positive batter piles this trend is quite the opposite and the horizontal displacements increase with batter angle.

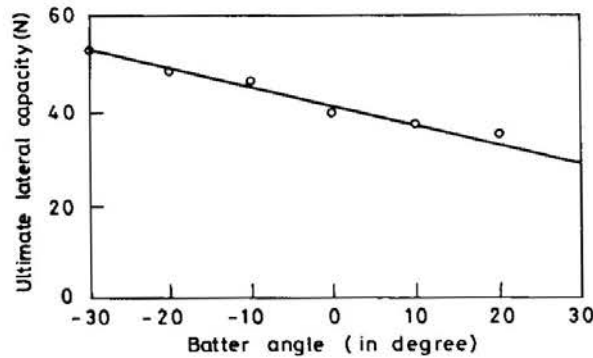


Fig. 4 Variation of Lateral Capacity with Batter Angle.

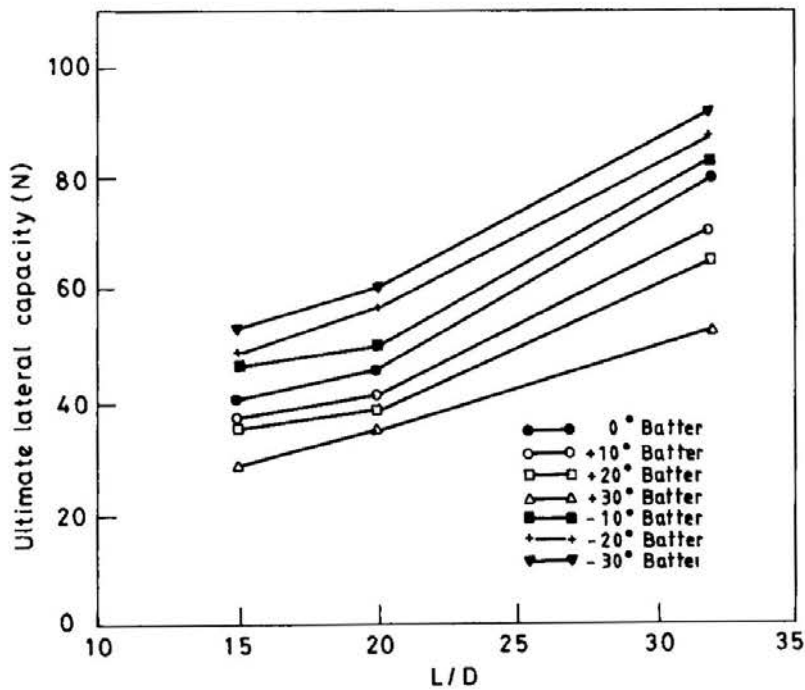


Fig. 5 Variation of Ultimate Lateral Capacity with Embedment Ratio.

From the literature, it can be seen that there are many methods suggested to determine the ultimate lateral capacity of vertical piles based on load deflection curves. The ultimate capacity is often taken as ultimate load based on the allowable deflection. According to Briaud et al (1983) permissible deflections are generally in the order of 10% of pile diameter. According to Broms (1964) the ultimate lateral resistance is reached when the deflection at the ground surface reaches a value approximately equal to 20% of the diameter or width of the pile. As there was no specific method suggested for batter piles, in this investigation the method suggested by Broms (1964) is used for estimating ultimate lateral capacity of batter piles and the same method is also used for vertical piles. From the load displacement curves it can be observed that the capacity of a negative batter pile is greater than the capacity of a vertical pile. In comparison, the capacity of a positive batter pile is less. The variation of ultimate lateral capacity with batter angle is presented in Fig. 4. As the batter angle increases from -30° to $+30^{\circ}$ the capacity is decreased. The trends

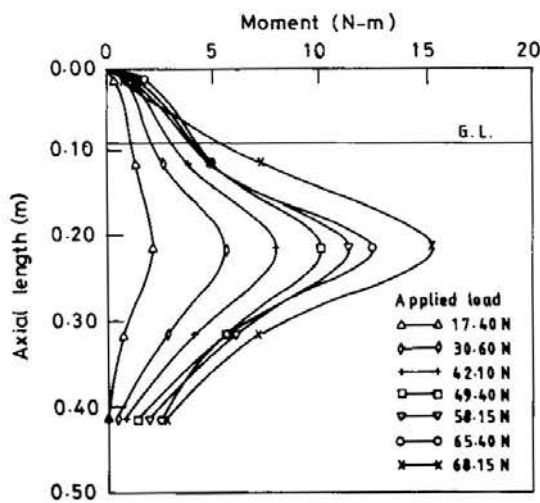


Fig. 6 Bending Moment Variation with Axial Length of Pile.

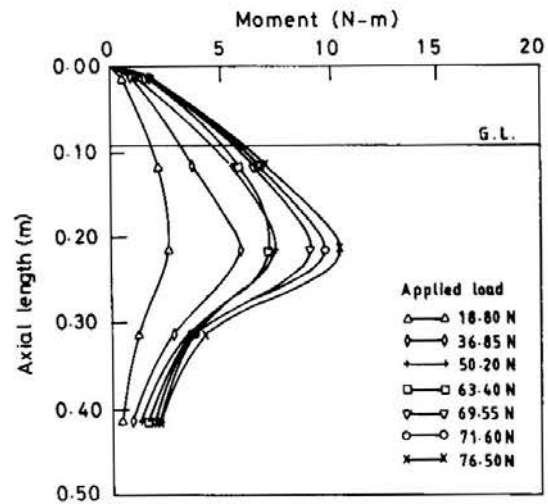


Fig. 7 Bending Moment Variation with Axial Length of Pile.

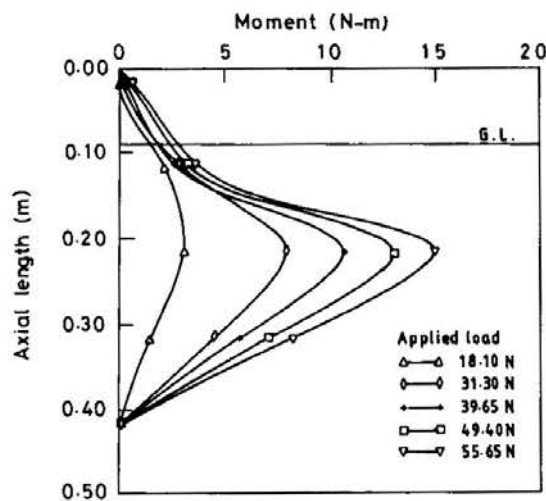


Fig. 8 Bending Moment Variation with Axial Length of Pile.

BEHAVIOUR OF MODEL BATTER PILES

obtained from piles with embedment ratios of 20 and 32 are similar to the trends obtained from piles with an embedment ratio of 15. The ultimate lateral capacities for different embedment ratios of 15, 20, and 32 for all the batter angles tested are summarized in Table. 2. The variation of ultimate lateral capacity with embedment ratio (L/D) is presented in Fig. 5. For a given batter angle, ultimate lateral capacity increases with embedment ratio.

The flexural strains along the axis of the pile were determined using electrical resistance type strain gauges. These flexural strains were converted to bending moments

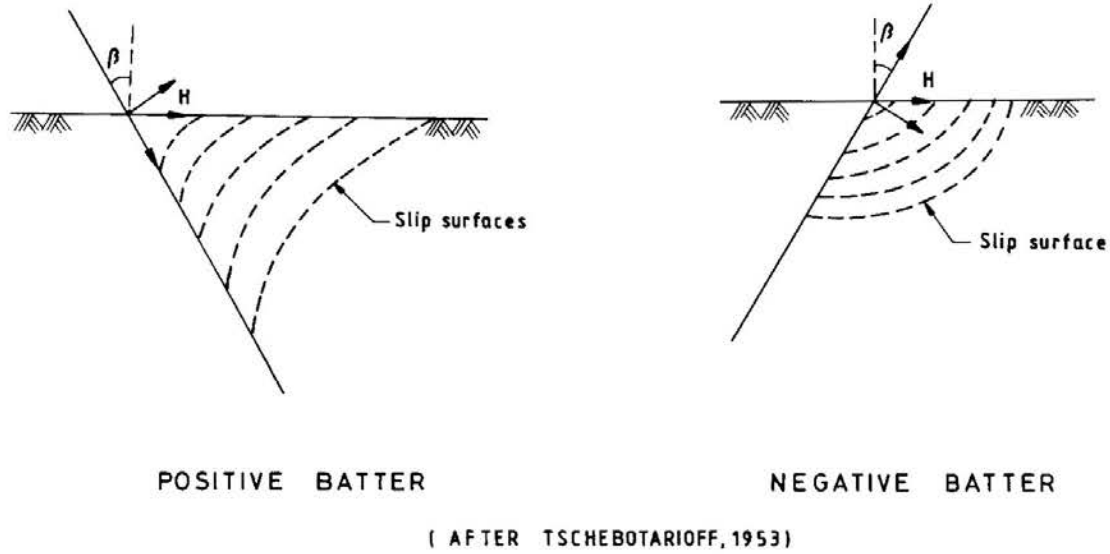


Fig. 9 Failure Surfaces (After Tschebotarioff, 1953).

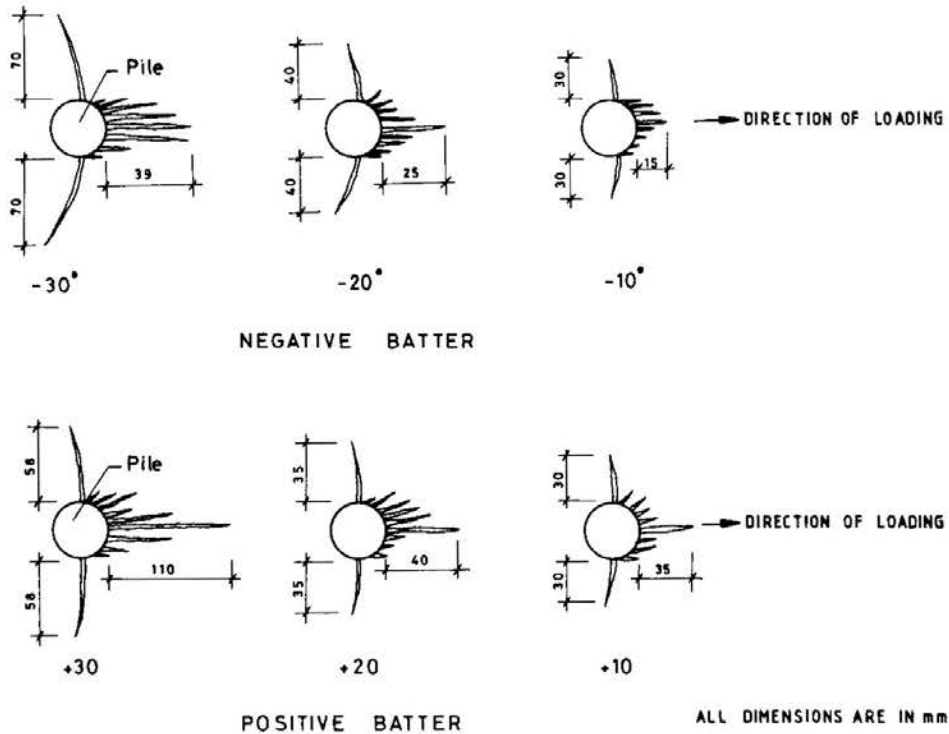


Fig. 10 Crack Pattern on the Surface of Soil.

Table 2 Ultimate Lateral Capacities .

S.No.	Batter angle	Ultimate lateral Capacity (N)		
		L/D = 15	L/D = 20	L/D = 32
1.	- 30°	52.8	60.0	92.0
2.	- 20°	48.2	55.5	87.0
3.	- 10°	46.4	49.0	83.0
4.	0°	40.2	46.0	76.0
5.	+ 10°	37.7	41.8	70.0
6.	+ 20°	35.5	38.2	65.0
7.	+ 30°	29.9	35.5	53.0

by multiplying the strains with the appropriate calibration constants. A typical variation in the bending moment with axial length of pile for embedment ratio (L/D) of 15 and batter angle 0° (vertical pile) is shown in Fig.6. It can be seen from the figure that the bending moment increases with axial length of pile after reaching a maximum value at mid-height of the pile embedded and thereafter it decreases. Further, the bending moments increase with load increments. Figs. 7 and 8 represent bending moment variation for embedment ratio (L/D) of 15 and for negative and positive batter piles respectively. By comparing the magnitudes of bending moments of vertical piles (Fig.6) and negative batter piles (Fig.7), it can be seen that the bending moments in the case of negative batter piles are less than the values recorded in vertical piles. In a similar way, the bending moment values, as obtained from vertical piles, can be compared with the values of positive batter piles and it can be seen from Fig.8 that the bending moments are greater. From Figs 6, 7 and 8 it can be concluded that the bending moments are larger for positive batter piles and smaller for negative batter piles as compared with vertical piles. This type of behaviour has been observed for all the tests conducted for all the embedment ratios (L/D) of 20 and 32.

As discussed above, the ultimate load versus displacement variations and bending moment variation with axial length suggest that a pile with negative batter offers more resistance than a positive batter pile and a vertical pile. This aspect can be further confirmed by the type of failure surfaces as suggested by Tschebotarioff (1953) and the same is presented in Fig.9. The slip surfaces in the case of positive batter piles deflect upwards and as a result of which there is a reduced soil resistance, but in the case of negative batter piles the slip surfaces deflect downwards and this results in improved soil resistance and hence the negative batter pile gives more resistance than the vertical pile. Fig.10. shows the soil crack pattern observed on the ground surface around the pile during the testing (for embedment ratio of 15) and it is observed that the soil around the pile in the direction of loading is heaved up, and a number of cracks were formed in this heaved up mass. These soil failure patterns extend over a distance of 0.5 to 4.5 times the diameter of the pile in the direction of load application. For negative batter piles these soil failure patterns extend over a short distance of 0.5 to 1.5 times the diameter of the pile, but in the case of positive

BEHAVIOUR OF MODEL BATTER PILES

batter piles the patterns extend over a distance of 1.5 to 4.5 times pile diameter. The load component normal to the pile axis causes the pile to push the soil outwards in the case of positive batter piles and this results in tension failure extending over a large distance. Consequently, there is a less resistance to lateral load. However, for negative batter piles the load component normal to the pile axis causes the pile to press the soil downwards and hence this results in a compressive failure over a relatively smaller distance and this results in an improved lateral load capacity.

CONCLUSIONS

In this study, experimental investigations on model aluminium pile instrumented with electrical resistance type strain gauges were carried out in a soft marine clayey soil. Based on this investigation the following conclusions are drawn:

- (i) Ultimate lateral capacity of piles in the case of both vertical and batter piles increases with the embedment ratio (L/D).
- (ii) The ultimate lateral capacity of a negative batter pile is more than a vertical pile and a positive batter pile is weaker than a vertical pile in resisting lateral loads.
- (iii) Bending moment variations with axial depth also indicate a reduced bending moment for a pile with negative batter.
- (iv) The failure patterns observed support the variations in the capacity.

REFERENCES

- AWAD, A. & PETRASOVITS, G. (1969): Considerations on the bearing capacity of vertical and batter piles subjected to forces acting in different directions, Proc. 3rd Budapest conf. on SM & FE, Budapest.
- BRIAUD, J.L., SMITH, T.P & MEYER, B. (1983): Pressure meter gives elementary model for laterally loaded piles, International symposium on in-situ testing, Paris, vol.2, pp. 217-221.
- BROMS, B.B. (1964): Lateral resistance of piles in cohesive soils, Journal of Soil Mechanics and Foundation Engineering, ASCE, Vol.90,SM-2, PP.127-163.
- FEAGIN, L.B. (1953): The lateral load tests on group of battered and vertical piles, Special Technical publication No.154, ASTM, pp.12-30.
- MURTHY, V.N.S. (1964): Behaviour of battered piles embedded in sand and subjected to lateral loads, Proc. Symposium on Bearing Capacity of piles, CBRI Roorkee, India, pp.142-153.
- PERRY, C.C. and LISSNER, H.R. (1955): The strain gauges primer, McGraw Hill book company, New York.

- PRAKASH and SUBRAMANYAM, G. (1965): Behaviour of battered piles under lateral loads, *Journal of Indian National Society of Soil Mechanics and Foundation Engineering*, Vol.4, No.2, pp.177-196.
- RAMASAMY, G. (1974): Flexural behaviour of laterally and axially loaded individual piles and group piles, Ph.D Thesis Department of Civil Engineering, I.I.Sc, Bangalore.
- RANJAN, G., RAMASAMY, G. and TYAGI, R.P. (1980): Lateral response of batter piles and pile bents in clay. *Indian Geotechnical Journal*, Vol.10, No.2, pp 135-142.
- TSCHEBOTARIOFF, G.P. (1953): The resistance to lateral loading of single piles and pile groups, Special Technical publication No.154, ASTM, pp.38-48.

LOAD TRANSFER THROUGH A GRAVEL BED ON STONE COLUMN REINFORCED SOIL

M.R. Madhav¹ and W.F. Van Impe²

SYNOPSIS

Treatment of soft or weak soil deposits with stone columns involves providing at the ground surface a dense gravel bed as a working platform and a drainage layer acting as a stiff raft. Whilst it is often presumed to be rigid no data are available to validate this hypothesis. A model is proposed for the analysis of the granular layer covering the stone column reinforced soil. The response of the system is shown to depend on the relative stiffness of the gravel bed. The load transferred to the stone column varies significantly with the stiffness of the gravel bed relative to the column and the soil. The design criterion proposed ensures the gravelbed deforms uniformly.

INTRODUCTION

Reinforcement of soft or weak compressible soils by stone columns helps to reduce the settlements and to improve the bearing capacity of the soil significantly (Van Impe & De Beer, 1983; Bergado et al, 1991, Van Impe & Madhav, 1992). Whenever stone columns are chosen as a design alternative, a gravel bed or mat is provided to cover the natural ground. The purpose of this raft or cushion is:

- (i) to provide a working platform for the machinery;
- (ii) to level the site and increase the elevation;
- (iii) to prevent upheaval during stone column installation by the vibrodisplacement technique;
- (iv) to provide a facility for drainage of water, since the columns act as drains as well; and
- (v) to distribute the load from the structure on to the soil and the stone columns and minimize the differential settlements.

The last mentioned function, i.e. the structural effect of the gravel bed in the distribution of the load, is very important for the success of this soil improvement technique. To be effective, the covering granular mat should be composed of well graded gravel-sand mixture and very well compacted to a high relative density. Most methods of analysis of

¹ Professor of Civil Engineering, Indian Institute of Technology, Kanpur-208016, India.

² Professor of Soil Mechanics and Foundation Engineering & Director of Soil Mechanics Department, Gent University, Gent, Belgium.

settlement of stone column reinforced soil, *e.g.* Priebe (1976), Goughnour & Bayuk (1979), Balaam & Booker (1981), Van Impe & De Beer (1983), Van Impe & Madhav (1992), implicitly consider the granular raft or layer to be rigid with settlements being uniform over both the soft soil and the stiff stone column implying arching action. From the available literature, it appears most engineers and researchers indeed treat the granular raft to be rigid even though no analysis exists which implements the structural effect of the gravel bed. Juille & Sherwood (1983) recommend the following criteria for the granular raft thickness, H_f :

$$(C-d_p) < 4H_f < H+H_f \quad (1)$$

where C is the axis to axis column spacing, $d_p = 2a$ is diameter of stone column, and H the thickness of compressible soil layer to be improved.

Table 1 Gravel Bed Over Stone Column Reinforced Soil.

Granular Pad Material	Thickness H_f (m)	Reference
sand + thin layer of gravel	2.0	Brons & De Kruijff (1985)
gravel	0.3-1.0	Mitchell & Huber (1983)
sand and gravel	0.7	
sand	2.0	Venmans (1990)
sand-medium to fine	0.9	Bachus & Barksdale (1984)
coarse sand + crushed stone	1.0	Bhandari (1983)

Table 1 summarises some of the recent available data regarding the thickness and the type of granular layer involved. Note that the thickness varies from as low as 0.3 m to as high as 2 m and the material type ranges from gravel to fine sand. Therefore it cannot be presumed that such a granular mat will always act as a rigid one. Madhav & Poorooshasb (1987) propose a Pasternak type of model for a stiff layer over soft soil. This concept is extended here to analyse the gravel bed over a stone column reinforced soil.

ANALYSIS OF THE COVERING 'GRAVEL' BED BEHAVIOUR

Fig. 1 represents a unit cell consisting of a stone column (axi-symmetric case) or a trench (plane strain case) of diameter or width, $d_p (= 2a)$, surrounded by treated soil extending up to a distance, $b = d_c/2$, where d_c is the diameter or the width of the unit cell. The stone column extends to the full depth, H , of the soft soil underlain by the rigid bearing stratum. The granular mat at the top has a thickness, H_f , and is characterised by its shear modulus, G_r . E_s and ν_s are respectively the modulus of deformation and Poisson's ratio of

LOAD TRANSFER THROUGH A GRAVEL BED

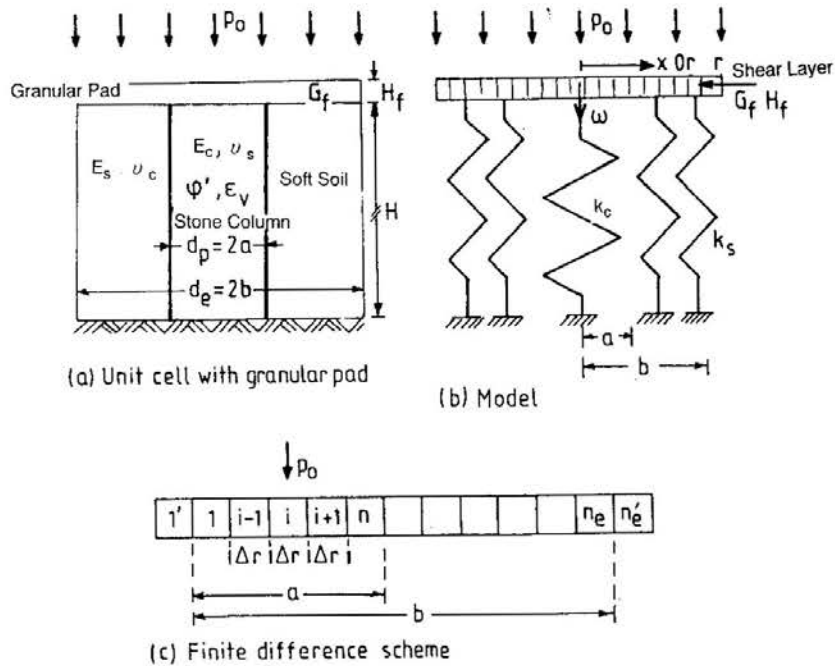


Fig. 1 Definition Sketch.

the soil. Following Van Impe & de Beer (1983) and Van Impe & Madhav (1992), the column is considered to yield at its peak resistance defined by its angle of shearing resistance, ϕ'_c and volumetric dilation, ϵ_v . A uniform load of intensity, p_o , acts on top of the gravel bed. For reasons of symmetry, there are no interacting shear stresses at the outer boundary of the unit cell.

The model proposed here is based on the following assumptions: (i) the gravel bed is incompressible and can distort only in shear; and (ii) the soil and the stone column deform in a linear stress-strain behaviour without slip at their interface.

Table 2 Typical Values of Shear Modulus for Granular Soils (Bowles, 1982).

Dense Sand	20-4 MPa
Dense Gravel and Sand	40-80 MPa

The coefficients of subgrade reactions for the stone column, K_c and for the soil, K_s can be estimated. For the stone column, assuming it to deform elastically,

$$K_c = E_c/H \tag{2}$$

where E_c is the modulus of deformation of the column material itself, obtained from a plate load test on the column. If the column material yields plastically, the approach of Van Impe

& De Beer (1983) extended by Van Impe & Madhav (1992) can be used for the estimation of pile settlements and stress concentration factor from which K_c can be evaluated. For the reinforced soil on the other hand:

$$K_s = D_s/H \quad (3)$$

where $D_s = E_s(1-\nu_s)/\{(1+\nu_s)(1-2\nu_s)\}$ is the constrained modulus of the soft soil estimated for the appropriate stress level and relevant stress path. It may also be possible to back-figure from DMT tests in the soft clay layer. The governing equations for the equivalent model considered are summarized as follows:

(a) *Granular Trench*

For a uniform load of intensity p_0 , acting on top of the granular fill:

$$p_0 = K_c w - (G_r H_r) \frac{d^2 w}{dx^2} \quad \text{for } 0 \leq x \leq a \quad (4)$$

$$\text{and } p_0 = K_s w - (G_r H_r) \frac{d^2 w}{dx^2} \quad \text{for } a \leq x \leq b \quad (5)$$

where w is the settlement of the fill at a distance x from the center of the unit cell. The boundary and the continuity conditions are

$$(i) \text{ At } x = 0; \quad \frac{dw}{dx} = 0 \quad (6)$$

$$(ii) \text{ At } x = a; \quad \left. \frac{dw}{dx} \right|_{a^+} = \left. \frac{dw}{dx} \right|_{a^-} \quad \text{and } w_{a^+} = w_{a^-} \quad (7)$$

$$(iii) \text{ At } x = b; \quad \frac{dw}{dx} = 0 \quad (8)$$

Equations (4) and (5) are easily solved and expressed in dimensionless form as

$$W = C_1 \{ \exp(\alpha_c X) + \exp(-\alpha_c X) \} + 1/K_r \quad \text{for } |X| \leq 1.0 \quad (9)$$

$$\text{and } W = C_4 \{ b_0 \exp(\alpha_s X) + \exp(-\alpha_s X) \} + 1 \quad \text{for } 1.0 < X \leq b/a \quad (10)$$

where $X = x/a$,

$$W = w/w_w,$$

$$w_w = p_0/K_s,$$

$$\alpha_c = \text{SQRT} \{ K_c \cdot a^2 / G_r H_r \},$$

LOAD TRANSFER THROUGH A GRAVEL BED

$$\alpha_s = \text{SQRT} \{K_s \cdot a^2 / G_r \cdot H_r\},$$

$$b_0 = \exp(-2\alpha_s \cdot b/a) \text{ and}$$

$$K_R = K_c / K_s.$$

The subscripts c and s refer to stone column and soft soil respectively. C1 and C2 are obtained from the boundary conditions as

$$C_1 = (b_4/b_3) \cdot C_4 \text{ and } C_4 = (1 - 1/K_R) / b_5 \text{ with}$$

$$b_1 = \{\exp(\alpha_c) + \exp(-\alpha_c)\};$$

$$b_2 = \{b_0 \cdot \exp(\alpha_s) + \exp(-\alpha_s)\};$$

$$b_3 = \alpha_c \cdot \{\exp(\alpha_c) - \exp(-\alpha_c)\};$$

$$b_4 = \alpha_s \cdot \{\exp(\alpha_s) - \exp(-\alpha_s)\} \text{ and}$$

$$b_5 = b_4 \cdot b_1 / b_3 - b_2.$$

The load carried by the granular trench, F_c , is:

$$F_c = 2 \int_0^a K_c w dx \quad (11)$$

and is expressed as the stress concentration factor, m , where

$$m = \frac{\text{Load carried by the trench, } F_c}{\text{Total load on unit cell, } F_t} \quad (12)$$

where $F_t = 2p_0 \cdot b$. If the granular raft is rigid i.e. $G_r \cdot H_r \rightarrow \infty$ and $\alpha_c = \alpha_s = 0$, the normalized uniform settlement, W_r , and the ratio m_r , for this case are

$$W_r = \frac{b/a}{(K_R + b/a - 1)} \quad (13)$$

$$m_r = \frac{K_R}{(K_R + b/a - 1)} \quad (14)$$

(b) Stone Column

The governing equations for the stone column reinforced soil (axi-symmetric conditions) become

$$p_0 = K_c \cdot w - G_r H_r \left\{ \frac{d^2 w}{dr^2} + \frac{1}{r} \frac{dw}{dr} \right\} \text{ for } 0 \leq r \leq a \quad (15)$$

$$\text{and } p_0 = K_s \cdot w - G_r H_r \left\{ \frac{d^2 w}{dr^2} + \frac{1}{r} \frac{dw}{dr} \right\} \quad \text{for } a \leq r \leq b \quad (16)$$

where r is the radial distance from the center. The boundary and continuity conditions are of the same form as Eqs. (6), (7), and (8) but with x replaced by r . Eqs. (15) and (16) can be solved analytically but a finite difference approach is found to be simpler and equally good. Eqs. (15) and (16) in nondimensional form are

$$\lambda_s = \lambda_s \cdot w - \left\{ \frac{d^2 W}{dR^2} + \frac{1}{R} \frac{dW}{dR} \right\} \quad \text{for } 0 \leq R \leq 1 \quad (17)$$

$$\text{and } \lambda_s = \lambda_s K_R \cdot w - \left\{ \frac{d^2 W}{dR^2} + \frac{1}{R} \frac{dW}{dR} \right\} \quad \text{for } 1 \leq R \leq b/a \quad (18)$$

where $R = r/a$,

$$\lambda_s = K_c a^2 / G_r H_r$$

$$\lambda_s = K_s a^2 / G_r H_r$$

The granular pad is discretised into elements of size $\Delta r = a/n$ or $\Delta R = 1/n$, and the total number of elements $n_e = n \cdot b/a$. Eqs. (17) and (18) in finite difference form become

$$\lambda_s = \lambda_c \cdot W_i - \left\{ \frac{W_{i-1} - 2W_i + W_{i+1}}{(\Delta R)^2} \right\} + \frac{1}{R_i} \left\{ \frac{W_{i+1} - W_{i-1}}{2\Delta R} \right\} \quad \text{for } 1 \leq i \leq n \quad (19)$$

$$\text{and } \lambda_s = \lambda_c / K_c \cdot W_i - \left\{ \frac{W_{i-1} - 2W_i + W_{i+1}}{(\Delta R)^2} \right\} + \frac{1}{\Delta R_i} \left\{ \frac{W_{i+1} - W_{i-1}}{2\Delta R} \right\} \quad \text{for } n \leq i \leq n_e \quad (20)$$

where $R_i = (i-0.5) \cdot \Delta R$. The continuity conditions are automatically satisfied and the boundary conditions (i) and (iii) give

$$W_1' = W_1' \quad \text{and } W_{n_e}' = W_{n_e}' \quad (21)$$

where W_1' and W_{n_e}' are the displacements at nodes to the left of node 1 and to the right of node n_e respectively. The n_e number of equations for the nodes 1 to n_e are written and solved iteratively satisfying the convergence criterion

$$\{W_{\text{new}}(i) - W_{\text{old}}(i)\} / W_{\text{new}}(i) < \epsilon$$

where $W_{\text{new}}(i)$ and $W_{\text{old}}(i)$ are the current and previously evaluated values of nodal

LOAD TRANSFER THROUGH A GRAVEL BED

displacements and ϵ is a small quantity. The load carried by the stone column, F_c , is

$$F_c = \int_0^{2\pi} \int_0^a K_c \cdot w \cdot r \cdot d\theta \cdot dr \quad (23)$$

while the total load F_t , on the unit cell is

$$F_t = \pi \cdot b^2 \cdot p_0 \quad (24)$$

The ratio, m , becomes

$$m = F_c/F_t = \frac{\sum_{i=1}^n \{i^2 - (i-1)^2\} W_i}{\sum_{i=1}^{p_0} \{i^2 - (i-1)^2\} W_i} \quad (25)$$

If the granular pad is rigid, the uniform settlement, W_r , and the ratio, m_r , of the load on the stone column are

$$W_r = (b/a)^2 / \{K_R + (b/a)^2 - 1\} \quad (26)$$

$$\text{and } m_r = K_R / \{K_R + (b/a)^2 - 1\} \quad (27)$$

RESULTS

The displacement, W , and the percentage ratio, m , of the load carried by the granular trench or the stone column to that on the unit cell are obtained analytically in the former and numerically in the latter case. By normalising the actual settlement, w , with the settlement, w_w , of the soft soil alone, the effects of the granular trench or the stone column and the gravel bed in reducing the total and the differential settlements get highlighted very well. The following are the ranges of parameters investigated:

<p>(a) Granular Trench</p> <p>$K_R = 3 - 50$</p> <p>$b/a = 1.5 - 10.0$</p> <p>$\alpha_c = 0 - 5.0$</p>	<p>(b) Stone Column</p> <p>$K_R = 3 - 50$</p> <p>$b/a = 1.7 - 4.0$</p> <p>$\lambda_c = 2 - 50$</p>
---	---

For the gravel bed on granular trench reinforced soil (plane strain case), the variation of displacement with distance is depicted in Fig. 2 for $K_R = 10$ and $b/a = 5$. The displacements are small for the portion of the gravel bed on the granular trench but increase significantly with increasing values of distance, X . In the case of relatively flexible gravel bed the difference in the displacements over the granular trench and the soft soil are large. The stiffness of the mat increases with decreasing values of α_c and the settlements over the unit cell tend to become uniform. For $\alpha_c \leq 0.1$, the gravel bed can be treated as rigid, there being negligible differential settlement over the full width of the unit cell.

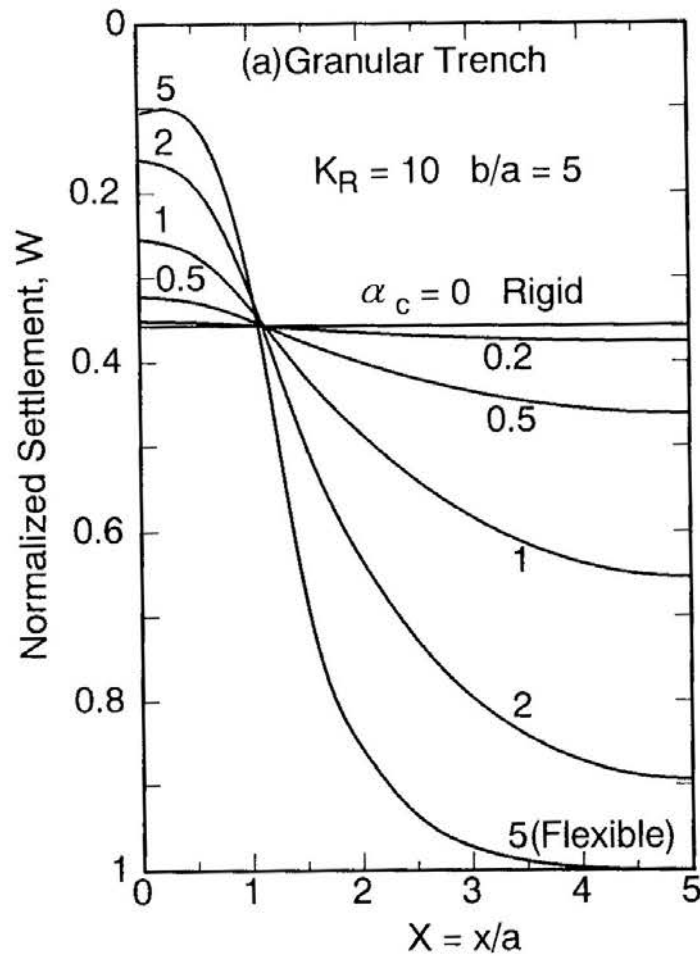


Fig. 2 Effect of α_c on Settlements - Granular Trench.

The settlement profile of the gravel bed is sensitive to the relative stiffness, K_R , of the granular trench material to that of the soft soil (Fig. 3). For $\alpha_c = 1.0$ and $b/a = 5.0$, the settlement of the gravel bed on a stiff granular trench ($K_R = 50$) is uniform while for a less stiff one the difference between the center and the edge settlements is large. The central and edge settlements are respectively 0.07 and 0.23 for K_R equal to 50, while they are 0.48 and 0.83 for K_R equal to 5. Thus, a stiff gravel bed is more effective on a stiff granular trench than on a softer one.

The effect of spacing between the granular trenches, i.e., of the ratio b/a , on settlement profile can be observed from Fig. 4. For close spacings ($b/a = 2$), the gravel bed is very effective in acting as an almost rigid base and the settlements are uniform. With increasing values of the ratio b/a , both the central and the edge settlements increase. The farther the distance of the point from the center, the lesser would be the effect of the stiff granular trench and larger would be the settlements. The total load on the unit cell increases with increasing values of b/a , leading to larger settlements. The rate of increase of the settlement at the edge is much more than the increase of the central settlement.

LOAD TRANSFER THROUGH A GRAVEL BED

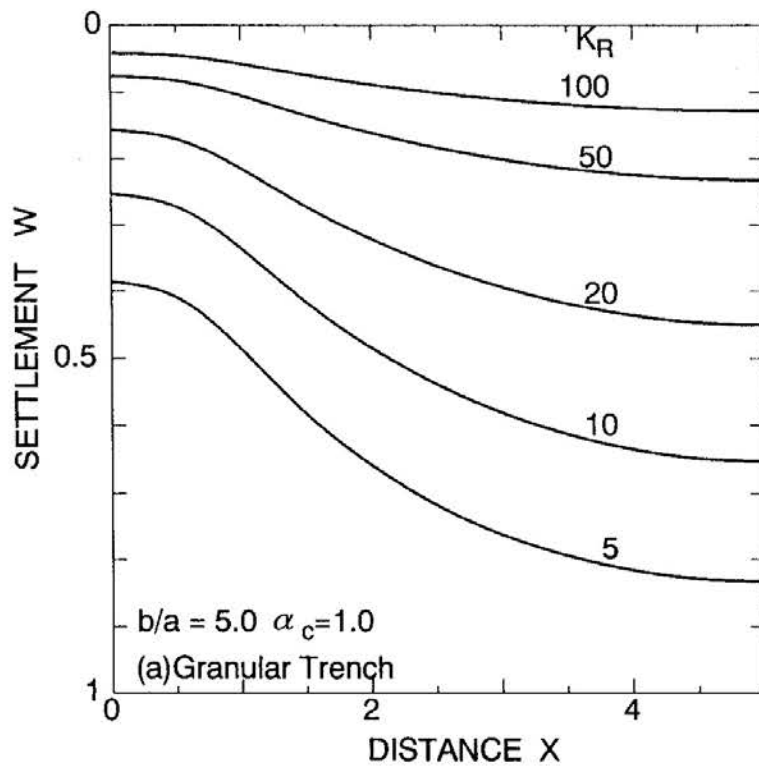


Fig. 3 Effect of K_R on Settlements - Granular Trench.

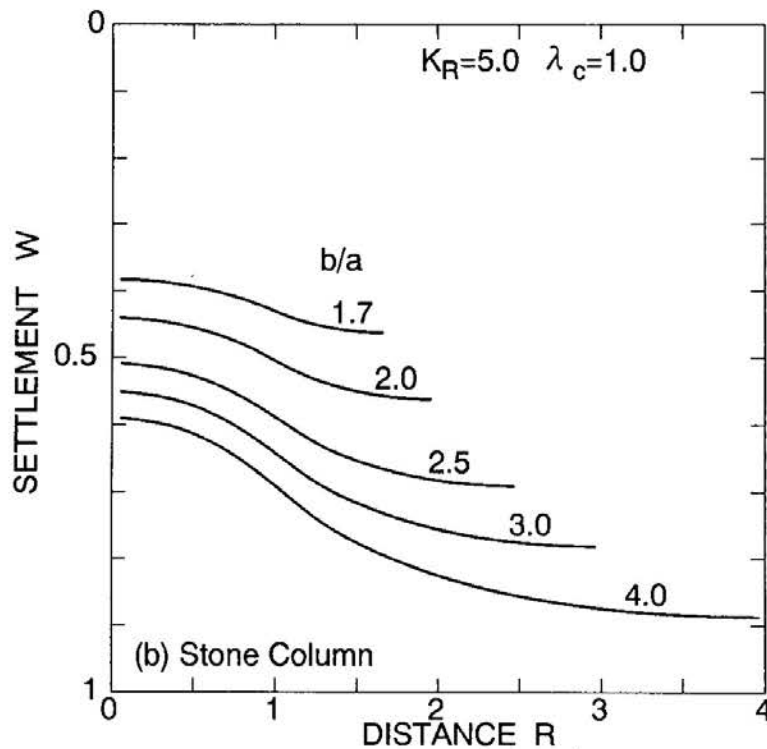


Fig. 4 Effect of b/a Settlements - Granular Trench.

Gravel Bed on Stone Column Reinforced Soil

The evaluation of load transfer through gravel bed on to stone columns is of much practical interest. For the evaluation of Eqs. (19) and (20), the number of elements, n , into

which the portion of the gravel bed over the stone column is divided, is varied. A value of $n = 20$ is found to be adequate. Similarly ϵ is chosen as 0.000001, as no improvement in the accuracy results by reducing ϵ further. The variation of settlement, W , of the gravel bed with distance is shown in Fig. 5 for $b/a = 2.5$ and $K_R = 5$. If $\lambda > 50$, the gravel bed has no stiffness and the unit cell deforms as per the stiffnesses of the stone column and the soft soil. Once again it may be noted that the settlement, W , increases significantly in case of flexible beds ($5 < \lambda < 50$). As the gravel bed becomes stiffer i.e. its shear stiffness tends to infinity, i.e. $\lambda_c \rightarrow \infty$, the settlements tend to become uniform. For λ_c values of 0.05, 0.5, and 1.0, the differential settlements are 0.01, 0.1, and 0.18, respectively. Thus, it can be noted that for $\lambda_c \leq 0.05$, the settlements are uniform implying that the gravel bed over the reinforced ground can be treated as rigid.

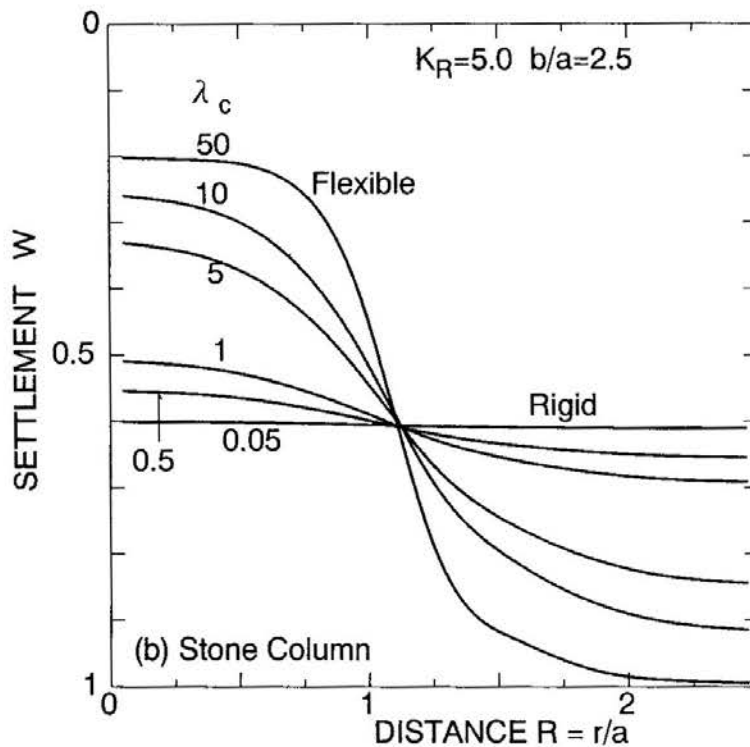


Fig. 5 Effect of λ_c on Settlements - Stone Column.

Stronger and stiffer stone columns provide better arching action and give rise to more uniform settlements (Fig.6). For K_R increasing from 5 to 50, the central normalized settlement decreases from 0.51 to 0.1, while the edge settlement decreases from 0.69 to 0.14. It should be noted that if K_R values increase for a given value of λ_c , it corresponds to a decrease in the value of K_s , the stiffness of the soft soil being improved. A smaller value of K_s implies a larger value of unreinforced settlement, W_w . For K_R increasing from 5 to 20, the differential settlement reduces from 0.18 to 0.09. A gravel bed on a stiff stone column is once again much more effective in reducing differential settlements.

The response of a gravel bed on a stone column reinforced soil is sensitive to the spacing ratio b/a (Fig. 7). For close spacings ($b/a = 1.7$), the normalised settlement increases from 0.38 at the center to 0.46 at the edge of the unit cell. For a spacing ratio of 2.5, the

LOAD TRANSFER THROUGH A GRAVEL BED

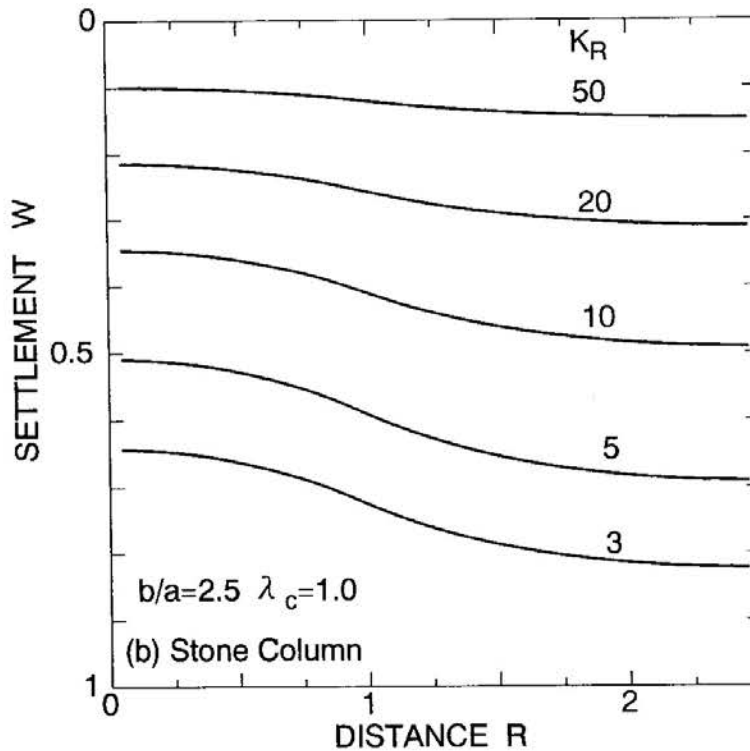


Fig. 6 Effect of K_R on Settlements - Stone Column.

corresponding settlement values are 0.51 and 0.68, respectively. The shear stiffness of the gravel bed is more effective at closer spacings of the stone columns.

Load Carried by Granular Trench/Stone Column

For design, it is imperative to know the sharing of the applied load by the stone columns or the granular trenches and the soft soil. The percentage of loads carried by the gravel trench or the stone column are evaluated by Eqs. (14) and (27) respectively and are presented in Figs. 8 and 9. The percentage of the load carried by the granular trench, m , increases with increase in the ratio a/b (Fig. 8). For a flexible gravel bed ($\alpha_c = 5$), the increase is linear. With increasing stiffness of the gravel bed i.e., decreasing values of the parameter, α_c , the percentage of load carried by the trench increases rapidly with a/b initially but the rate of increase decreases with a/b . The initial rate of increase of m with a/b is more if the parameter α_c is smaller. From the above results, it is apparent that if $\alpha_c < 0.2$, the gravel bed can be treated to be rigid.

The effect of the relative stiffness of the gravel bed in transferring the applied load on to the stone columns is highlighted in Fig. 9. Low values of the parameter λ_c imply a stiffer gravel bed and lead to higher loads to be transferred to the stone columns. The values of m for $\lambda_c = 0.1$ correspond nearly to the values for a rigid raft. The percentage, m , of the load carried by the stone columns decreases with increasing values of λ_c . The influence of the gravel bed is more if the stone columns are spaced closely. For λ_c increasing from 0.1 to 50.0, the percentage values of the loads on the stone columns are 77 and 42 for a spacing of 2.0, and 54 and 18 for a spacing of 3.0. For closer spacings the percentage of load on the stone column is nearly constant for $\lambda_c < 0.2$. Thus, from consideration of load transfer, gravel beds with $\lambda_c < 0.2$ can be treated as rigid.

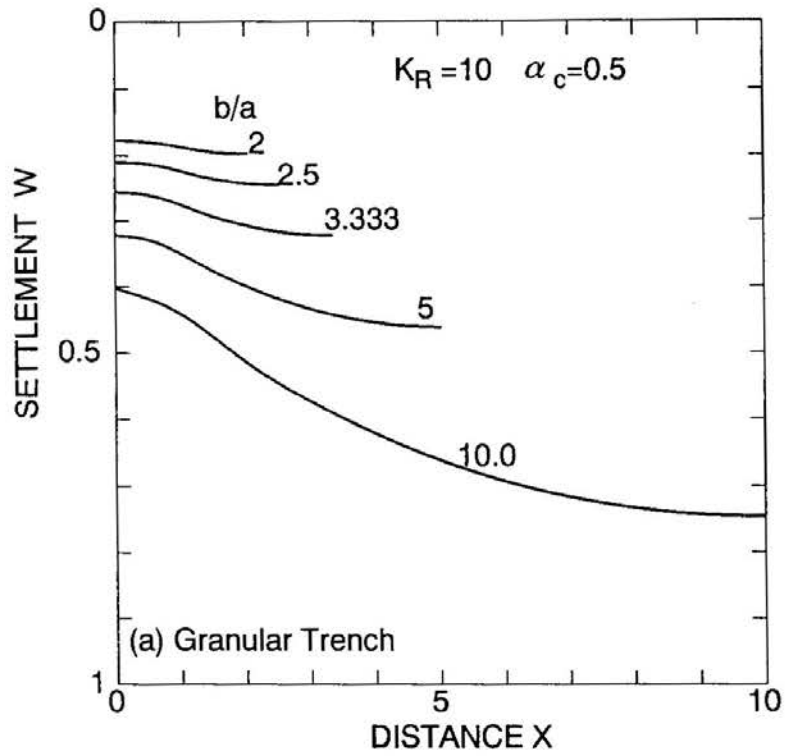


Fig. 7 Effect of b/a on Settlements - Stone Column.

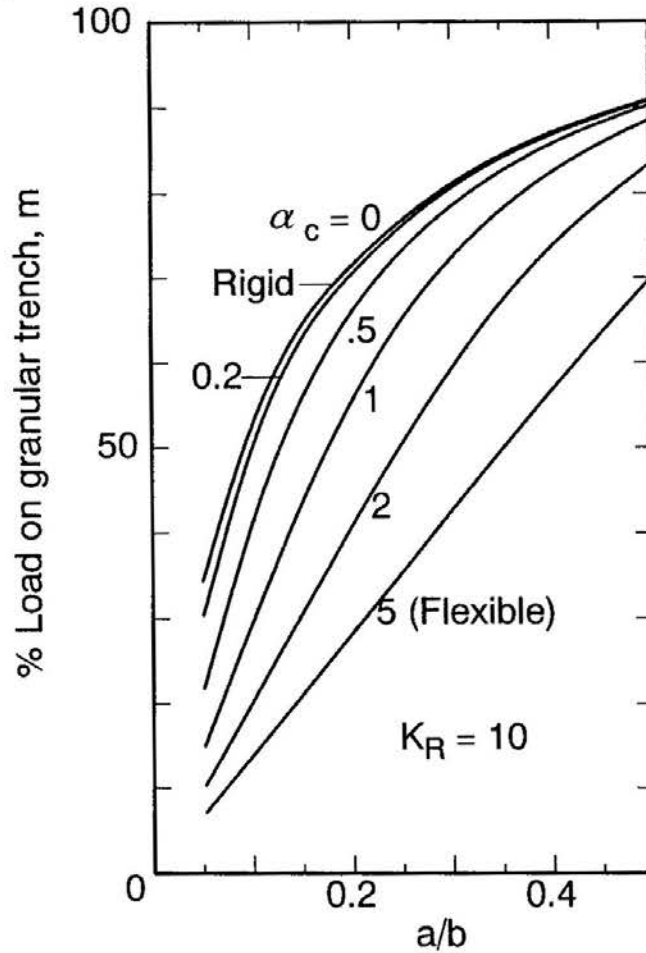


Fig. 8 Load on Granular Trench.

LOAD TRANSFER THROUGH A GRAVEL BED

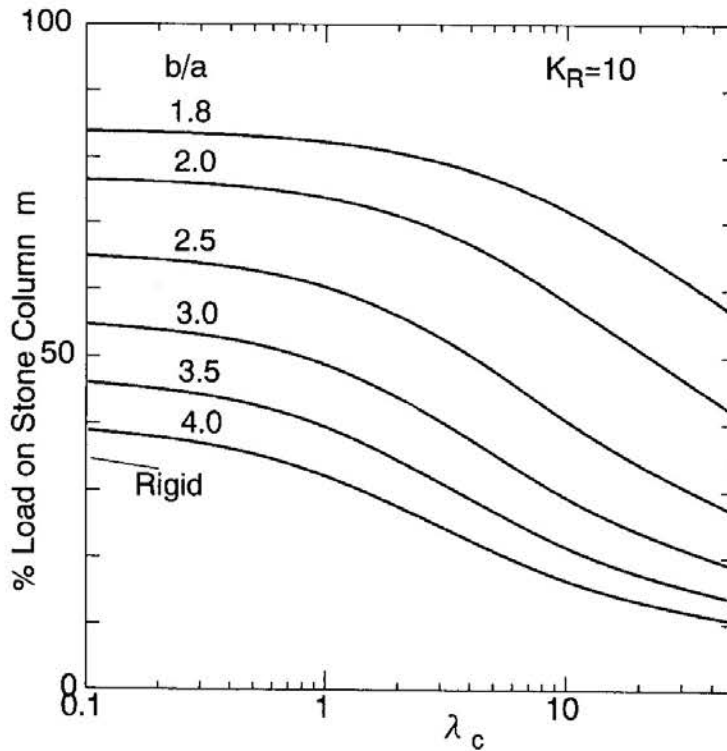


Fig. 9 Load on Stone Column

Settlement, W_r , and Percentage of Load, m_r , on Granular Trenches and Stone Columns under Rigid Gravel Bed

Table 3 Limiting Values of Displacement Factor W_r /Load Factor m_r .

(a) Granular Trench						
K_R	1.5	2.0	b/a 2.5	3.0	3.5	4.0
3	.429/.857	.500/.750	.555/.667	.600/.600	.637/.545	.667/.500
5	.273/.909	.333/.833	.383/.769	.429/.714	.467/.667	.500/.625
10	.143/.952	.182/.909	.217/.870	.250/.833	.280/.800	.308/.769
20	.073/.976	.095/.952	.116/.930	.136/.909	.155/.889	.174/.869
(b) Stone Column						
K_R	1.5	2.0	b/a 2.5	3.0	3.5	4.0
3	.618/.572	.667/.500	.758/.364	818/.273	859/.210	.889/.167
5	.447/.691	.500/.625	.610/.488	.692/.385	.754/.308	.800/.250
10	.265/.817	.308/.769	.405/.656	.500/.555	.576/.471	.640/.400
20	.146/.899	.174/.869	.247/.792	.321/.714	.392/.640	.454/.571

Table 3 summarises the values of the uniform settlement, w_u , and the percentage of load, m_p , carried by the granular trench or the stone column beneath a rigid gravel bed. These values are applicable provided the gravel bed is designed as a rigid one.

CONCLUSIONS

Improvement of ground with a regular array of stone columns is commonly resorted to in case significant reduction in settlement is desired. A unit cell is analysed as typical of the treated area. The design usually implies uniform settlement of the stone column and the soft soil. A simple model for a gravel bed laid over the stone column reinforced soil is proposed and analysed for both plane strain (granular trench) and axi-symmetric (stone column) conditions. The variation of settlements with distance in a unit cell are shown to be dependent on the shear stiffness (product of shear modulus and the thickness) of the gravel bed, the relative stiffness of the stone column to that of soft soil, and the spacing of the stone columns. The load transferred to the stone column by the gravel bed also varies with the above specified parameters. For the covering gravel bed over stone columns to be considered rigid, the relative stiffness ratio, λ_c , should be less than about 0.2. For higher values of λ_c , differential settlements could be significant.

ACKNOWLEDGEMENT

The authors acknowledge the financial support from the Belgian National Fund for Scientific Research to Prof. M.R. Madhav during his stay in Belgium.

REFERENCES

- BACHUS, R.C., and BARKSDALE, R.D. (1984). 'Vertical and Lateral Behaviour of Model Stone Columns', International Conference on In Situ Soil and Rock Reinforcement, Paris, pp. 99-110.
- BALAAM, N.P., and BOOKER, J.R. (1981). 'Analysis of Rigid Rafts supported by Granular Piles', International Journal, Numerical Analytical Methods in Geomechanics, Vol 5, pp. 374-403.
- BERGADO, D.T., ALFARO, M.C., and CHAI, J.C. (1991). 'The Granular Pile: Its Present State and Future Prospects for the Improvement of Soft Bangkok Clay', Geotechnical Engineering, Vol. 22, pp. 143-175.
- BHANDARI, R.K.M. (1983). 'Behaviour of a Tank Founded on Soil Reinforced with Stone columns', Proceedings of 7th ECSMFE, Helsinki, Vol. 1, pp. 65-68.
- BOWLES, J.E. (1982). 'Foundation Analysis and Design', McGraw Hill Book C., New York, p. 67.
- BRONS, K.F., and DE KRUIJFF, H. (1985). 'The Performance of Sand Compaction Piles', Proceedings; XI ISSMFE, San Francisco, Vol. 3, pp. 1683-1686.
- GOUGHNOUR, R.R., and BAYUK, A.A. (1979). 'Analysis of Stone Column - Matrix

LOAD TRANSFER THROUGH A GRAVEL BED

- Interaction under Vertical Load', International Symposium on Reinforcement of Soils, Reinforced Earth and other Methods, Paris, Vol. 1, pp. 271-277.
- JUILLIE, Y., and SHERWOOD, D.E. (1983). 'Improvement of Sabka Soil at the Arabian Gulf Coast', Proceedings of 7th ECSMFE, Helsinki, Vol. 2, pp. 781-788.
- MADHAV, M.R., and POOROOSHASB, H.B. (1987). 'Pasternak Concept for Modelling Soft Soil Overlain by Stiff Soil', Ind. Geotech. Conf., Bangalore, Vol. 1, pp. 107-110.
- MITCHELL, J.K., and HUBER, T.T. (1983). 'Stone Column Foundations for a Waste Treatment Plant - A Case History', Geotechnical Engineering, Vol. 14, No. 2.
- PRIEBE, H. (1976). 'Abschätzung des Setzungsverhaltens eines durch Stopppverdichtung verbesserten Baugrundes', Die Bautechnik, Vol. 53, pp. 160-162.
- VAN IMPE, W.F., and DE BEER, E. (1983). 'Improvement of Settlement Behaviour of Soft Layers by means of Stone Columns', Proceedings of 7th ECSMFE, Helsinki, Vol. 1, pp. 309-312.
- VAN IMPE, W.F., and MADHAV, M.R. (1992). 'Analysis and Settlement of Dilating Stone Column Reinforced Soil', Osterreichische Ing. und Arch. - Zeitschrift, Vol. 137, pp. 114-121.
- VENMANS, A.A.M. (1990). 'Widening of a Road Embankment using Stone Columns', Young Geotechnical Engineers Conference, The Hague.

APPENDIX - NOTATION

a	= $d_p/2$;
b	= $d_e/2$;
$b_0 - b_5$	- functions of a and b;
C	- center to center spacing between stone columns;
$C_1 - C_4$	- integration constants;
D_s	- constrained modulus of the soft soil;
d_e	- diameter of the unit cell;
d_p	- diameter of the stone column;
E_s	- modulus of deformation of the soft soil;
F_c and F_t	- loads carried by the granular trench/stone column and unit cell respectively;
G_f	- shear modulus of granular bed material;
H	- thickness of soft soil;
H_f	- thickness of granular bed;
K_c and K_s	- coefficients of subgrade reaction of granular trench/stone column and soft soil respectively;
K_R	= K_c/K_s ;
m	= F_c/F_t - ratio of load carried by trench/stone column with respect to the load on the unit cell;
m_r	- ratio of load carried by trench/stone column in case of rigid granular bed;
n, n_e	- number of elements in the stone column and the unit cell respectively;
p_0	- uniform stress acting on the granular bed;
R	= r/a ;
r	- radial distance;

MADHAV and VAN IMPE

W	= w/w_w - normalized settlement;
W_i	- normalized nodal displacement at node i ;
W_r	- normalized uniform settlement of rigid granular bed;
w	- settlement at distance r or x ;
w_w	= p_0/K_s - settlement of untreated soft soil;
X	= x/a ;
x	- distance from center of granular trench;
α_c, α_s	= $\text{SQRT} \{K_c(K_s).a^2/G_r h_f\}$;
ϵ	- a small parameter;
ϵ_v	- volumetric dilation;
λ_c, λ_s	= $K_c (K_s).a^2/G_r H_f$ - stone column case;
V_s	- Poisson's ration of soft soil;
ϕ'_c	- angle of shear resistance of granular trench/stone column material;

A COMPARISON OF THE CYCLIC PULLOUT BEHAVIOUR OF MODEL PLATE AND PILE ANCHORS IN SOFT CLAY

M. Datta¹, S.K. Gulhati² and N.U. Khan³

SYNOPSIS

The movement of model plate anchors and model pile anchors buried in soft clay and subjected to cyclic pullout loading is compared in this paper. In particular, the influence of number of cycles of loading, of cyclic stress level and of water content of the soil on pullout behaviour is highlighted.

The comparative study reveals the following differences and similarities between plate and pile anchors: (a) plate anchors show much larger movement than pile anchors under identical cyclic loading; (b) pile anchors show sudden failure due to slippage between the pile wall and the surrounding soil whereas no such failure is observed in plate anchors despite much larger movement; (c) the movement in both types of anchors is governed by the maximum cyclic stress level; and (d) an increase in the water content of the soil results in an improved performance in both types of anchors.

The study reveals that for satisfactory performance of plate and pile anchors, the maximum cyclic stress level should be kept below a threshold value which is significantly lower than the static breakout capacity.

INTRODUCTION

The search for ocean resources is progressing from the continental shelves into the deep seas where water depths are more than 200 m. Compliant floating structures are more economical than fixed offshore structures for recovery of ocean resources from such deep-water locations. These floating structures are held in position by foundations anchored to the seabed. Pullout loads transmitted by floating structures to the foundations are primarily cyclic in nature on account of the large environmental forces experienced by the floating structures. The design of foundation anchors is governed by their ability to resist cyclic pullout loads.

Presence of significant petroleum resources has been registered off the east coast of India at the mouth of the river Godavari where water depths are of the order of 200 metres and the seabed soil comprises of very soft to soft underconsolidated clay. Tension leg platforms (TLPs) are envisaged as one feasible type of production structure for this site. An understanding of the pullout behaviour of anchors in very soft to soft clays, under cyclic

¹ Associate Professor, Civil Engg. Dept., Indian Institute of Technology, New Delhi-110016, India

² Managing Director, Educational Consultants (India) Ltd., New Delhi, India

³ Reader, Civil Engg. Dept., Jamia Millia Islamia, New Delhi, India

pullout loading has thus been a subject of indepth research over the last few years.

The pullout behaviour of different types of anchors (Fig-1) is governed by the mechanisms by which resistance to pullout load is developed. For example, in plate anchors buried in clays, resistance to pullout load is induced on account of the resistance offered by the soil above the plate, R_v , as well as suction which may develop below the plate, P_s (Fig. 1 (b)). In pile anchors, resistance develops on account of skin friction along the pile surface, F_v (Fig. 1 (c)). In gravity anchors, resistance can develop on account of all the factors mentioned above as well as the submerged weight of the anchor, W_a , which is quite substantial (Fig. 1 (a)).

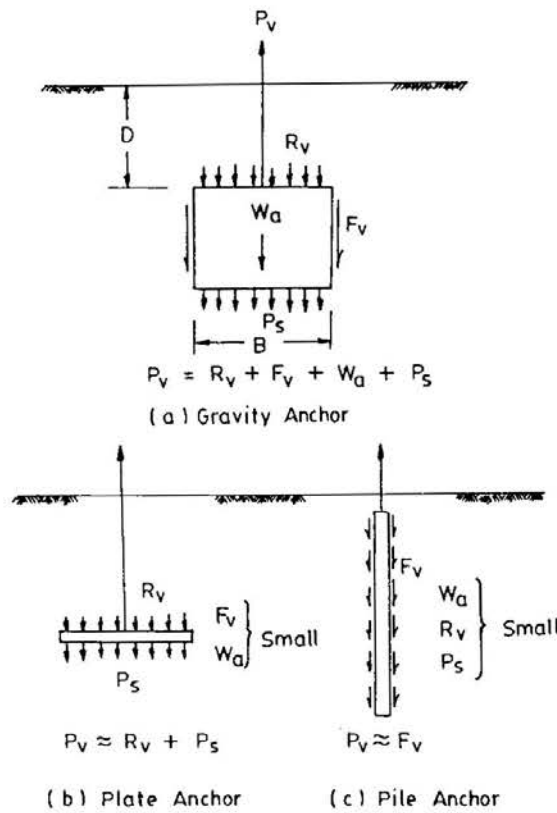


Fig. 1 Vertical Breakout Capacity of Gravity, Plate and Pile Anchors.

This paper presents a comparative study of the results obtained by conducting model tests on plate and pile anchors buried in soft clay under identical conditions and subjected to cyclic pullout loading.

LITERATURE REVIEW

The behaviour of plate anchors buried in clay and subjected to cyclic pullout loading has been studied in model laboratory tests by Bembem et. al (1973), Bembem and Kupferman (1975), Ponniah and Finlay (1988) and Datta et. al. (1990). Their findings can be summarised as follows:

A COMPARISON OF THE CYCLIC PULLOUT BEHAVIOUR

- (a) Plate anchors show significant upward movement under cyclic pullout loading;
- (b) The rate of movement per cycle decreases as the number of cycles increase;
- (c) The magnitude of total movement is governed primarily by the maximum cyclic stress level and not by the cyclic stress amplitude;
- (d) Though plate anchors show significant movement, they do not fail by shearing even when the maximum cyclic stress level is as high as 70% of the static pullout capacity.

Data on behaviour of piles in clay subjected to cyclic loading has been reported by Holmquist and Matlock (1976), Poulos (1979 & 1981), Steenfelt et. al. (1981) and Matlock et. al. (1982). These investigations pertain to two-way (compression-tension) cyclic loading or to strain controlled loading, both of which are not relevant for pile anchors of TLP foundations. The behaviour of piles under one-way stress controlled cyclic pullout loading has been studied by Puech (1982), Karlsrud and Haugen (1985) and Khan et. al. (1992).

Their finding can be summarised as follows:

- (a) Below a threshold stress level of cyclic loading, piles show very low movement with number of cycles. The rate of movement rapidly falls to zero as number of cycles increase. The total accumulated movement remains below 4.0 percent of pile diameter.
- (b) Above the threshold stress level, rapid accumulation of upward movement takes place with number of cycles, finally resulting in failure of the pile.
- (c) The threshold level lies in the range of about 50 to 80 percent of ultimate static pullout capacity.

SCOPE

All studies reported in the literature on plate anchors and pile anchors have been conducted by different investigators using different soil conditions & loading conditions. As a consequence, it is not possible to draw a comparison between the behaviour of these two types of anchors. In the present study, the pullout behaviour of plate and pile anchors has been studied using identical soil conditions as well as similar cyclic loading conditions and a comparison has been made vis-a-vis the following aspects:

- (a) influence of number of cycles of loading on the movement of anchors;
- (b) influence of cyclic stress level on the movement of anchors;
- (c) influence of water content on the pullout behaviour of anchors.

On the basis of this comparison, implications for the design of anchors of TLP foundations are summarised.

EXPERIMENTAL INVESTIGATION

Test Set-up

Circular plate anchors 5 cm in diameter were embedded in soft clay to a depth of 30 cm in model test tanks having a diameter of 30 cm and height of 50 cm (Fig. 2 (a)). The embedment depth to diameter ratio was kept at 6 to simulate deep anchor behaviour.

Tubular aluminium piles, having a length of 30 cm and diameter of 5 cm (Fig. 2 (b)) were used for model tests on pile anchors, in the same tests tanks as used for plate anchors. The outer surface of these piles was thoroughly and evenly roughened by knurling. The piles had a cone at the bottom end which was used during installation of the pile by pushing. The cone was detached from the bottom prior to application of pullout load.

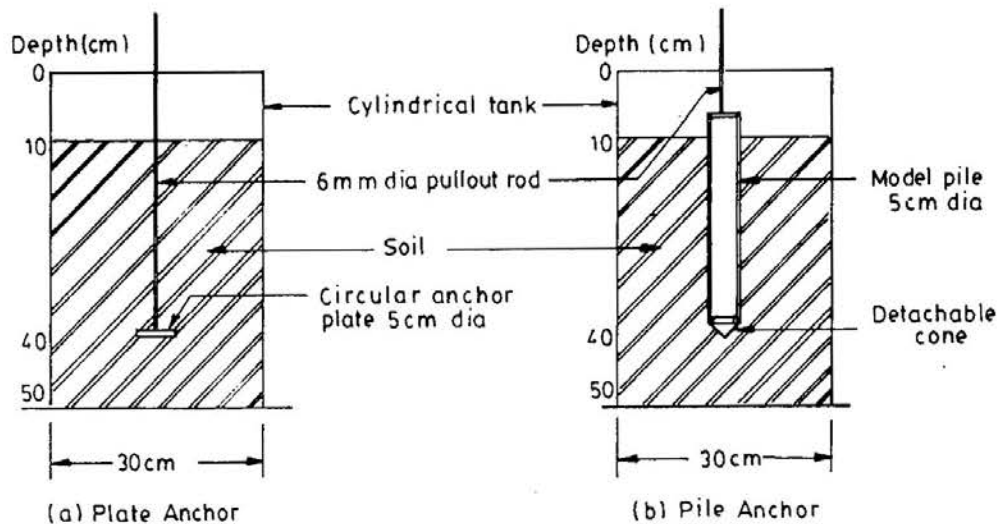


Fig. 2 Model Testing Arrangement for Plate and Pile Anchors.

A multipurpose mobile loading frame was used for applying static as well as cyclic pullout loading to the anchors (Fig. 3). A pneumatic system was used for the application of cyclic loads (Fig. 4) and a motorised gearbox was used for static pullout. The air cylinder (see H in Fig. 3 & Fig. 4) formed the heart of the cyclic pullout load application system. A constant pressure was maintained in the air in the top part of the cylinder. In the bottom part of the cylinder, below the piston, the air pressure was varied between the maximum and minimum levels corresponding to the cyclic pullout load to be applied. This was achieved by means of two solenoid valves and a timer which changed the pressure in the bottom part as per the time period specified. This arrangement resulted in a square wave loading pattern (Fig. 5). The maximum and minimum values of the cyclic pullout load applied were recorded by a load cell. The upward movement of the anchor was measured by an LVDT as well as a dial gauge. A strip chart recorder was used for recording of results.

At the end of the cyclic load tests, static strain controlled pullout tests were conducted with the same frame using the motorised gearbox.

A COMPARISON OF THE CYCLIC PULLOUT BEHAVIOUR

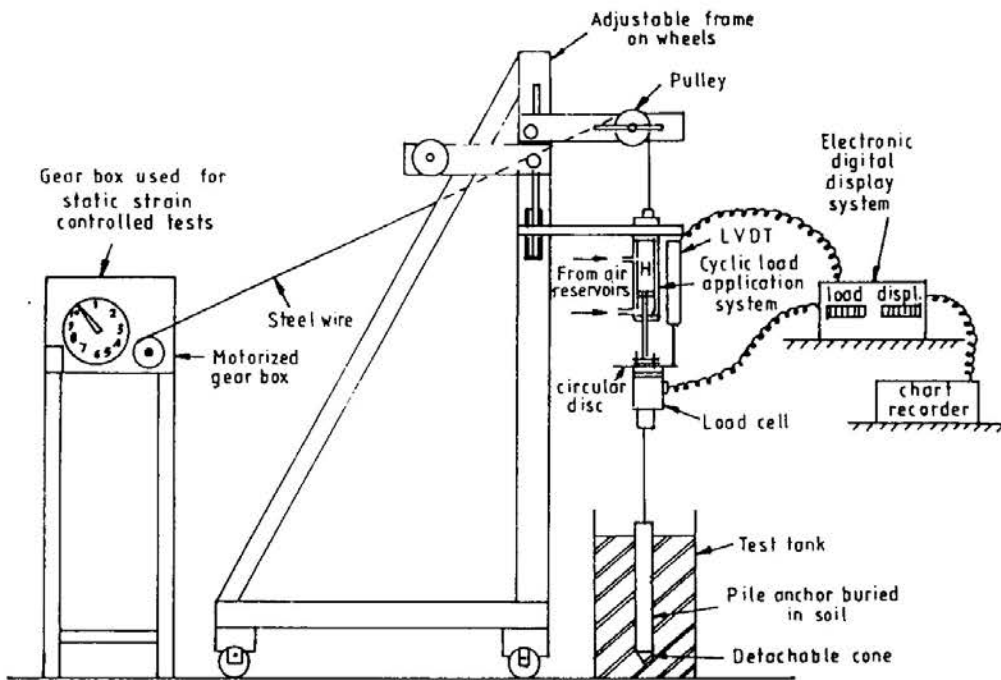


Fig. 3 Experimental Set-up for Pulling out Plate and Pile Anchors Under Cyclic Loading and Strain Controlled Static Loading.

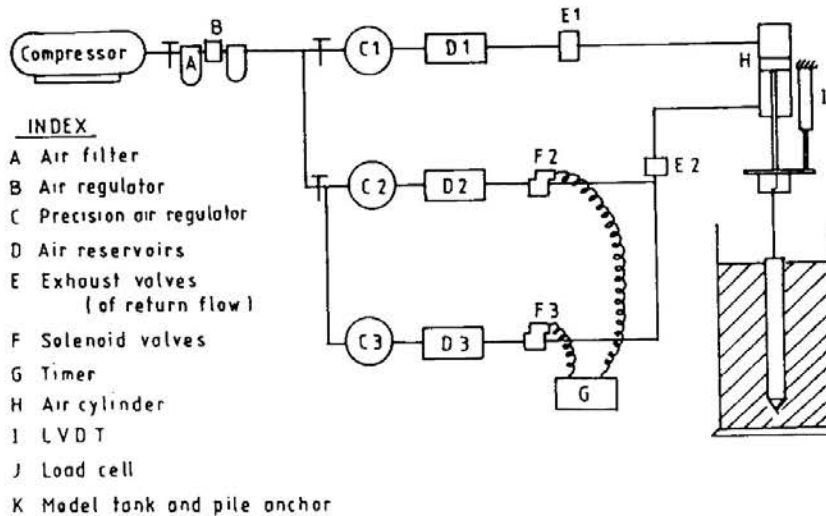


Fig. 4 Pneumatic System for Applying Cyclic Load.

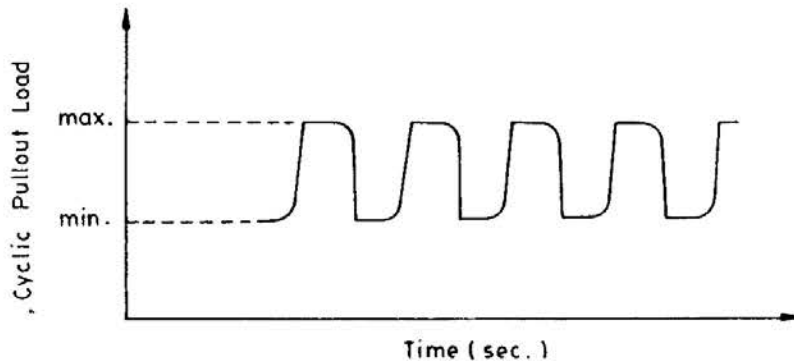


Fig. 5 Square Wave Pattern of Cyclic Loading.

Soil Used

The soil used in the model tests was Dhanauri Clay, a river bed clay deposit having plastic limit of 28 of liquid limit of 51. The range of water contents used in model tests varied from 32 to 41 percent. In this range of water content the undrained strength, S_u , of the soil varied from 0.016 to 0.06 kg per sq. cm (1.57 to 5.88 kPa) indicating that the soil strength fell within the range of strengths normally associated with very soft clays.

About 40 kg of dry pulverised soil was required for each model test. This soil was mixed with the appropriate amount of water in a separate container, kneaded thoroughly to break down any lumps and then passed through 10 mm aperture sieve to achieve a uniformly mixed soil. Small quantities of the soil were placed in the test tank by hand. These were patted and spread evenly to avoid entrapment of air. The tank was filled up in layers and care was taken to ensure that no air was trapped between successive layers as well as between the soil and the tank wall.

A detailed study was conducted to establish the variation of strength of remoulded Dhanauri clay with time. The study indicated that Dhanauri clay did exhibit thixotropic properties and that the strength did not increase appreciably after 4 days. In all model tests, pullout loading was applied after allowing Dhanauri clay to remain undisturbed for 7 days.

Testing Programme

Tests were conducted on anchors embedded in Dhanauri clay at three water contents varying from 32% to 41%.

At each water content one static test was performed in the beginning. Thereafter a series of cyclic tests were conducted; each cyclic test was followed by a static pullout test.

In static pullout tests, a strain rate of 0.2 mm/min was used. On the basis of the failure load observed in the static test at the start of each test series, the maximum and minimum cyclic load limits were fixed as a percentage of the static breakout capacity. In each cyclic test, a total of 500 cycles of pullout load were applied between the prefixed minimum and maximum load limits using a time period of 15 seconds per cycle. At the end of the cyclic test, the anchor was pulled out under strain controlled static loading.

In the series of cyclic tests on plate anchors, the minimum cyclic stress level was fixed at 0 and 25% whereas the maximum cyclic stress level was fixed at 25, 33, 50 and 66% in different tests at each water content.

In the series of cyclic tests on pile anchors, the minimum cyclic stress level was fixed at 25% and the maximum cyclic stress level was fixed at 50, 66 and 75% in different tests at each water content.

RESULTS

Load-Displacement Behaviour Under Static Pullout

The load-displacement behaviour of plate and pile anchors observed under static pull-

A COMPARISON OF THE CYCLIC PULLOUT BEHAVIOUR

out at a strain rate of 0.2 mm/min is compared in Fig. 6. The following observations can be made:

(a) As load is applied to a plate anchor, the anchor is displaced and load increases as displacement increases; load does not reach a peak.

(b) On the other hand, pullout load increases to a peak value at very low displacement for a pile anchor.

(c) The displacement necessary to generate maximum soil resistance in pile anchors is, therefore, very low as compared to the displacement required to generate maximum soil resistance in plate anchors.

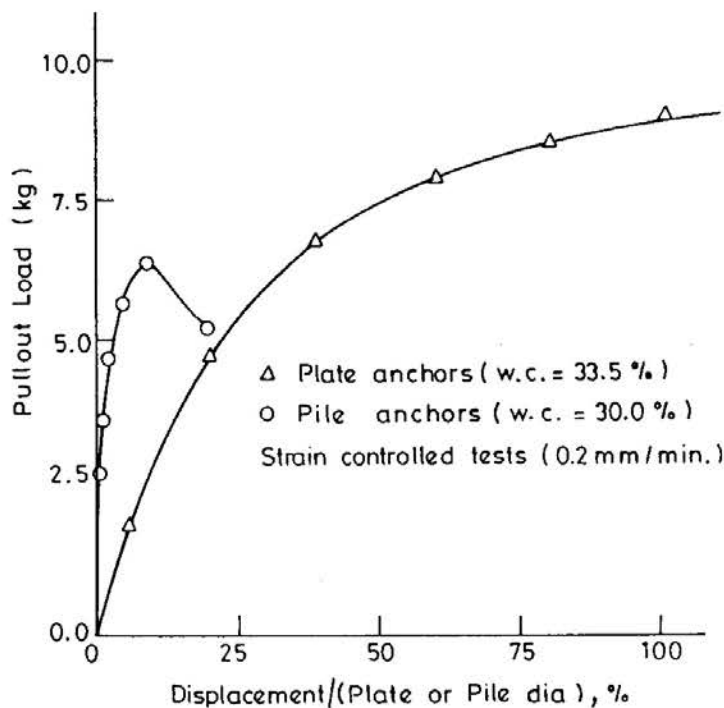


Fig. 6 Pullout Load - Deformation Behaviour of Plate and Pile Anchors.

Displacement Behaviour Under Cyclic Loading

Figs. 7 and 8 depict the movement of plate anchors with number of cycles for cyclic stress levels of 0 to 33% (min. to max) and 0 to 66% respectively. One notes from these figures that plate anchors show significant movement under cyclic loading. The rate of increase in movement decreases as the number of cycles increase. Plate anchors do not fail by rapid upward movement.

Figs. 9 and 10 depict the movement of pile anchors with number of cycles for cyclic stress level of 25 to 50% and 25 to 75% respectively. One notes from Fig. 9 that pile anchors show insignificant displacement even after 500 cycles. However, in contrast, Fig 10 depicts that piles experiencing higher cyclic stress show sudden failure by rapid upward movement despite initially showing very little movement. The number of cycles in Fig. 10 have been

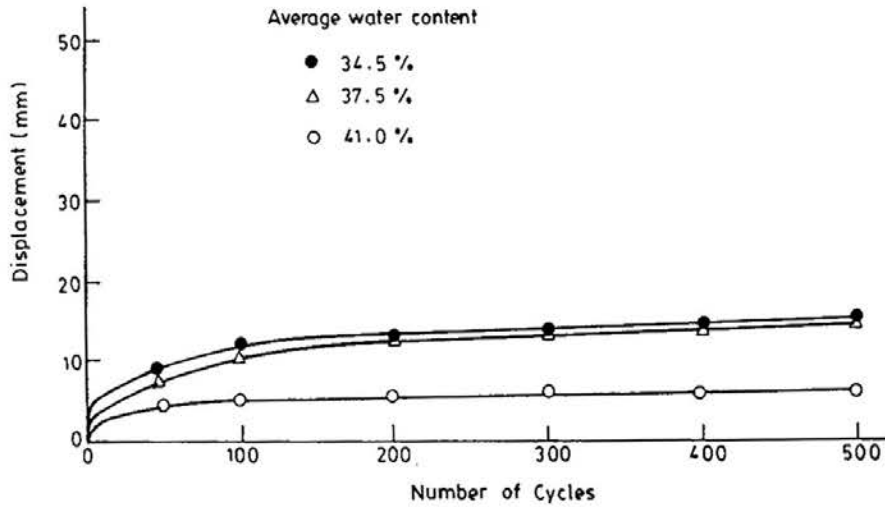


Fig. 7 Movement of Plate Anchors with Number of Cycles (cyclic stress level: 0 to 33%).

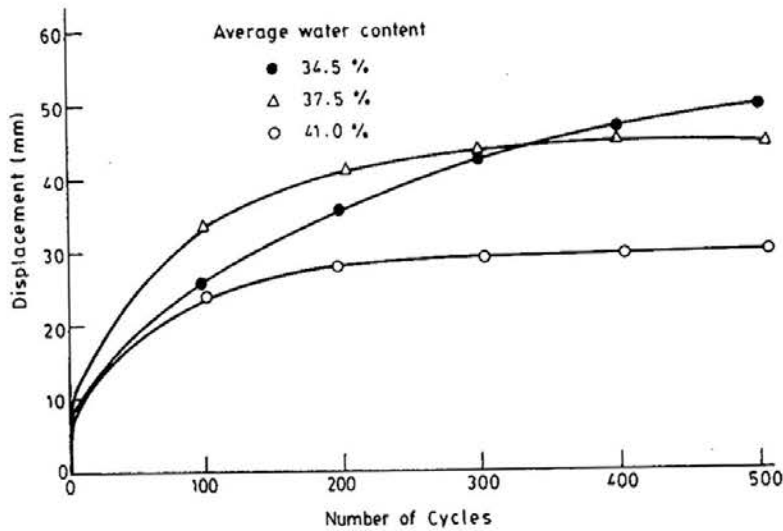


Fig. 8 Movement of Plate Anchors with Number of Cycles (cyclic stress level: 0 to 66%).

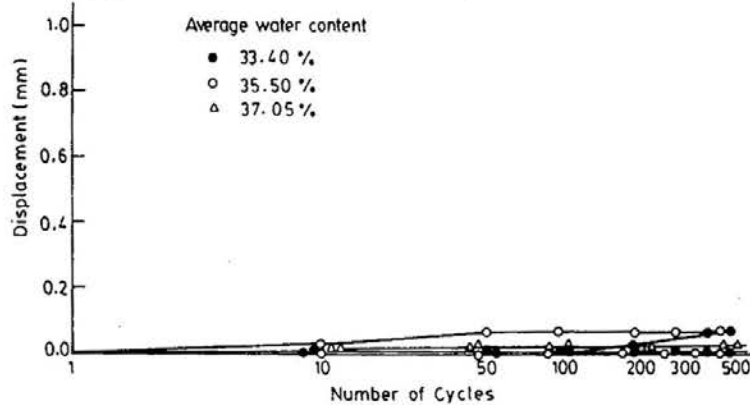


Fig. 9 Movement of Pile Anchors with Number of Cycles (cyclic stress level: 25 to 50%).

A COMPARISON OF THE CYCLIC PULLOUT BEHAVIOUR

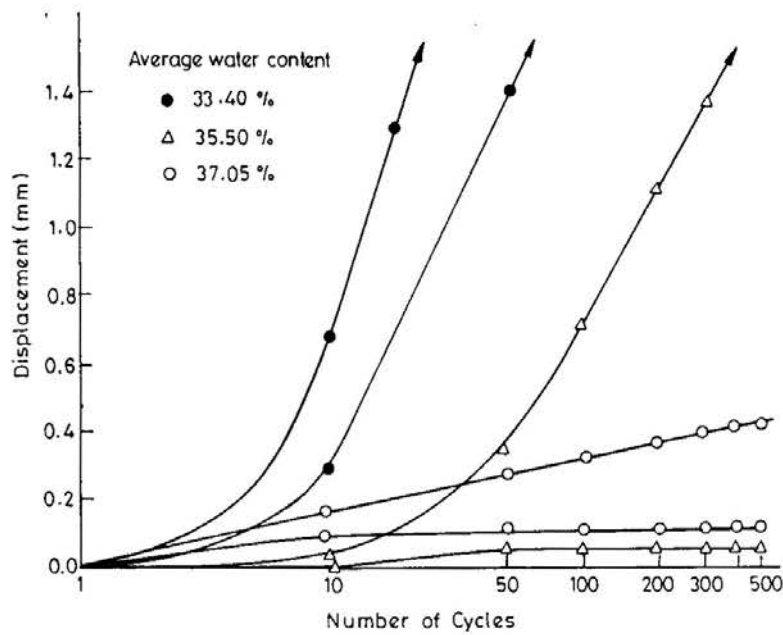


Fig. 10 Movement of Pile Anchors with Number of Cycles (cyclic stress level: 25 to 75%).

plotted on a log scale to highlight the low initial movement before sudden failure.

The contrasting behaviour of model plate and pile anchors is depicted in Fig. 11 for a maximum cyclic stress level of 50% and in Fig. 12 for a maximum cyclic stress level of 66%. When the maximum stress level is 50% (or less) pile anchors show much smaller displacement than plate anchors (Fig. 11). However at higher maximum stress level (Fig. 12), pile anchors fail without any warning despite showing low initial movement. Plate anchors show much larger initial movements than pile anchors but they never show sudden failure. This difference in behaviour can be attributed to the fact that the mechanism of generation of soil resistance for piles is very different from that for plates. In piles, once significant movement

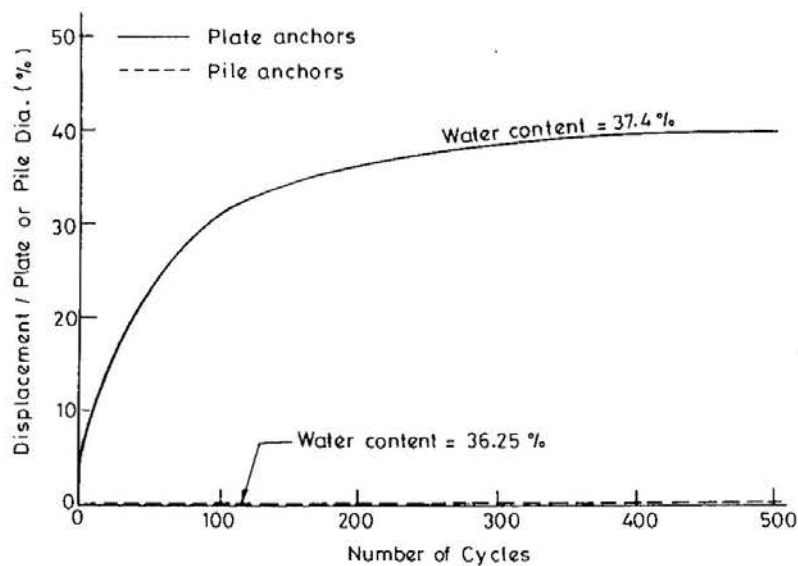


Fig. 11 Movement of Plate and Pile Anchors Under Cyclic Loading (maximum cyclic stress level: 50%).

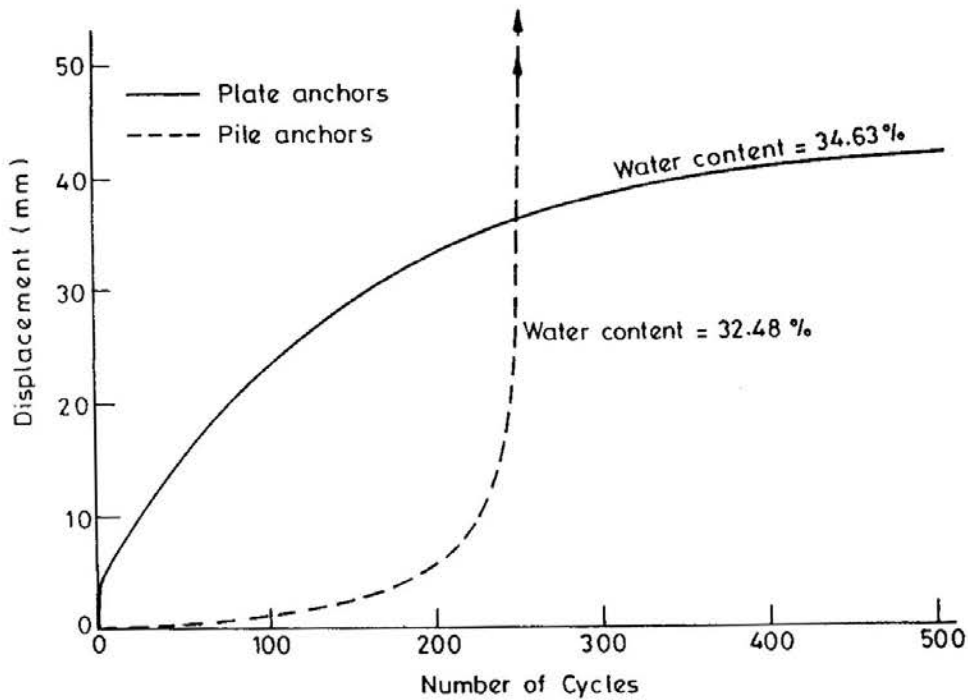


Fig. 12 Movement of Plate and Pile Anchors Under Cyclic Loading (maximum cyclic stress level: 66%)

occurs, there is slippage between the pile wall and the soil and the pile moves up rapidly. In contrast, for plates, rapid upward movement is restricted by the fact that soil above the plate has to be progressively displaced as the plate moves up.

Influence of Maximum Cyclic Stress Level

That the behaviour of plate anchors under cyclic loading is governed by the maximum cyclic stress level and not by the cyclic stress amplitude has been highlighted in detail by Datta et. al. (1990). For pile anchors also, Khan et. al. (1992) have shown that the maximum cyclic stress level substantially controls the pullout behaviour under cyclic loading.

The influence of the maximum cyclic stress level on the total displacement after 500 cycles is brought out in Fig. 13 for plate anchors and in Fig. 14 for pile anchors for each series of model tests conducted at the three water contents. One notes from Fig. 13 that in the case of plate anchors the total displacement increases with increase in the maximum cyclic stress level and that for a given maximum cyclic stress level the total movement is lower for model tests in soil at a higher water content.

Pile anchors show a similar trend although their total displacements are much smaller than those of plate anchors. As the maximum cyclic stress level increases, model piles show failure in soils at low water content though this is not observed in tests at higher water content.

To ensure that the movement of plate anchors lies below a prespecified limit, it is necessary to restrain the maximum cyclic stress level below a threshold value which may be designated as the critical maximum cyclic stress level. For example, if the limit on movement

A COMPARISON OF THE CYCLIC PULLOUT BEHAVIOUR

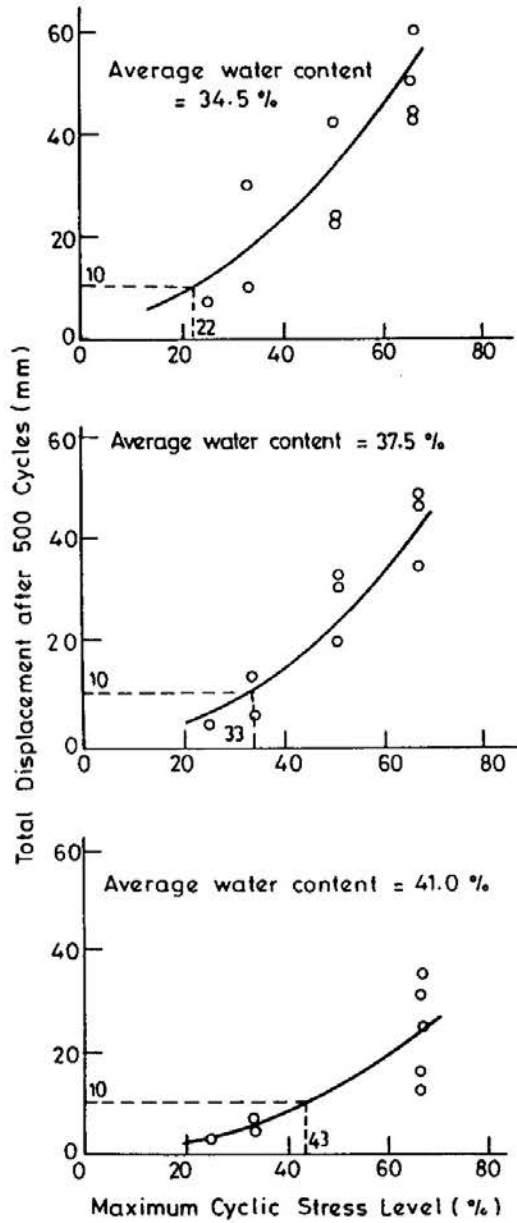


Fig. 13 Influence of Maximum Cyclic Stress Level on Movement of Plate Anchors.

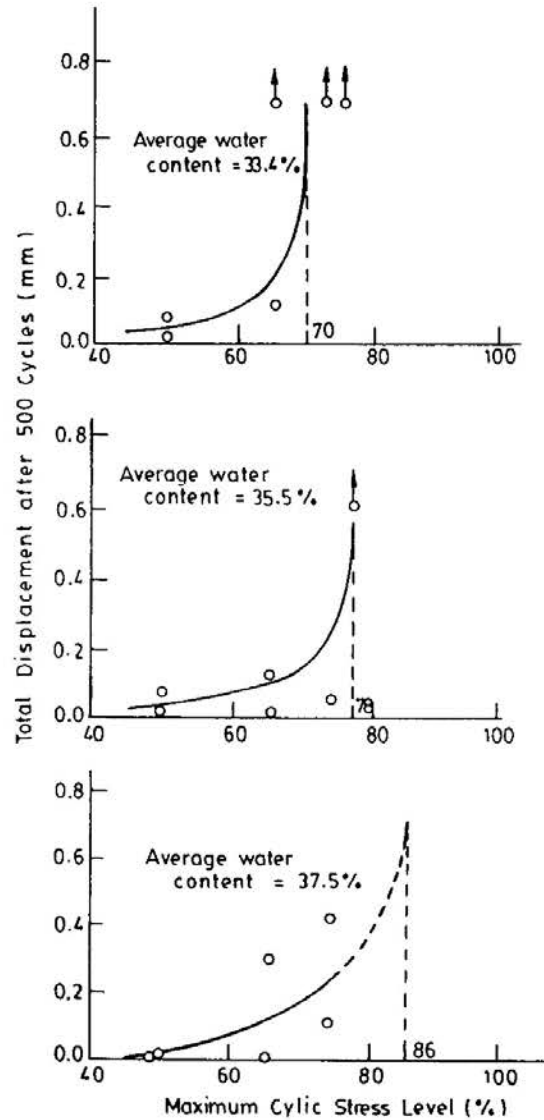


Fig. 14 Influence of Maximum Cyclic Stress Level on Movement of Pile Anchors.

is 20% of the plate diameter, one can determine the critical maximum cyclic stress level as shown in Fig. 13 for each water content of the soil. A plot of the critical maximum stress level versus the water content of soil is shown in Fig. 15 from which one notes that as the water content increases, the critical value also increases, indicating better performance of anchors in softer soils.

The criterion for identifying the critical maximum cyclic stress level in pile anchors is different from that in plate anchors because one has to prevent the occurrence of failure rather than control the movement. To prevent failure, the maximum cyclic stress level must be kept

below the critical stress level. This critical value can be obtained from the plot of pile movement versus maximum cyclic stress level as shown in Fig. 14 for each water content of the soil. A plot of the critical maximum stress level versus the water content is shown in Fig. 16 from which one notes that as the water content increases, the critical value also increases. This trend is similar to that observed for plate anchors.

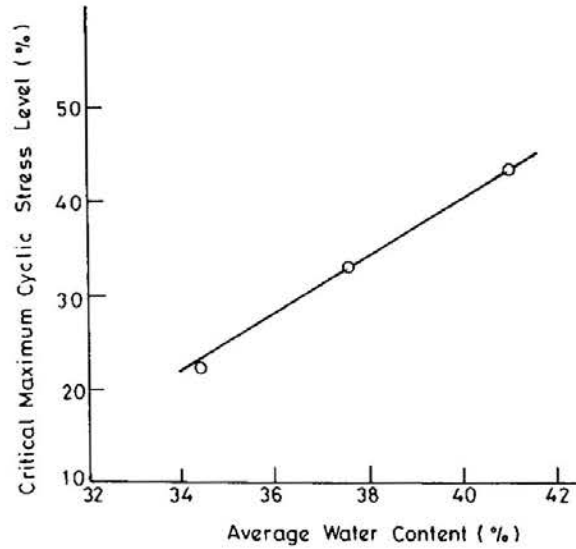


Fig. 15 Influence of Water Content on Critical Maximum Cyclic Stress Level for Plate Anchors.

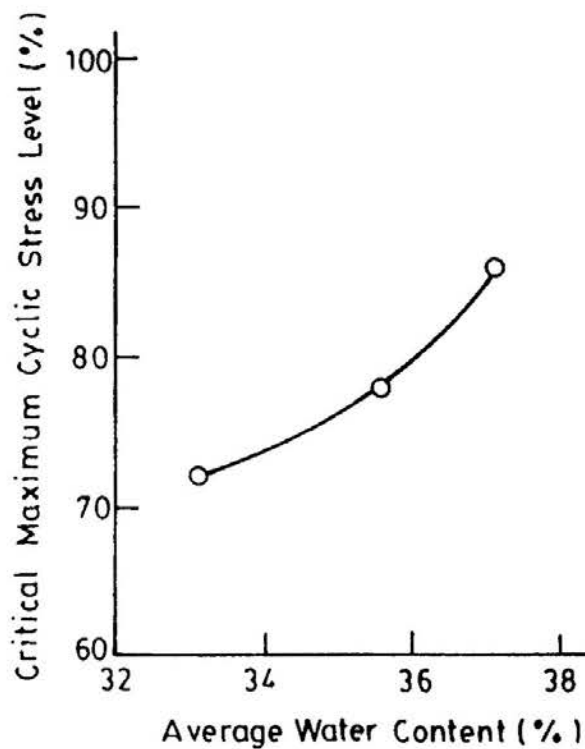


Fig. 16 Influence of Water Content on Critical Maximum Cyclic Stress Level for Pile Anchors.

A COMPARISON OF THE CYCLIC PULLOUT BEHAVIOUR

IMPLICATIONS FOR DESIGN

For the design of plate anchors subjected to cyclic loading, it is necessary that the peak cyclic load be substantially lower than the static pullout capacity of the anchor. The level to which the peak load must be restricted depends upon the maximum permissible movement. It is useful to allow for some movement, since plate anchors show significant initial movement under cyclic loading which tapers off rapidly as the number of cycles of loading increase. Nevertheless the peak cyclic load would have to be restricted to less than 50% of the static pullout capacity even when movements as large as 20% of anchor diameter are allowed. Pile anchors for TLPs must be designed keeping in view the fact that piles can fail even when the maximum cyclic load is well below the static pullout capacity. Though the critical level of the maximum cyclic load lies in the range of 60% to 80% of the static pullout capacity, it would be appropriate to apply a factor of safety of 2.0 to this critical maximum cyclic load to preclude the possibility of sudden failure.

CONCLUSIONS

The present comparative study shows that model plate anchors and model pile anchors buried in soft clay subjected to cyclic pullout loading exhibit the following differences and similarities.

- (a) The magnitude of movement under identical cyclic loading varies widely - plate anchors show much larger movement than pile anchors.
- (b) The mechanism of failure under cyclic loading is not the same - pile anchors show sudden failure due to slippage between pile wall and the surrounding soil whereas no such failure is observed in plate anchors.
- (c) The behaviour of both types of anchors under cyclic loading is governed by the maximum cyclic stress level.
- (d) An increase in water content of the clay results in an improvement in the behaviour of both types of anchors - the movements decrease and sudden failure is not observed.
- (e) Satisfactory performance of both types of anchors requires that the maximum cyclic stress level be kept below a threshold value which is significantly lower than the static breakout capacity.

REFERENCES

- BEMBEN, S.M., KALAJIAN, E.H. KUPFERMAN, M. (1973), "The Vertical Holding Capacity of Marine Anchors in Sand and Clay Subjected to Static and Cyclic Loading", *Proc. Offshore Technology Conf.*, 2 : 871-880.
- BEMBEN, S.M. and KUPFERMAN, M., (1975),: "The Vertical Holding Capacity of Marine Anchor Flukes Subjected To Static and Cyclic Loading", *Proceedings Offshore*

- Technology Conference*, OTC 2185, 363-374.
- DATTA, M., GULHATI, S.K. and ACHARI, G. (1990), "Behaviour of Plate Anchors in Soft Cohesive Soils Under Cyclic Loading", *Indian Geotechnical Journal*, 20, 3 : 207-224.
- HOLMQUIST, D.V. and MATLOCK, H. (1976), "Resistance - Displacement Relationship for Axially-Loaded Piles in Soft Clay", *Proc. of 8 th Offshore Technology Conf.*, Houston, Texas, OTC 2474: 553-569.
- KARLSRUD, K. and HAUGEN, T. (1985), "Behaviour of Piles in Clay Under Cyclic Axial Loading - Results of Field Model Tests", *Proc. of 4th Int. Conf. on Behaviour of Offshore Structures*, Amsterdam: 589-600.
- KHAN, N.U., DATTA, M., and SHASHI K. GULHATI. (1992). "Pullout Behaviour of Pile Anchors In Soft Clay", *Proceedings Fourth Indian Conference On Ocean Engineering*, Goa, Vol. 1.
- MATLOCK, H., BOGARD, D. and CHEANG, L. (1982), "A Laboratory Study of Axially Loaded Piles and Pile Groups Including Pore-pressure Measurements", *Proc. of Int. Conf. on Behaviour of Offshore Structures*, 1982: 105-121.
- PONNAIAN, D.A., and FINLAY, T.W., (1988), "Cyclic Behaviour of Plate Anchors", *Canadian Geotechnical Journal*, Vol. 25, pp. 374-381.
- POULOS, H.G. (1979), "Development of an Analysis for Cyclic Axial Loading of Piles", *Proc. of 3rd Int. Conf. on Numerical Methods in Geomechanics*, Aachen, Vol. 4.
- POULOS, H.G. (1981), "Cyclic Axial Response of Single Pile", *Journal of Geotechnical Engg. Div.*, ASCE, Vol. 107, No. GT 1 : 41-58.
- PUECH, A.A. (1982), "Basic Data for the Design of Tension Piles in Silty Soils", *Proc of Int. Conf. on Behaviour of Offshore Structures*, 1982: 141-157.
- STEENFELT, J.S., RANDOLPH, M.F. and WORTH, C.P. (1981), "Instrumented Model Piles Jacked into Clay", *Proc. of 10th Int. Conf. on Soil Mech. and Foundn. Engg.*, Stockholm, Vol. 2: 857-864.

GEOTECHNICAL PROPERTIES OF THE COHESIVE SUNGSHAN DEPOSITS, TAIPEI

C.T. Chin¹, J.H.A. Crooks², and Z.C. Moh³

SYNOPSIS

The cohesive soil deposits in Taipei are mainly slightly plastic clays with varying silt content in various depositional environments in the Taipei basin. For the design and construction of Taipei Rapid Transit Systems, it is essential to have a comprehensive understanding of the behaviour of these cohesive soils. The results of an extensive laboratory testing program indicate that the state concept for defining undrained strength applies well to the cohesive soils in Taipei. The results of K_0 consolidated undrained triaxial compression tests on samples reconsolidated to their in-situ stresses are in good agreement with the SHANSEP strengths. A generalized yield envelope has been defined for the lower cohesive soils in Taipei.

INTRODUCTION

Deep open excavations are common in Taipei for construction of basements for buildings which are supported on floating or semi-floating raft foundations. Internally braced diaphragm wall systems are traditionally used for support of open excavations.

At present, there is a significant increase in excavation work due to the construction of the Priority Network of the Taipei Rapid Transit Systems (TRTS) which includes 88 km of track with 80 stations (Fig. 1). The total length of the underground section is about 44 km. Thirty nine stations are to be constructed below grade in open excavations typically 200 to 300 m long and between 15 to 28 m deep. An additional 12.5 km of running track, crossovers and pedestrian shopping malls will also be constructed by cut-and-cover method. The remaining 18 km of underground track will be in paired 5.6 m diameter bored tunnels. The deeper open excavations will be supported by internally braced diaphragm walls; the total length of diaphragm wall construction is estimated at about 45 km. As with all underground construction in densely populated urban environments, the effects of ground deformation on existing structures is a significant consideration on the TRTS project.

Accurate definition of the engineering properties of the soils along the route of the subway is critical. Of particular interest is the undrained strength of the softer cohesive deposits through which much of the route will pass. For example, the predicted deformations

¹ Project Manager, Moh and Associates, 11/Fl., No. 35, Lane 11, Kwangfu N. Rd., Taipei, Taiwan, R.O.C.

² Principal, Golder Associates, 54-70 Moorbridge Rd., Maidenhead, Berkshire SL6 8BN, England. Formerly GESC Project Manager, Moh and Associates.

³ President, Moh and Associates, 11/Fl., No. 35, Lane 11, Kwangfu N. Rd., Taipei, Taiwan, R.O.C.

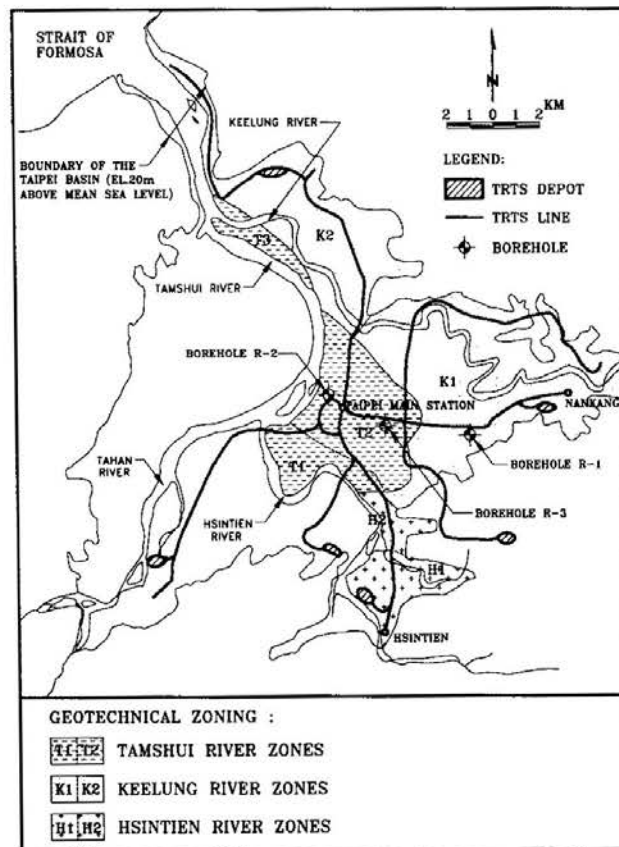


Fig. 1 Geotechnical Zoning in the Taipei Basin .

of supported excavations depend directly on the undrained strength assumed in analysis. An assumed strength which is too low will result in conservative design (ie extra struts, ground treatment, etc) and higher costs than is necessary. On the other hand, if the assumed strength is too high, performance during construction will be worse than expected and higher costs then are anticipated as well as claims will result.

As part of the TRTS project, a study of the strength behaviour of the recent cohesive deposits within the Taipei basin has been carried out by Moh and Associates (MAA), the TRTS Geotechnical Engineering Specialty Consultant. This paper reports the results of this work and establishes a basis for strength definition for these materials.

GROUND CONDITIONS

Regional Geology

The Taipei basin is relatively flat lying at a general elevation of 5-10 m above mean sea level. The total area of the Taipei basin is approximately 243 sq. km. Within the basin, the Hsintien and Keelung rivers join the Tamshui river and flow northwest to the Strait of Formosa (Fig. 1). The area is heavily developed and densely populated.

The basin was formed as the result of tectonic activity and is bounded to the east, south

GEOTECHNICAL PROPERTIES

and west by hills consisting of sedimentary rocks of Tertiary age. To the north, the basin boundary is formed by mountains consisting of rocks of volcanic origin.

The Quaternary deposits which infill the basin, comprise upper recent deposits of the Sungshan formation which are up to 70 m thick in the city center area (Table 1). The Sungshan deposits overlie an extensive gravel deposit, the Chingmei deposit, and the lower hard sandy clay deposits of the Hsinchuang formation. Most of the TRTS underground construction work in the downtown area will take place in the Sungshan formation. The permeable and water-bearing Chingmei gravels also have a major impact on the project in terms of groundwater control requirements.

Table 1 Profile of Sedimentary Deposits in Taipei Basin.

Formation	Thickness (m)	Soil Description
Top Soil (CL/ML)	1-6	Yellowish Brown Clay
Layer VI (CL/ML)	2-8	Grayish Black Clayey Silt/Silty Clay
Layer V (SM)	2-20	Gray Silty Fine Sand
Sungshan Formation Layer IV (CL)	6-29 40-70	Gray Silty Clay
Layer III (SM)	0-19	Gray Silty Fine Sand
Layer II (CL/ML)	0-19	Gray Silty Clay
Layer I (SM)	0-15	Gray Silty Fine Sand
Chingmei Formation	0-200	Yellowish Brown Gravel
Hsinchuang Formation	0-120	Gray to Yellowish Brown Sandy Clay with Occasionally Interbedded Thick Gravel Layer
Tertiary Sedimentary Rock (Volcanic Rock in Peitou, Shihlin, and the Vicinity of Kungkuan)		

Stratigraphy

Based on collation and synthesis of available data, Moh and Associates (1987) subdivided the Sungshan deposits into areal zones based on depositional history and material type. Most of the deeper excavations for the TRTS project will be located in the T2 and K1 zones (Fig. 1).

The stratigraphy in the T2 zone is relatively uniform, consisting of six alternating layers of clays and sands. The uppermost layer VI together with layers IV and II consist of cohesive soils while layers V and III consist of silty sands. The lowermost layer I is variable and contains both clayey and sandy materials. In the K1 zone, sandy layers are thin or absent and the profile is dominated by cohesive soils. Typical index properties for the various layers are summarized in Table 2.

Table 2 Physical Properties of Sungshan Deposits.

Sublayer	Soil Description	w _n (%)	w _l (%)	I _p (%)	Particle Size Distribution (%)			
					Gravel	Sand	Silt	Clay
VI	Brownish Yellow to Grayish Black Clayey Silt/Silty Clay	31.2	35.8	12.9	0	10	58	32
V	Gray Silty Sand	26.3	-	-	1	75	19	5
IV	Gray Silty Clay/Clayey Silt	32.1	34.3	12.0	0	8	61	31
III	Gray Silty Sand	23.9	-	-	0	60	34	6
II	Gray Silty Clay/Clayey Silt	27.2	30.3	9.2	0	9	67	24
I	Gray Silty Sand	20.3	-	-	1	63	29	7

A typical east-west section along the TRTS Nankang Line (from Taipei Main Station to Nankang, Fig. 1) illustrates the gradual change in stratigraphy from the alternating clayey/sandy layers in the T2 zone in the city center area to the thick clay deposits in the K1 zone to the east (Fig. 2). Figure 3 shows a typical north-south section along the TRTS Hsintien Line (from Taipei Main Station to Hsintien, Fig. 1). Typical T2 stratigraphy occurs in the northern section of this line; a promontory of sandstone and tuff abruptly delineates the T2 zone from the gravelly H2 area which occupies the southern section of the line.

As indicated on Figs. 2 and 3, layer IV of the Sungshan deposits frequently occurs at about the invert of open excavations and is the medium through which tunnels will pass in the T2 area. In the downtown area, this material is silty with low plasticity. To the east, it becomes more clayey and construction performance in this area will be dominated by deep

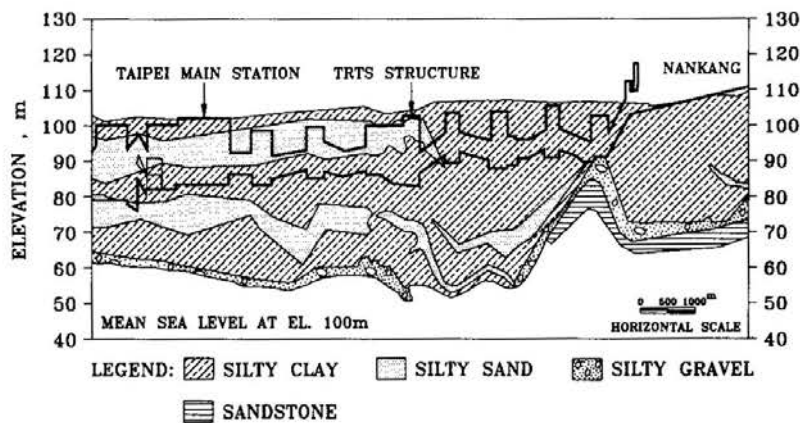


Fig. 2 Stratigraphy along the E-W Nankang Line.

GEOTECHNICAL PROPERTIES

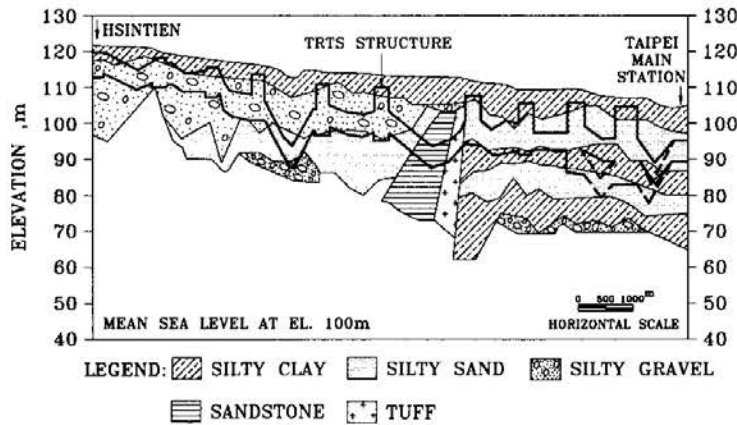


Fig. 3 Stratigraphy along the N-S Hsintien Line.

deposits of soft clay. The strength of these layer IV materials which vary in terms of material type, is the focus of this study.

Groundwater Conditions

The groundwater regime in the Taipei basin has experienced complex changes during the past 30 years as a result of extensive pumping from the Chingmei formation to supply water for the city. Figure 4 shows typical water pressure drawdown and associated settlement data for the downtown area. Pumping of groundwater from the Chingmei gravel began prior to 1960 and continued until the mid-1970s. By that time, a maximum draw-down of about 40 m had occurred in the lower Sungshan deposits; water pressures in the

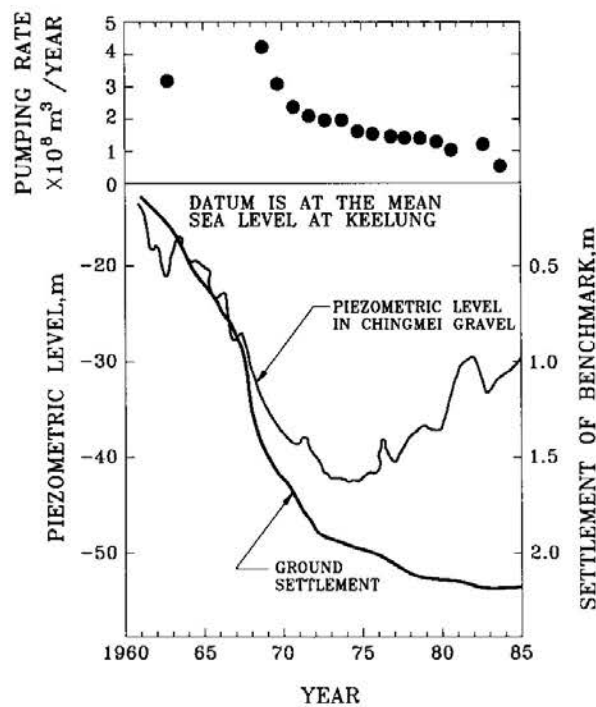


Fig. 4 Drawdown and Settlement due to Past Pumping in Taipei.

upper Sungshan deposits (layers V and VI) were not significantly affected. Surface settlement up to 2 m occurred as a result of the drawdown. As shown on Fig. 4, the ground surface settlement associated with pumping followed the drawdown curve closely. Drawdown and settlement were maximum in the city center area and progressively decreased toward the edges of the basin.

Since the mid-1970s, pumping has been restricted and there is a well-defined trend of recovery of water pressures in the gravel and the lower Sungshan deposits. Further, the rate of settlement has slowed down dramatically and has been close to zero throughout most of the basin in recent years. In the central basin area, water pressures in the lower Sungshan deposits and Chingmei gravel are still sub-hydrostatic. Recovery of water pressures is continuing and is a major factor in the design and construction of underground works (Chin et al, 1991a).

STRENGTH BEHAVIOUR IN TERMS OF STATE

State of Soils

It is inevitable that different methods of measuring strength will give different results because of differences in boundary conditions, mode of failure in relation to strength anisotropy, rate of testing and degree of disturbance. Understanding the reasons for these differences and selecting the correct values for design require that a consistent approach is used. In this study, state concepts have been used to evaluate the strength behaviour of the cohesive Sungshan deposits.

The strength behaviour of a soil is controlled in a first order sense by its void ratio and the effective stresses to which it is subjected. Together, void ratio and effective stresses define the current state of the soil which is represented as a point on a void ratio - effective stress plot. Current state is quantified by its distance from a reference line as follows (Fig. 5):

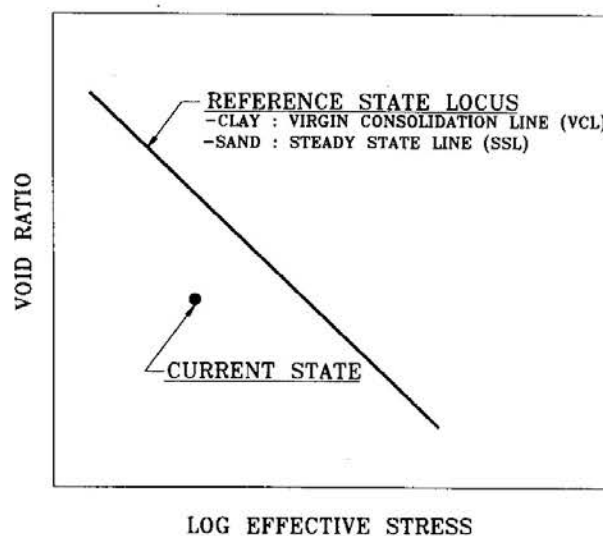


Fig. 5 State of Soils.

GEOTECHNICAL PROPERTIES

- * For clays, the virgin consolidation line (VCL) is used as a reference. Current state is quantified as the ratio of the current stress to the maximum past pressure (ie OCR).
- * For sands, the steady state line (SSL) is used as a reference. Current state is quantified as the void ratio difference between the current state and the SSL at the same stress level (ie state parameter, ψ).

Because ψ and OCR quantify current state, they provide a rational basis for correlations with the strength properties of sands and clays respectively. The use of OCR to represent the behaviour of clays is the basis of the SHANSEP concept (Ladd & Foott, 1974). The state parameter concept for sands was introduced by Been & Jefferies (1985). Examples of state – property correlations for different types of soils are shown on Fig. 6 (Ladd & Edgers, 1972) and Fig. 7 (Been & Jefferies, 1985).

The basic procedure for characterizing the soil properties at a site using the state approach is as follows:

- * Establish the OCR/ ψ profile for the site based on laboratory and/or field testing (eg CPT).
- * Determine the generic OCR/ ψ – property correlations for the relevant materials based on laboratory tests.
- * Use the OCR/ ψ – strength correlations to determine the strength profile at the site.

Normally, current state is defined in terms of vertical effective stresses. This approach is satisfactory if K_0 can be reasonably represented by expressions relating K_0 to OCR for

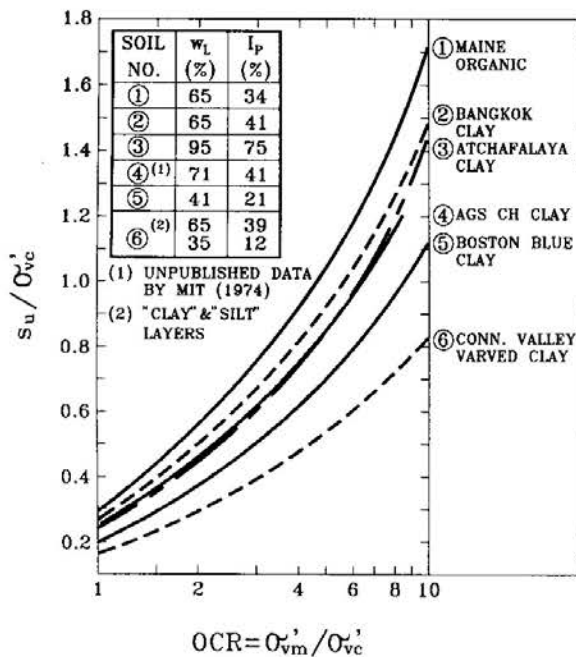


Fig. 6 Undrained Strength Ratio vs. OCR from CKoUDSS Tests on Six Clays (Ladd & Edgers, 1972).

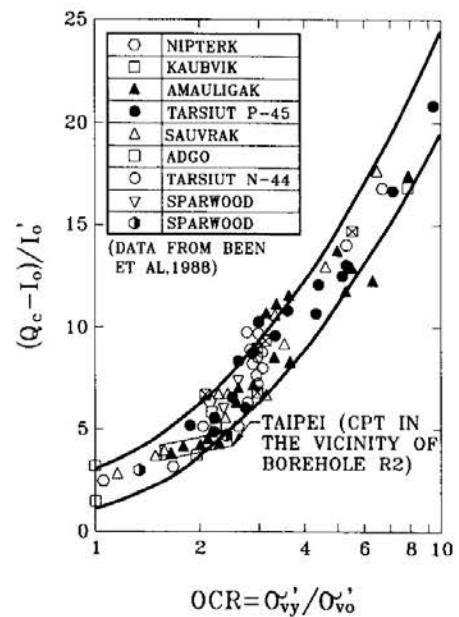


Fig. 7 Angle of Shear Resistance for Several Sands (Been & Jefferies, 1985).

clays or ϕ' for sands. Such relationships are reasonable for many soil deposits. However, in some materials, particularly clays, K_o can vary significantly from this expectation. Further in some tests (eg CPT and field vane), the horizontal effective stress has at least as much or greater influence than the vertical effective stress on the measurement being made. For this reason, it is more appropriate to define state in terms of mean stress level:

$$I'_o = (\sigma'_{vo} + 2 \times \sigma'_{ho})/3 \quad (1)$$

$$I'_y = (\sigma'_{vy} + 2 \times \sigma'_{hy})/3 \quad (2)$$

$$OCR'_i = I'_y / I'_o \quad (3)$$

The incorporation of σ'_{ho} is a relatively new concept because it requires the measurement of K_o . While this may be a difficult task, it is not impossible as discussed below.

Defining the State of Clays

As noted above, the state of clays is defined in terms of OCR which requires the accurate measurement of the following effective stresses:

- * σ'_{vo} Vertical in-situ stress.

This is more difficult in Taipei than is often the case because of the current complex groundwater conditions caused by past pumping from the Chingmei gravels and incomplete recovery of water pressures since pumping stopped. Total stresses are readily calculable but piezometers are required to define the in-situ water pressure. An estimate of σ'_{vo} can also be obtained from conventional oedometer tests using the “work/unit volume” approach (Becker et al, 1987) described below.

- * σ'_{vy} Vertical yield stress.

These values are estimated from the results of oedometer tests. However, for the cohesive Sungshan deposits, the $e - \log$ stress curves from oedometer tests are rounded with indistinct yield points. Thus interpretation of these data is best carried out using the “work/unit volume” approach.

- * σ'_{ho} and σ'_{hy} and Horizontal in-situ and yield stresses.

These values can be measured in-situ by self bored pressuremeter tests (not carried out as part of this study) or estimated using the “work/unit volume” interpretation of the results of oedometer tests carried out on vertically trimmed samples.

Based on the above, it is evident that significant reliance is placed on oedometer tests to define the state of clays. A problem exists in the interpretation of these tests for soils such as the cohesive Sungshan deposits, which exhibit rounded $e - \log$ stress curves. However, many of these problems can be overcome by using the “work/unit volume” approach developed by Becker et al (1987). This procedure is illustrated on Fig. 8 and described below:

- * The increment of work/unit volume is calculated for each load as follows:

GEOTECHNICAL PROPERTIES

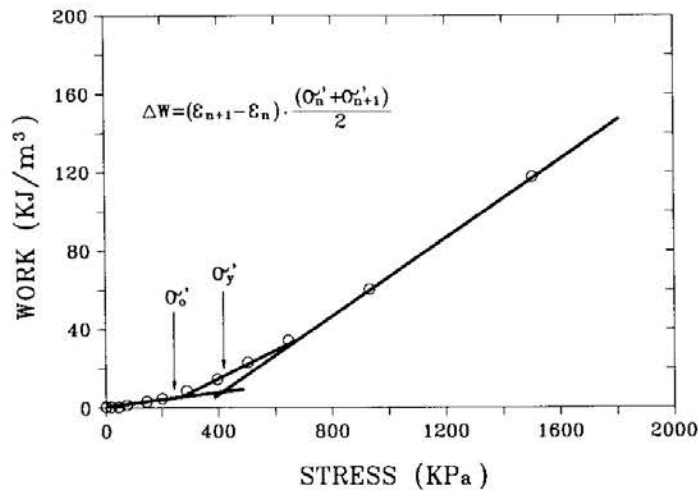


Fig. 8 Work/Unit Volume Interpretation of Oedometer Test Data .

$$\Delta W = (\epsilon_{n+1} - \epsilon_n) \times (\sigma'_{n+1} + \sigma'_n) / 2 \quad (4)$$

- * Cumulative work/unit volume is plotted vs final stress. The data can then be represented by linear relationships.
- * The intersection of the initial line and the post yield line occurs at σ'_y (ie σ'_{vy} or σ'_{hy} depending on the sample orientation).
- * In over-consolidated soils, there is a third line between the initial line and the post yield line. The intersection of the initial line and this third line occurs at σ'_o (ie σ'_{vo} or σ'_{ho} depending on the sample orientation).

It should be noted that the work/unit volume approach does not alter the data; it is simply a different method of presenting the data in a form in which it is easier to interpret. This is because the data are more easily represented by straight lines on arithmetic scales. The same data will provide the same result regardless of whether the conventional Casagrande or any other approach is used. However, natural strains must be used if the same form of relationship is to be preserved.

Regardless of the approach used to interpret the results of oedometer tests, only end of primary consolidation strains should be used. Since time effects vary in different soils, the inclusion of arbitrary quantities of secondary compression in test interpretation is not rational. The effects of unload-reload cycles should also be removed.

STATE OF COHESIVE SUNGSHAN DEPOSITS

To obtain data for evaluating the strength behaviour of the cohesive Sungshan deposits, detailed sampled borings were put down at the locations shown on Fig. 1. Cone penetration tests were also carried out in the vicinity of Borehole R-2. The sites were chosen to reflect the varying nature of the materials across the basin. The results of testing to define state profiles at each location are described below.

K1 Area

This site is predominantly underlain by clayey silt except for a 4 m thick sandy zone at about 30 m depth (Fig. 9). The nature of the clayey soil changes slightly but consistently with depth with the clay content increasing down to about 15 m and then decreasing again below this depth. This variation is reflected in the index properties as indicated on Fig. 9.

There is also an apparent difference in material type between 19 - 21 m depth where the water content is about 5% lower than the adjacent materials and the plasticity index is 2 to 3% higher. The specific gravity in this zone also appears to be lower than the adjacent material.

Piezometric pressures were determined from inspection of piezometers installed in the boring and in other borings drilled in the past near to this location. While the latter show some variation with time, the most likely values provide a reasonably definitive linear trend with depth. No information is available above a depth of 15 m; it is assumed that the current piezometric profile continues upward until it intersects the hydrostatic line associated with a groundwater level at a depth of 1 m. This would represent the upper bound of piezometric pressure.

Information on the state of the materials at the K1 site is summarized on Fig. 10 and discussed below.

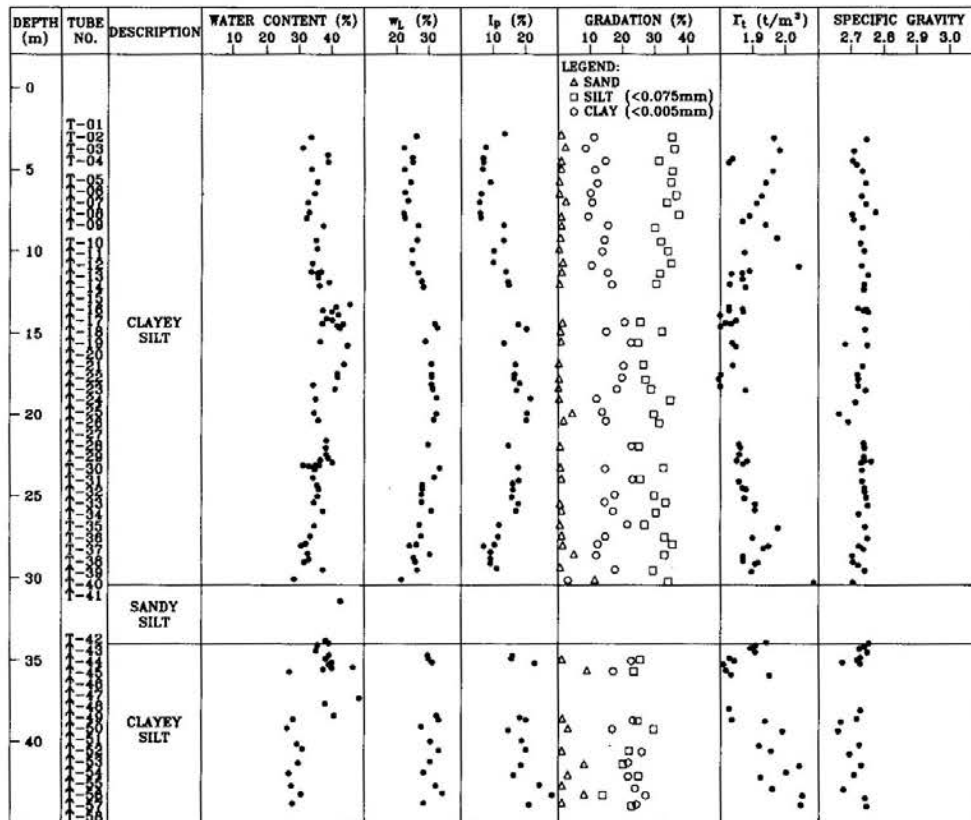


Fig. 9 Index Properties of K1 Soil.

GEOTECHNICAL PROPERTIES

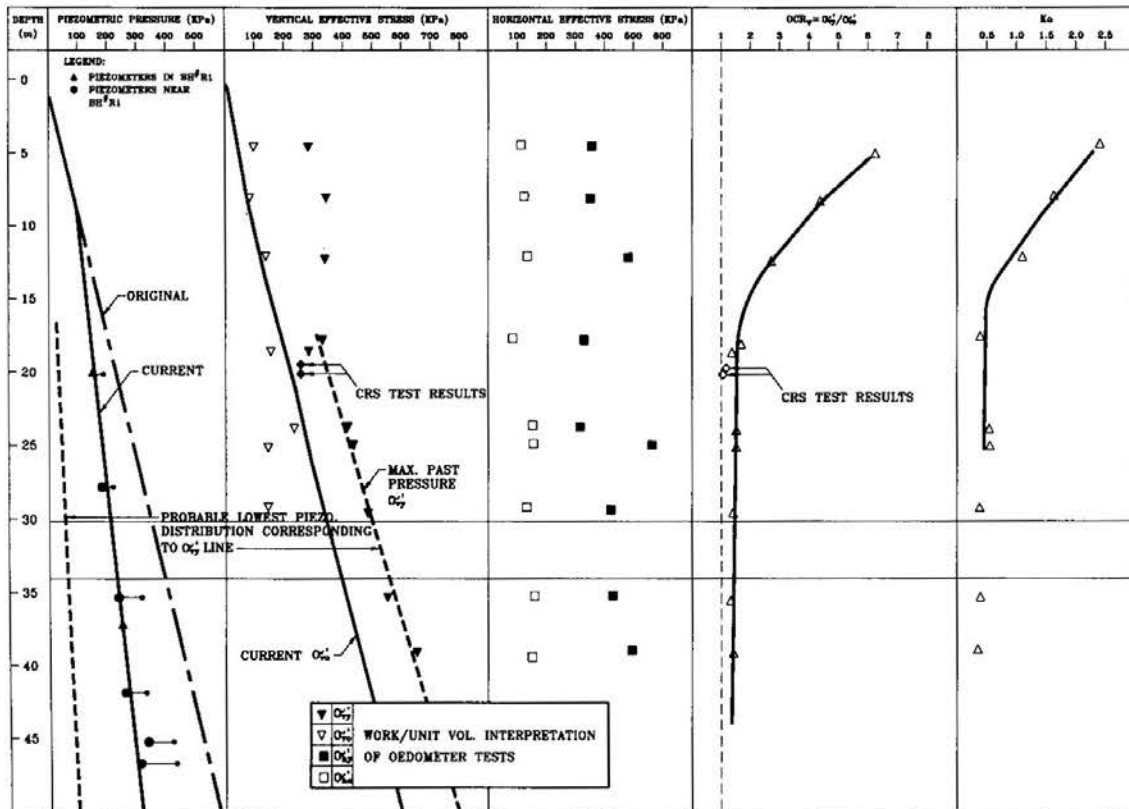


Fig. 10 State Profile of K1 Soil .

Based on the measured piezometric profile and calculated total stresses, the current in-situ vertical effective stress profile can be accurately determined. The σ'_{vo} values estimated from vertically loaded oedometer tests are reasonably consistent with the calculated σ'_{vo} profile.

Above 15 m depth, σ'_{vy} values are approximately constant but are relatively high given the depth and assumed stress history. The σ'_{hy} values are as high as σ'_{vy} values. OCR_v values are also high at shallow depth decreasing to about 1.5 - 2 at about 15 m. High K_0 values which also show a decreasing trend with depth are also evident above 15 m depth.

The state data below 15 m are readily understood in terms of the known stress history of the deposit. Thus, the σ'_{vy} values form a consistent trend and lie above the current σ'_{vo} profile. The magnitude of over consolidation is consistent with a past piezometric profile which reflects a 35 - 40 m water level lowering in the underlying Chingmei gravels. As a result of this stress history, OCR decreases slightly from about 1.7 - 1.4 with depth.

The σ'_{vy} values from the constant rate of strain (CRS) compression tests at about 20 m depth lie somewhat below the trend given by incrementally loaded tests. It is not known if this difference is due to the apparent difference in material type between 19 - 21 m as discussed above or a difference resulting from test type.

Given the stress history below 15 m, the K_0 values which range from 0.45 - 0.66 appear reasonable. Unrealistically low values were measured at depth and have been ignored.

T2 Area

The stratigraphy of Borehole R-2 is typical of the T2 area with all of layers I - VI easily recognized. Stratigraphic and state data for the relevant layers are summarized on Figs. 11 and 12 and discussed individually below.

The piezometric conditions in the depth range of interest (ie in layers IV - VI) are well defined based on the 2 piezometers installed in layer IV and the piezometric pressures measured in the overlying layer V at the end of CPT dissipation tests. The measured piezometric profile at this location is consistent with other data in the general T2 area. Based on the measured piezometric profile and the calculated total vertical stress profile, the σ_{vo}' profile is readily determined.

Layer VI: Based on the oedometer test results, this 3 m thick silty clay layer is moderately over-consolidated. However, the degree of over-consolidation is not as high as in the upper portion of the K1 site.

Layer IV: This layer consists of a moderately plastic clayey silt to silty clay material which is typical of layer IV soils throughout the T2 area. Two sets of oedometer tests indicate slight over-consolidation with an OCR of about 1.6. The magnitude of over-consolidation above the current σ_{vo}' profile is consistent with the fact that the piezometric pressure at the top of the underlying sandy layer (and probably the base of layer IV) was zero during the period of maximum groundwater lowering when pumping took place from the underlying Chingmei gravels.

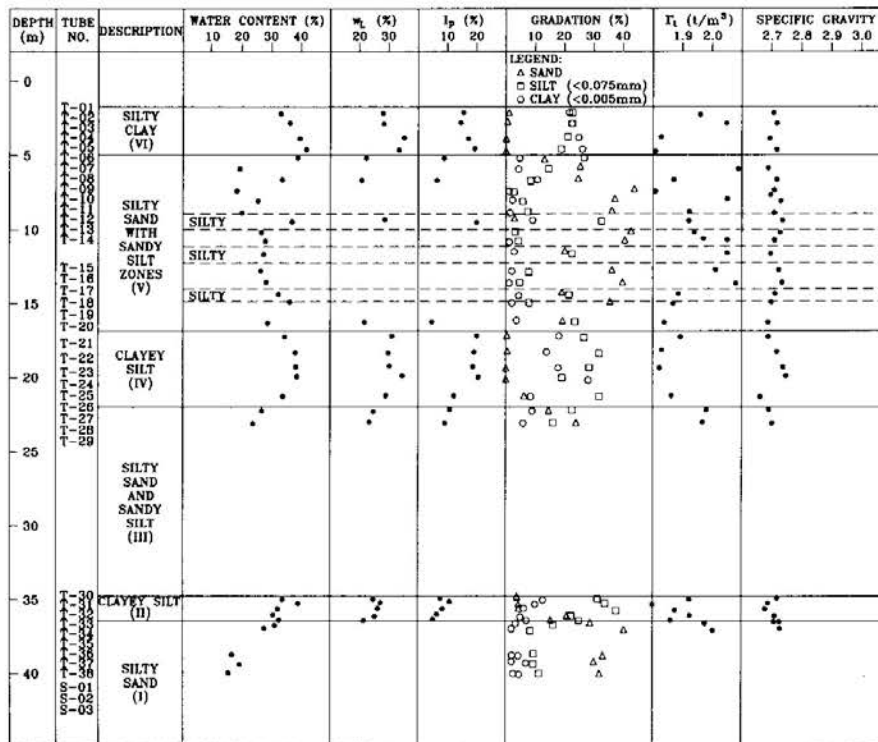


Fig. 11 Index Properties of T2 Soil.

GEOTECHNICAL PROPERTIES

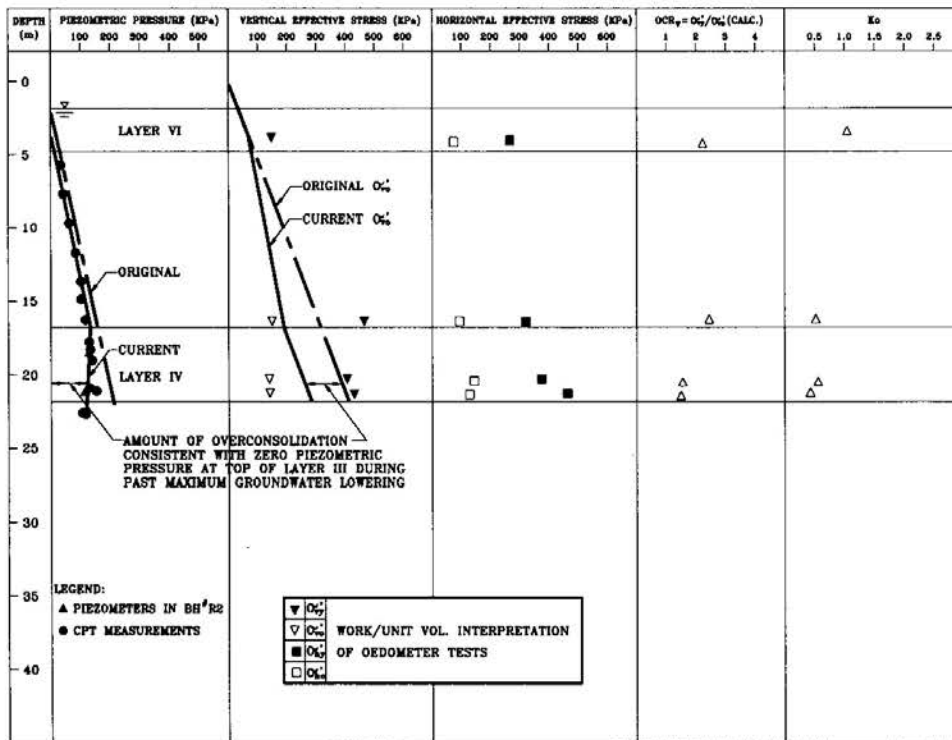


Fig. 12 State Profile of T2 Soil.

The σ'_{vo} values obtained in the vertically loaded oedometer tests do not correspond well to the calculated σ'_{vo} profile. However, the σ'_{ho} values from the horizontally loaded oedometer tests provide reasonable K_o values of about 0.5.

K1/T2 Transition Area

Borehole R-3 was put down in the “transition zone” between the T2 and K1 areas. As expected, the typical Sungshan deposits stratigraphy was encountered (ie layers I-VI) but with the cohesive layers more dominant than is the case in the T2 zone (Fig. 13). At this location the more sandy layer V is reasonably well defined between 5.5 and 13 m depths although the layer III material is more silty at depth than is the case in the T2 area. Layers I-III are poorly defined below 29 m; this zone is best described as silt - clayey silt with silty sand interbeds and is not considered further in this review.

The piezometric profile is reasonably well defined by the piezometers installed in the borehole together with others previously installed in the general vicinity and is very similar to that measured at the K-1 site.

From the piezometric profile and computed vertical total stresses, the current effective stress profile can be readily established. The σ'_{vo} values estimated from oedometer tests are in reasonable agreement with the calculated values. The state data for the relevant layers is summarized on Fig. 14 and discussed individually below:

Layer VI: As is the case for the K1 location, layer VI in the T2/K1 “transition” zone is over-consolidated with high K_o values.

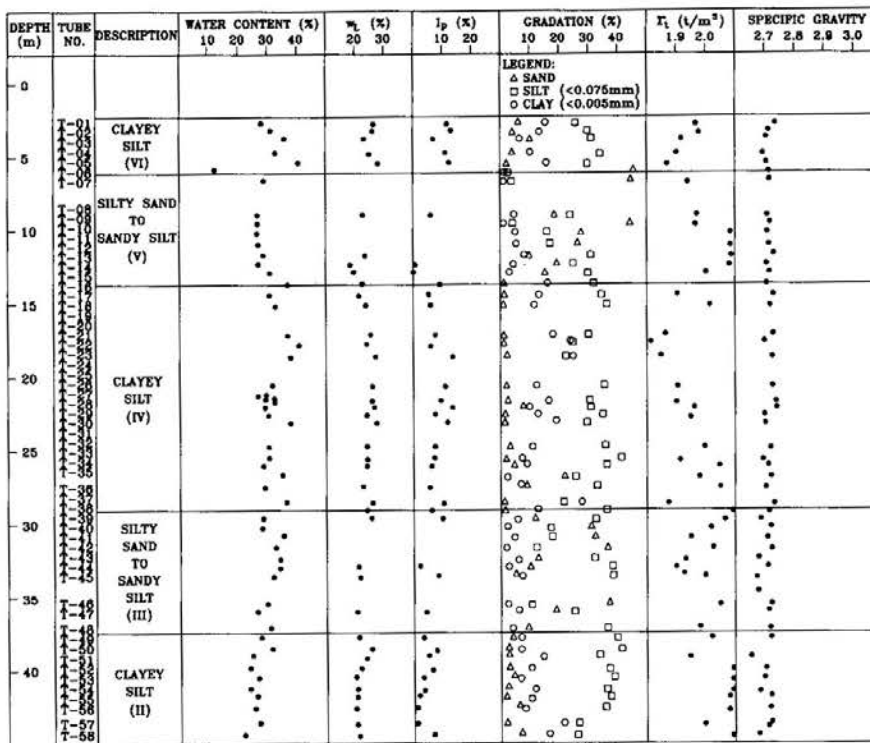


Fig. 13 Index Properties of K1/T2 Soil.

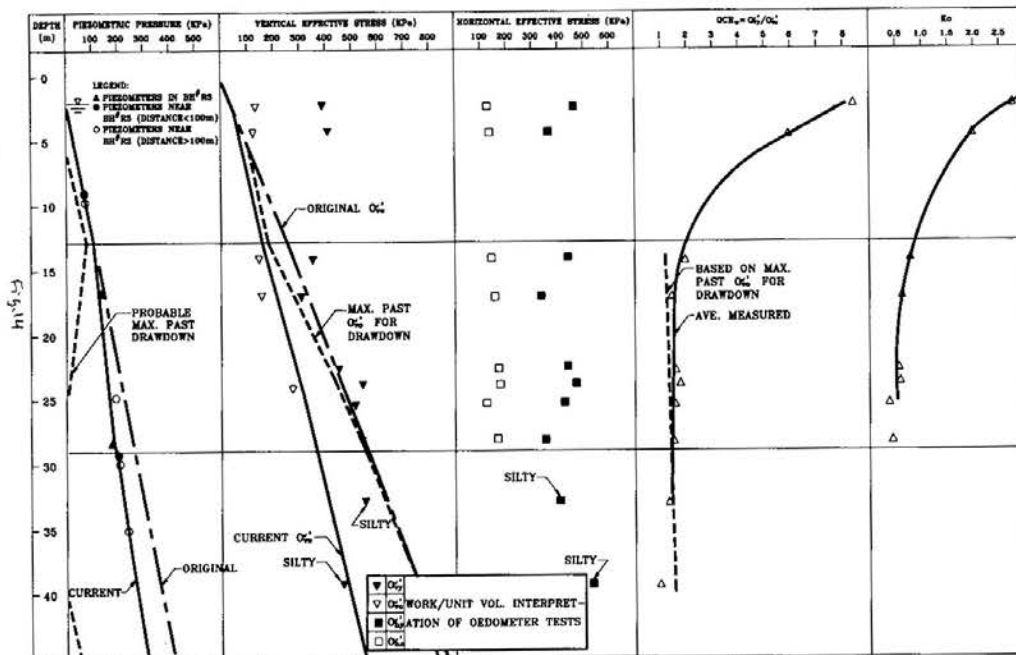


Fig. 14 State Profile of K1/T2 Soil.

Layer IV: The results of 6 pairs of vertically and horizontally loaded oedometer tests within this layer provide a good definition of the state of the soil. The σ'_{vy} profile is reasonably consistent with the maximum vertical effective stress calculated based on

GEOTECHNICAL PROPERTIES

the maximum past groundwater lowering due to pumping from the Chingmei gravels. The measured σ'_{hy} values also lie in the same range. The resulting OCR is approximately constant at about 1.4 - 1.6. Ko values are consistently equal to about 0.6. It is noted that slightly higher OCR and Ko values occur at the top of the layer.

State of the Layer VI Clays

In the layer VI materials at both the K1 and K1/T2 locations, the test data indicate a relatively high degree of over-consolidation together with high Ko values. Both OCR and Ko decrease with depth. The reason for this phenomenon is not clear. There are two possible explanations for this phenomenon:

- * either the test data are incorrect, or
- * the observed state data is correct and there is a rational reason for this condition based on the history of the deposit.

The data which indicate an unusual state in the layer VI materials is developed solely from the work/unit volume interpretation of vertically and horizontally loaded oedometer tests. Thus the possibility that this type of interpretation is invalid for the Sungshan materials must be considered. The following points are noted:

- * The σ'_{vy} data for each site are consistent and the σ'_{hy} values are similar to the σ'_{vy} values. Regardless of the magnitude of the yield values, the decreasing trend in OCR instinctively seems reasonable. The σ'_{vy} values determined in the same manner at greater depth clearly match the known stress history of the deposit based on known groundwater level changes. Thus it appears that the approach is correct at depth. There is no reason to suspect that the same method of interpretation should be correct in the layer IV soils and incorrect in the layer VI soils.
- * The σ'_{vo} values estimated from oedometer test results are reasonably close to those calculated from total stresses and piezometric pressures. While the latter are not well defined in the layer VI materials, variation from the profiles assumed in this review is not likely to alter this conclusion significantly.
- * The σ'_{ho} values estimated from horizontally loaded oedometer tests seem entirely reasonable at depth given the known stress history of these lower materials. Again, there seems to be no reason that the same method of interpretation should be correct for the layer IV soils and incorrect for the layer VI soils. Further, if the work/unit volume approach to estimating σ'_{vo} gives reasonable results in the layer VI soils, there is no reason to suspect that it will not provide reasonable estimates of σ'_{vo} .

Based on the above, the apparently unusual state of the layer VI soils does not appear to be the result of incorrect measurements. Rather, it appears to be a real phenomenon. Possible reasons are discussed below.

- * Over-consolidation can be caused by surface loading which is applied for a sufficiently long time to allow full consolidation of the underlying materials. Man-made surface loads (ie fills) would have to be in the order of 10 - 15 m high in order to cause the

observed degree of over-consolidation. This is highly unlikely to have occurred at the K1 and K1/T2 sites.

- * A second form of past surface loading is natural soil which is subsequently eroded. This mechanism would require a past ground surface level at about El 120 - 125 m (mean sea level at El 100 m). There is no information to support this hypothesis.
- * As discussed previously, the groundwater level in the Taipei basin has been at shallow depth below the existing ground surface and there is no evidence to suggest that there has been significant lowering of the upper groundwater level to say a depth of 15 m. Thus it does not appear that this mechanism can explain the apparent degree of over-consolidation. Further, there is no evidence of significant weathering except at shallow (< 5 m) depth.

The relationships between K_o and OCR_v for the layer IV and layer VI soils are shown on Fig. 15. For the layer IV soils within the tested range, the data are in a reasonable agreement with the "generally" expected relationship based on other materials (Mayne & Kulhawy, 1982). For the layer VI soils, this expected relationship does not apply.

It should be noted that traditional relationships between K_o and OCR have been developed based on laboratory measurements. Thus they reflect only the effect of OCR on K_o . However, depositional and post depositional factors also affect K_o and much higher values have been measured for other clays in self-bored pressuremeter tests and horizontally loaded oedometer tests. Jefferies et al (1987) report similar results for Arctic clays and

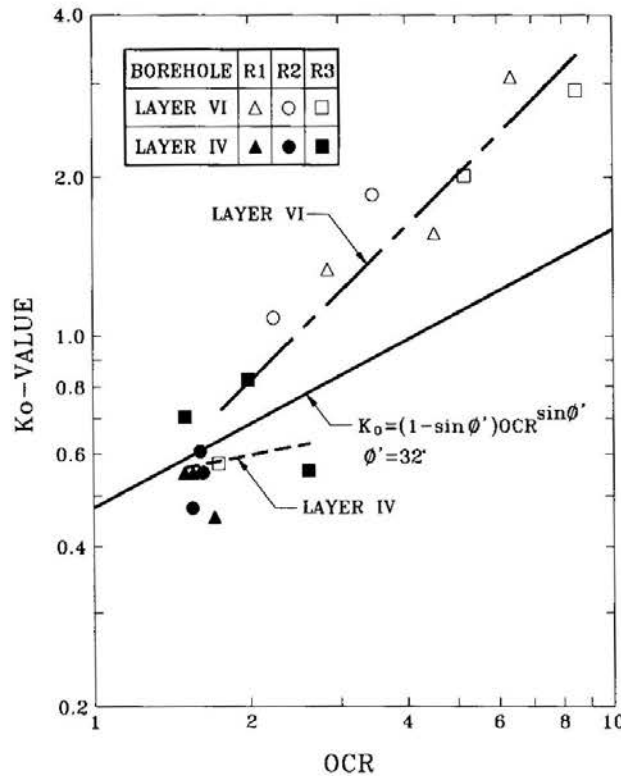


Fig. 15 K_o -OCR Relationships.

GEOTECHNICAL PROPERTIES

postulate that the measured high K_o values are the result of wave action during deposition in shallow water. Since the influence of wave action would decrease with increasing water depth, K_o would also be expected to decrease with depth as is the case for the Sungshan deposits. While the measured K_o - OCR relationship may appear "unusual", there is precedent for such behaviour. Thus the layer VI data should not be dismissed simply because it does not conform to what is generally thought of as typical.

UNDRAINED SHEAR BEHAVIOUR

Normalized Strength Behaviour

Samples of layer IV soils from various depths and locations were normally consolidated under K_o conditions in triaxial cells (CKoU tests). At the K1 site, the samples were at sufficient depth to be below the highly over-consolidated upper zone. Some were tested at $OCR = 1$ while others were allowed to swell to OCR values of approximately 2, 4 and 6 prior to shearing. Both compression and extension tests (CKoUC and CKoUE tests) were performed. These tests provide the basic SHANSEP type relationships between the state of the samples (expressed as OCR) and undrained strength ratios in compression and extension.

The majority of the compression strength test data lie in a relatively narrow band regardless of location (Fig. 16) and the average relationship between OCR_v and compression strength can be represented by the following expression:

$$s_u / \sigma'_{vc} = 0.32 \times OCR_v^{0.82} \quad (5)$$

A similar relationship, with equally narrow scatter, applies when the data is interpreted in terms of OCR_i .

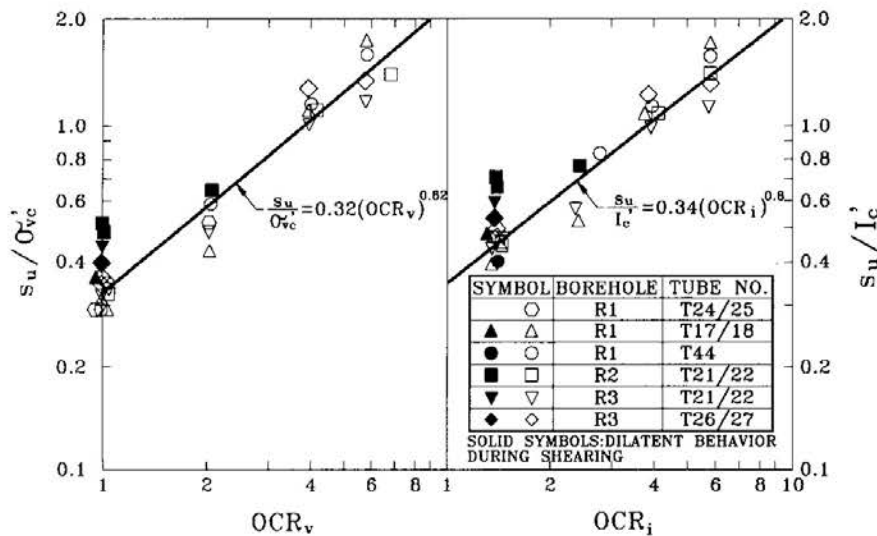


Fig. 16 Undrained Compression Strength Ratio vs. OCR from CKoUC Tests.

Some normally consolidated samples exhibited higher normalized strengths. This is attributed to dilation; as a result the SHANSEP approach does not apply and these data have not been included in the interpretation.

The porewater pressure response observed during undrained shear in compression is typical of a wide range of clays except for those samples which exhibit dilation (Fig. 17).

Although only 2 sets of SHANSEP undrained extension tests were carried out (Fig. 18), the results provide a consistent relationship as follows:

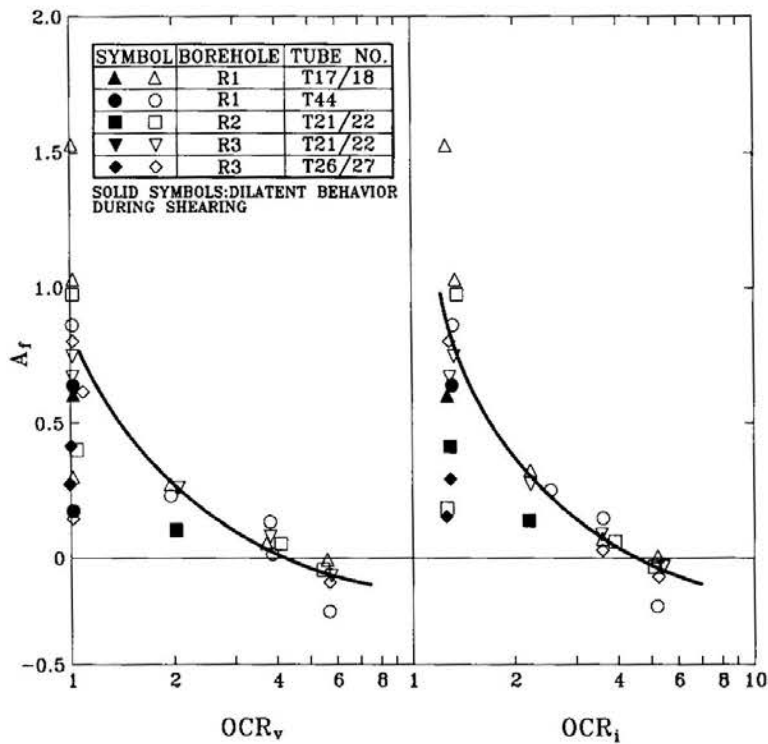


Fig. 17 Porewater Pressure Response during Shearing.

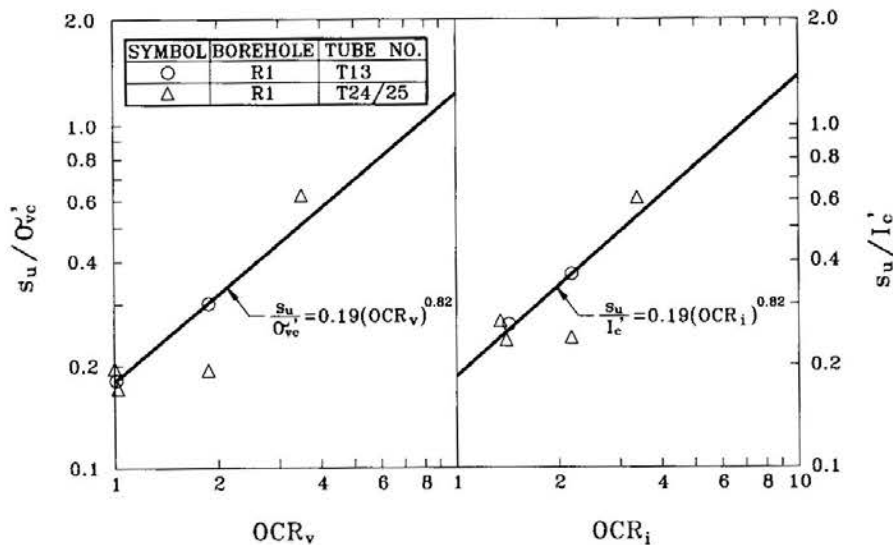


Fig. 18 Undrained Extension Strength Ratio vs. OCR from CKoUE Tests.

GEOTECHNICAL PROPERTIES

$$s_u / \sigma_{vc}' = 0.19 \times OCR_v^{0.82} \quad (6)$$

A similar relationship applies when the data is plotted in terms of OCR_t .

Samples Reconsolidated to In-Situ Stresses

CK₀UC tests were also carried out on samples from all three locations reconsolidated to the in-situ effective stress state (Recompression approach, Bjerrum, 1973). The purpose of this consolidation procedure is to ensure that the material is in as undisturbed state as possible. These tests provide a check on the OCR - compression strength relationships.

The results of all six tests tests of this nature are in excellent agreement with the strengths predicted using the SHANSEP approach described above (Fig. 19).

UUU and SUU Tests

Pairs of UUU and SUU tests were carried out on samples from the K1 and K1/T2 locations. These results are consistently lower than those derived from the normalized strength relationships and from samples which were tested after being reconsolidated to their in-situ effective stresses (Fig. 20). The results of SUU tests are particularly poor.

The reason for this difference is simply that the effective stresses under which the UUU and SUU tests were carried out are unknown because porewater pressures are not measured. It is obvious that the actual effective stresses in the UUU and SUU tests are significantly lower than those which exist in-situ.

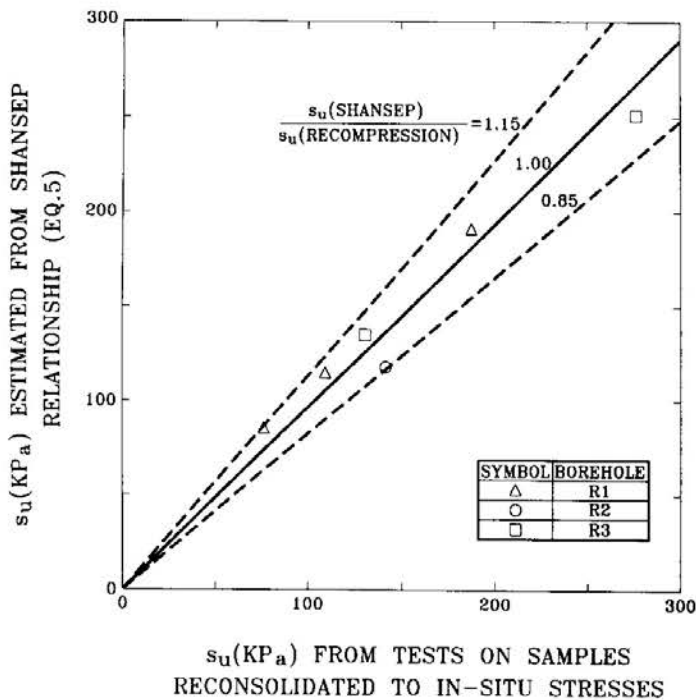


Fig. 19 Comparison of s_u between Recompression and SHANSEP Type of Tests.

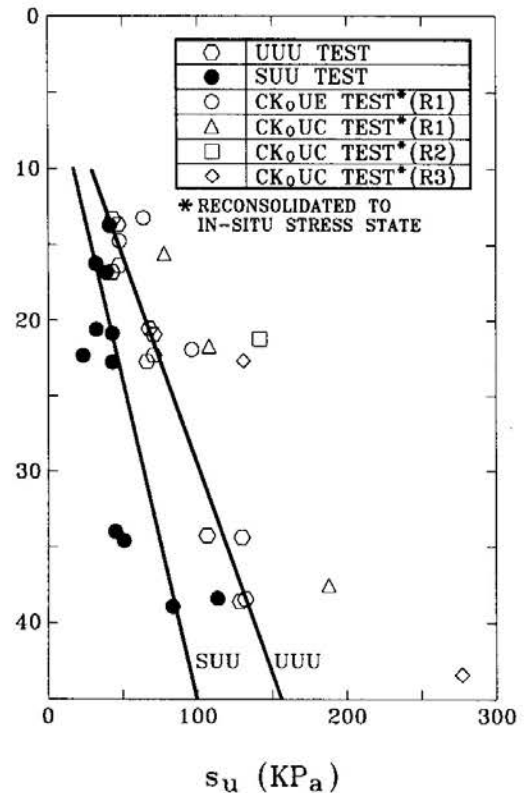


Fig. 20 Comparison of s_u from Various Test Types.

Large Strain Strength Behaviour

The effective stress states at the end of consolidated undrained compression and extension tests also provide information on the effective stress friction angle of soils. The combined results of tests on all K_0 consolidated undrained triaxial tests (Fig. 21) show little scatter and indicate that the average effective angle of shearing resistance ϕ' for all of the cohesive Sungshan deposits is about 32 degrees. This value applies to both extension and compression shearing modes.

Information from field monitoring has allowed effective stresses in the passive zone in front of diaphragm walls in Taipei to be calculated (Chin et al, 1991b). Based on the assumption the angle of wall friction is one third of the friction angle of the soil, field monitoring data confirms that the laboratory measured effective friction angle is reflected in the field.

Normalized CPT Behaviour

Since the tip resistance (Q_c) measured in a CPT test is controlled by the undrained strength of the soil (s_u), it can be expected that there will be a relationship between OCR - Q_c in the same way that there is a well defined relationship between OCR and s_u . Correlations of this nature have been developed for other soils, particularly for silty Arctic clays which are similar in many respects to the cohesive Sungshan deposits (Been et al, 1988).

Although only very limited data is available for the Sungshan deposits, it appears that the layer IV soils at the T2 location agree well with this correlation (Fig. 22). Thus the CPT provides the capability to provide reasonable estimates of in-situ state and therefore strength.

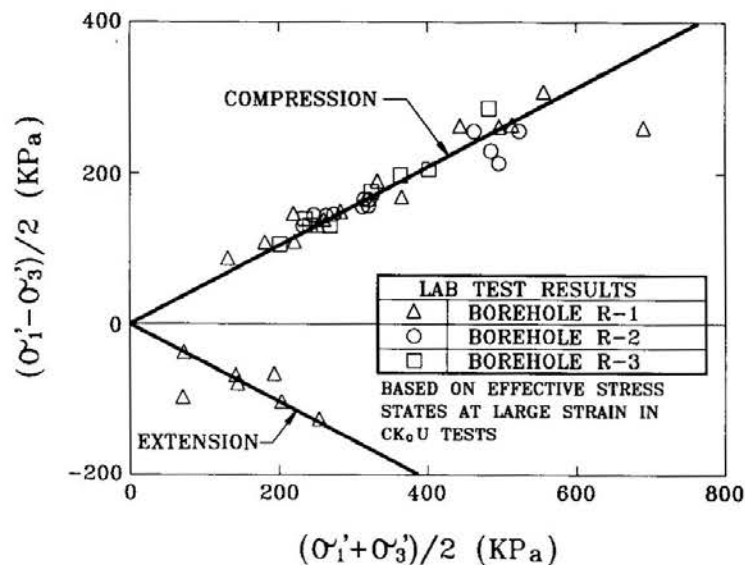


Fig. 21 Effective Stress Strength Envelopes.

GEOTECHNICAL PROPERTIES

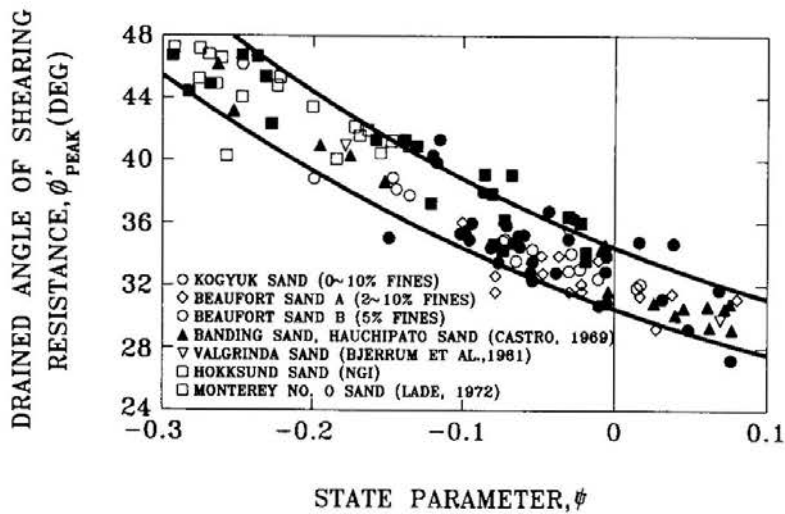


Fig. 22 Normalized Tip Resistance vs. OCR from Cone Penetration Tests.

Dilation Effects

Dilation occurs in over-consolidated clayey soils. However, in some undrained compression tests on normally consolidated samples of cohesive Sungshan soils, dilation occurred and resulted in undrained strengths significantly higher than would be expected based on normalized behaviour.

Evidence of similar behaviour is available from the results of a large body of CIUC tests carried out for various stages of the TRTS project. It is emphasised that these results should not be used to define undrained strength because consolidation stresses are not representative of field conditions. Nevertheless, they do provide a qualitative indication of the material types which would exhibit dilatant behaviour.

Based on the CIUC data (Fig. 23) there is a strong correlation between s_u/σ'_c and the porewater pressure parameter at failure (A_f). Basically, as s_u/σ'_c increases, A_f decreases

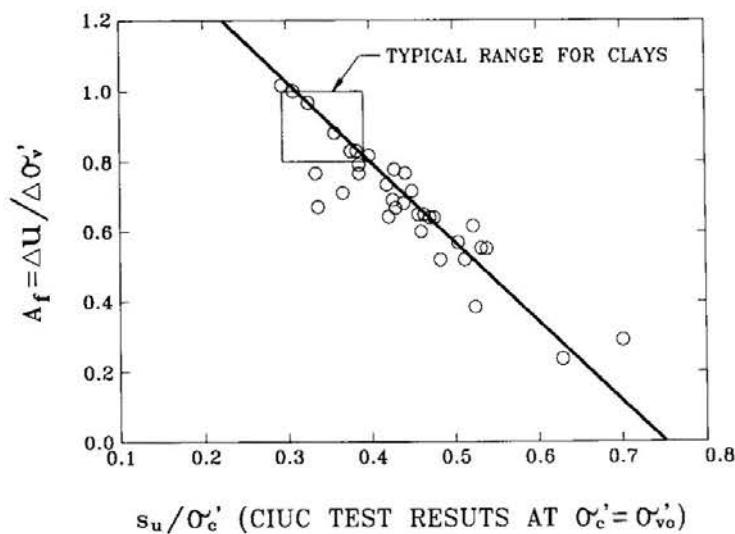


Fig. 23 $s_u - A_f$ relationship from CIU Tests.

which is indicative of dilatant behaviour. Sufficient data is available from the CIUC tests to relate the degree of dilation to material type (ie D_{60} and water content) as summarized on Fig. 24. Normal clay behaviour (ie $s_u/\sigma'_c = 0.3 - 0.4$; $A_f = 0.8 - 1$) is observed for samples with greater than 40% clay sizes which corresponds to water contents $> 40\%$. As the material becomes coarser and water contents decrease, the effect of dilation increases.

The problem of how to represent the strength of dilatant cohesive soils for design is difficult and poses the question as to whether or not the higher strength resulting from dilation can be relied on in the field. Clearly, this depends on the field problem. For example, for a tunnel where the loading condition is transient (ie short term), equalization of water pressures which would increase the porewater pressure and decrease strength, is less likely to occur. Thus the higher dilatant shear strength could provide significant "stand up time" which is beneficial.

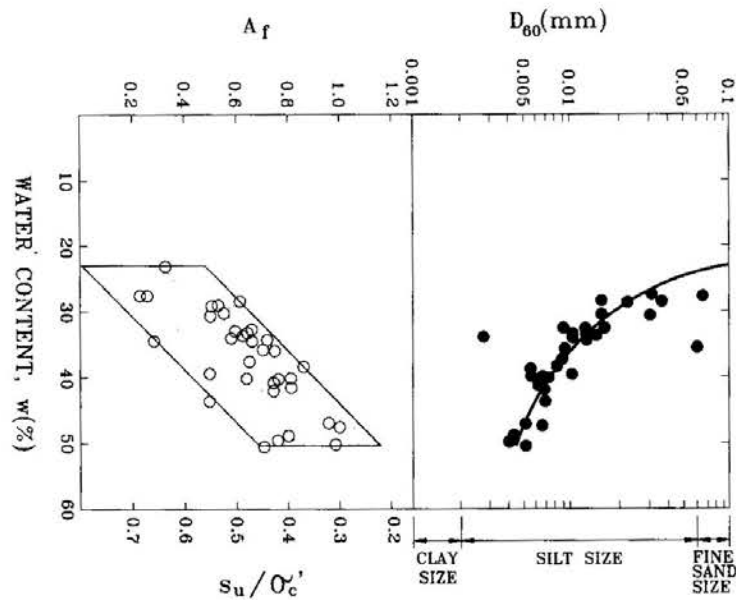


Fig. 24 Effect of Material Type on Dilation.

For longer term loading such as occurs in deep excavations, there is a greater likelihood that the soil will swell with porewater pressures increasing to the average surrounding conditions. Thus strength will decrease. This situation has to be evaluated on a case-by-case basis depending on the geometry of the problem and the coefficient of consolidation value of the soil.

YIELD BEHAVIOUR

The Yield Envelope Concept

Most cohesive soils exhibit both small strain and large strain behaviour. Small strain behaviour is characterized by undrained strength in compression and to a lesser extent, in

GEOTECHNICAL PROPERTIES

extension. A common example of small strain behaviour in a drained test is the yield stress evident in an oedometer test.

Large strain behaviour occurs in undrained strength tests when the material state reaches the ϕ' line. In an oedometer test, large strain behaviour occurs at stresses in excess of the yield stress (ie the normally consolidated stress range).

The total stress paths imposed in triaxial strength tests and oedometer tests are limited by the test conditions. However, under field loading conditions, the soil can be loaded along a wide variety of stress paths depending on the nature of loading. While the response of the soil to varying stress paths will vary in detail, there is a distinction between small and large strain behaviour regardless of stress path.

Small strain behaviour under various stress paths can be investigated in the laboratory by carrying out drained triaxial tests along various stress paths. For each stress path in $q' - p'$ stress space, a yield point can be identified which indicates the boundary between small strain and large strain behaviour. The locus of these yield points in $q' - p'$ stress space is termed the *yield envelope*. At stress states within the yield envelope, small strain behaviour occurs while large strain behaviour occurs outside the yield envelope.

The undrained compression strength will coincide with the upper surface of the yield envelope while the extension strength will coincide with the lower surface of the yield envelope. The apex of the yield envelope is typically defined by the preconsolidation pressure and the axis of the envelope will be approximately symmetrical around the K_0 line. Except for bonded or highly structured soils, the large strain lines in compression and extension will define the upper and lower limits of the yield envelope at lower stress levels; by definition stress states beyond the ϕ' lines in compression and extension cannot exist.

The yield envelope concept represents a simple qualitative stress-strain-strength model for lightly over-consolidated soils. It is useful for understanding the behaviour of soils under field loading (Folkes & Crooks, 1985; Crooks et al, 1984). It is also useful for evaluating the consistency of laboratory and field strength data.

Yield Envelopes for Cohesive Sungshan Deposits

The yield envelopes for samples of the cohesive layer IV Sungshan deposits from each of the three locations were determined in drained triaxial tests. The test samples were reconsolidated to their in-situ stresses prior to testing. Because the samples were obtained from different depths, the yield data were normalized with respect to their respective in-situ vertical yield stresses. The yield data from these tests is shown on Fig. 25 and describe a consistent generalized yield envelope for the layer IV deposits. Data from other tests also fit well with the generalized yield envelope:

- * The results indicate a consistent yield behaviour regardless of sample origin (ie the normalized yield envelope for each material type is essentially the same).
- * The compression and extension strengths predicted based on normalized (SHANSEP) strength behaviour using a typical OCR value of 1.6 correlate closely to the upper and

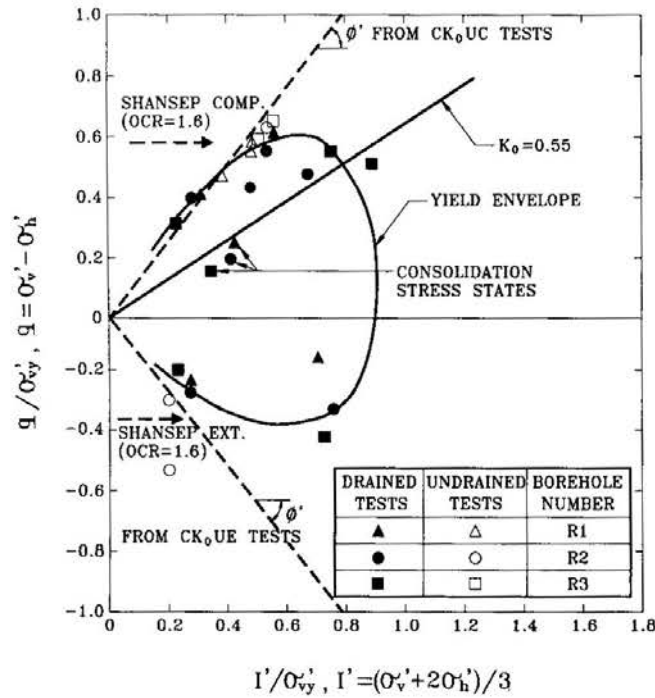


Fig. 25 Yield Envelope for Layer IV Soils.

lower portions of the generalized yield envelope.

- * The apex of the generalized yield envelope is reasonably well defined by the yield stress measured in oedometer tests and is consistent with a K_0 value of 0.55.
- * The large strain effective stress lines clearly provide upper and lower limits for the generalized yield envelope.

CONCLUSIONS

State concepts for defining undrained strength behaviour apply well to the cohesive Sungshan deposits.

At all locations, careful oedometer tests on good quality samples provide information on stress history which is consistent with the known stress history within the lower cohesive Sungshan deposits. The upper clayey soils at the K1 and K1/T2 locations are in a relatively highly over-consolidated state with associated high K_0 values. It is considered that this is a real phenomenon and is not the result of the test procedures.

The normalized strength (SHANSEP) approach to defining undrained strength in compression and extension applies well to the cohesive Sungshan deposits. Generalized relationships were found to apply to all of the materials tested in this program. Similar relationships apply when OCR is expressed in terms of mean stress. Some normally consolidated materials exhibit dilatant behaviour during undrained shear; the degree to which dilation occurs depends on the gradation of the soil. The strength of these materials cannot be represented by the normalized relationships.

GEOTECHNICAL PROPERTIES

The results of CKoUC tests on samples reconsolidated to their in-situ stresses are in good agreement with the strengths predicted using the normalized strength approach. The results of UUU tests and particularly SUU tests are significantly lower than the CKoUC data and do not provide a reasonable representation of undrained strength.

Although only limited data is available from this program, it appears that the CPT would be useful for providing rapid information on the state and strength of the cohesive Sungshan deposits.

The results of drained stress path testing indicates consistent yield behaviour for the layer IV soils at all locations. A generalized yield envelope has been defined for these materials. The yield behaviour is consistent with the results of other tests.

ACKNOWLEDGEMENTS

The authors wish to thank the Department of Rapid Transit Systems, Taipei Municipal Government for their support in the development of the information contained in this paper. Thanks are also due to our colleagues at Moh and Associates, Taipei, particularly Dr. R. N. Hwang and Mr. L. W. Wong, for their advice and assistance in the preparation of the paper.

REFERENCES

- BECKER, D.E., CROOKS, J.H.A., BEEN, K. and JEFFERIES, M.G. (1987). Work as a Criterion for Determining In-situ and Yield Stresses in Clays. *Canadian Geotechnical Journal*, Vol. 24, No.4, pp 549-564.
- BEEN, K. and JEFFERIES, M.G. (1985). A State Parameter for Sands. *Geotechnique*, Vol. 35, No. 2, pp 99-112.
- BEEN, K., CROOKS, J.H.A., and JEFFERIES, M.G. (1988). Interpretation of Material State from the CPT in Sands and Clays, *Proc. I.C.E. Conference on Penetration Testing in the U.K., Birmingham*, pp.215-218.
- BJERRUM, L. (1973). Problems of Soil Mechanics and Construction on Soft Clays. *State-of-the-Art Report*, Session 4, Proc. 8th ICSMFE, Moscow, Vol.3, pp.109-159.
- CHIN, C.T., CHIEH, T.T. and DUANN, S.W. (1991a). Groundwater Effect on MRT Construction. *Proc. 1st Young Asian Geotechnical Engineers Conference, AIT, Bangkok*, Vol.1, pp.1-12.
- CHIN, C.T., CROOKS, J.H.A., ENRIQUEZ, A. and PATRON, B.C. (1991b). Design and Performance of Open Excavations in Taipei. *Proc. 44th Canadian Geotechnical Conference, Edmonton*.
- CROOKS, J.H.A., BECKER, D.E., JEFFERIES, M.G. and MCKENZIE, K. (1984). Yield Behaviour and Consolidation: Part 1. *Pore Pressure Response. Proc. ASCE Symposium on Sedimentation Consolidation Models: Predictions and Validation, San Francisco*, pp 356-381.
- FOLKES, D.J. and CROOKS, J.H.A. (1985). Effective Stress Paths and Yielding in Soft

- Clays Below Embankments. *Canadian Geotechnical Journal*, Vol.23, No. 3, pp 357-374.
- JEFFERIES, M.G., CROOKS, J.H.A., BECKER, D.E. and HILL, P.R. (1987). Independence of Geostatic Stress from Over-consolidation in Some Beaufort Sea Clays. *Canadian Geotechnical Journal*, Vol 24, No. 3, pp 342-356.
- LADD, C.C. and EDGERS, L. (1972). Consolidated-Undrained Direct Simple Shear Tests on Saturated Clays. *Research Report R72-82, No. 284, Dept. of Civil Engrg., MIT, Cambridge, MA*, 354p.
- LADD, C.C. and FOOTT, R. (1974). New Design Procedure for Stability of Soft Clays. *Journal of Geotechnical Engineering Division, ASCE*, Vol. 100, GT7, pp. 763-786.
- MAYNE, P.W. and KULHAWY, F.H. (1982). Ko-OCR Relationships in Soil, *Journal of the Geotechnical Engineering Division, ASCE*, Vol. 108, GT6, pp. 851-872.
- MOH AND ASSOCIATES, INC. (1987). Engineering Properties of the Soil Deposits in the Taipei Basin. *Report No. 85043, Submitted to the Ret-Ser Engineering Agency and Taipei Public Works Department*.

APPENDIX: NOTATION

The following symbols are used in this paper:

A_f	= pore pressure parameter at failure
CIUC	= isotropically consolidated undrained triaxial compression
CKoUC	= Ko consolidated undrained triaxial compression
CKoUE	= Ko consolidated undrained triaxial extension
CKoUDSS	= Ko consolidated undrained direct simple shear
CPT	= cone penetration test
CRS	= constant rate of strain
D_{60}	= diameter at which 60% of the soil is finer
I_p	= plasticity Index
I'	= mean effective stress
I'_c	= mean effective consolidation stress
I'_o	= mean effective in situ stress
I'_y	= mean effective yield stress
Ko	= coefficient of earth pressure at rest
OCR	= over consolidation ratio
OCR_i	= over consolidation ratio in terms of I'_o and I'_y
OCR'_v	= over consolidation ratio in terms of σ'_{vo} and σ'_{vy}
Q_c	= tip resistance
q'	= $\sigma'_v - \sigma'_h$
SSL	= steady state line
SUU	= saturated unconsolidated undrained triaxial compression
u	= pore pressure
s_u	= undrained shear strength
UUU	= unsaturated unconsolidated undrained

GEOTECHNICAL PROPERTIES

VCL	= virgin consolidation line
ΔW	= work increment
w_l	= liquid limit
w_n	= natural water content
ϵ	= strain
γ_t	= total unit weight
σ'	= effective stress
σ_c'	= effective consolidation stress used in CIUC
σ_h'	= effective horizontal stress
σ_{ho}'	= in situ initial horizontal effective stress
σ_{hy}'	= effective horizontal yield stress
σ_v'	= effective vertical stress
σ_{vo}'	= in situ initial vertical effective stress
σ_{vc}'	= effective vertical consolidation stress
σ_{vm}'	= maximum effective vertical stress
σ_{vy}'	= effective vertical yield stress
σ_1'	= effective major principal stress
σ_3'	= effective minor principal stress
ϕ'	= friction angle in terms of effective stress
ψ	= state parameter